**Doctoral Dissertation**

# Fabrication and Characterization of Large-area Oriented Floating Films of Semiconducting Polymer

# 大面積配向半導体ポリマーフローティングフィルムの

# 作製と評価

**HERIYANTO SYAFUTRA**

**Graduate School of Science and Technology**

**Nara Institute of Science and Technology**

**2021**

*Dedicated*

*To*

*My Parents and Wife*

# Acknowledgments

The results of the work reported in this thesis have been carried out at the Organic Electronics Laboratory, Division of Materials Science, Nara Institute of Science and Technology, Japan, under the supervision of Prof. Masakazu Nakamura and Prof. Manish Pandey. I want to express my sincere gratitude to Prof. Masakazu NAKAMURA, allowing me to join this laboratory. I acknowledge that the achievements of this research work cannot be separated from the joint discussion activities carried out with Prof. Manish Pandey and Prof. Masakazu Nakamura to explore, plan, and/or solve my research problem. I have gained valuable research experience during my Ph.D., and I will apply it at the university in Indonesia where I work. I sincerely acknowledge in-depth discussions with Prof. Manish Pandey and Prof. Masakazu Nakamura to explore, plan, and/or solve my research problem. Their in-depth knowledge in the fabrication and characterization of organic electronic devices enabled me to do my best.

I am also very grateful to Prof. Yukiharu Uraoka and Prof. Ken Hattori for discussing and evaluating my research progress every year during this doctoral study. I want to express my gratitude to Prof. Shyam S. Pandey from Kyushu Institute of Technology, Japan, for providing experimental facilities for my research work. I am grateful to Prof. Hiroaki Benten, Prof. Hirotaka Kojima, Dr. Nikita Kumari, Mr. Ryo Abe for their valuable help and discussion regarding experiments.

I want to thank all the members of the Organic Electronics Laboratory and other staff members of Nara Institute of Science and Technology for their support in completing this study. I would like to thank the member of the Indonesian student community “NAISTER” for all the fun and togetherness. I am also very thankful to my colleagues of the physics department at faculty of mathematics and natural sciences, Bogor Agricultural University, for their support and motivation during the completion of this study.

I am very grateful to my mother, Zunaidah, who passed away 10 years ago, and I hope she is happy with my success and my father, Johan Syafri. They have instilled the character to keep fighting spirit and never give up. The results of their education are one of the reasons I was able to survive to face all difficulties while completing my studies. I also thank all the other family members for their support and motivation.

Finally, I would like to express my gratitude to my beloved wife and children. My wife Fifia Zulti and my three children Fadhil Fayyad Hamizan, Farhani Hakima, and Fazli Haritsah thank you for all the motivation, inspiration, and always standing together on every journey to complete doctoral studies, which are certainly not easy.

.

September 2021,

Heriyanto Syafutra

# Table of Contents

# Table of Figures

# Chapter 1. General Introduction

## 1.1 Why electronic devices based on organic materials and market opportunity

The electronics sector is one of the largest industrial sectors in the world, and in the last decade, the global electronics market has grown considerably. Companies in this sector are engaged in manufacturing, designing, assembling, and servicing electronic products. The electronics sector has led to increased productivity in research, development, innovation, trade, and investment and has contributed to economic growth in developed and developing countries. The growth of the electronics sector is largely motivated by increasing consumer demand and increasing competition, which continues to seek to reduce manufacturing costs to make electronic products affordable and available to a wider population.

In recent years, electronics industries have more intense to apply organic semiconductor-based electronic devices for different applications, such as smartphones, TV sets, sensors, IoTs, etc. The electronic devices based on organic semiconductors can be fabricated using lightweight materials, with low-temperature processes, in thin-films and offer more space in chip design for various electronic products and even customization to meet customers specification. Furthermore, organics electronic devices can be produced in bulk with a low cost. Devices can be superflexible and can go through extreme bending tests suitable for wearable electronics and compatible with biological systems. Organic materials do not require very expensive techniques, such as zone refining, for purification and also purified sample is commercially available. Secondly, there is no need for a clean room of any class while processing these materials. A laboratory atmosphere or glove box environment is sufficient for the handling of organic semiconductors.

Today, the most developed semiconductor-based devices are Organic Light-Emitting Diodes (OLEDs). They are prospective for creating emissive displays as new display screen

technology used on smartphones, tablets, laptops, and TVs. Organic semiconductors can also be used as active layers of photovoltaic cells (PV), and field-effect transistors (OFETs). Solar cells and sensors with integrated organic semiconductors are very popular today due to high scalability, processability, bendability, and more. The demand and sales of OLED display panels are increasing because they are thinner than LCD panels. The Organic FETs (OFETs) market tends to develop towards a demand for flexible OLED displays. One of the main reasons is the increased investment from original equipment manufacturers such as Apple and Samsung in flexible display technology.

IDTechEx Research is one of the independent market research company that continuously monitors companies engaged in the marketing and development of organic electronic devices reported that the total market for printed, flexible and organic electronics will grow from $41.2 Billion in 2020 to $74 billion in 2030. The majority of that is OLEDs; printed biosensors; and printed conductive ink for photovoltaics. On the other hand, logic and memory, flexible batteries and capacitive sensors, and stretchable electronics are much smaller segments but with strong growth potential.[1]

Some of market players in organic electronics devices are AU Optronics Corporation (Taiwan), BASF SE (Germany), Bayer Material Science AG (Germany), DuPont or E. I. du Pont de Nemours and Company (U.S.), LG Display (South Korea), Merck KGaA (Germany), Novaled GmbH(Germany), Koninklijke Philips N.V. (Philips) (The Netherlands), Samsung Display (South Korea), Sony Corporation (Japan), Sumitomo Corporation (Japan), Universal Display Corporation (U.S).[2]

### 1.2 Organic Semiconductor

Organic semiconductors can exist in a crystalline or amorphous phase. In general, organic semiconductors are electrical insulators; however, when charges are injected into them

from the electrode, or after doping, or by photoexcitation, they become semiconducting. Organic semiconductors are attracting a lot of interest from both academia and industry. Over the last few decades, huge scientific progress has been made ranging from basic studies to their applicability in different devices. Interest in organic semiconductors is their ease of processing compared to inorganic semiconductors and their potential for application photoelectronic devices and printable on flexible substrates. In OSC, the charge transport is controlled by intramolecular charge transport along the conjugated backbone and intermolecular charge transport hopping. [3–7] Various efforts are being made to design versatile OSC. By molecular engineering, small molecules or conjugated polymers can result in high-performance, printable OSCs, making them suitable for large-scale industrial production.

Organic semiconductors (OSCs) can be small molecules or polymers with alternating single and double carbon atom bonds. Carbon atoms have six electrons and, in their ground states, show the electronic configuration $1s^2 2s^2 2p^2$, wherein the 2*p* atomic orbitals contain two unpaired electrons. The low energetic difference between the 2*s* and 2*p* states leads one of two electrons in 2*s* orbitals to move to vacant 2*p* orbital, which results in an excited electronic state with the configuration $1s^2 2s^1 2p^3$. The alternating single and double carbon bonds in OSCs cause the overlapping of $2p_z$ orbitals between adjacent carbon atoms to form bonding ($\pi$) and antibonding ($\pi^*$) orbitals.

An increase in the number of conjugates causes the energy levels of the $\pi$ and $\pi^*$ orbitals split and start to form the $\pi$ and $\pi^*$ bands. All the $\pi$ orbital in the $\pi$ band will be occupied with electrons, and the highest energy orbital that contains electrons call the highest-occupied molecular orbital (HOMO). At the same time, the lowest-unoccupied molecular orbital (LUMO) in the $\pi^*$ band is the lowest energy orbital that doesn't contain electrons. The gap between HOMO and LUMO is the bandgap energy ($E_g$). The typical $E_g$ of OSC is between 1.5 to 3.5 *e*V that offer capability to exited electrons from HOMO to LUMO only by the thermal

energy. [8] The $E_g$ could be tuned by changing the conjugation or molecule. Improving molecules conjugation will increase the number of delocalization in π-electron that leads decrease in the $E_g$.

The central element of OSCs is carbon and hydrogen atoms in combination with other elements such as sulfur, phosphorous, nitrogen, etc. The chemical structure of OSCs is largely determined by kinds of atom, and the number of constituent atoms, which in the end determines the optical and electrical properties of the OSCs. The charge transport properties in OSC are determined by the molecular structure and its assembly in a solid state.

In thin films OSCs, uniaxial alignment of the backbone chains during film formation usually provides higher mobilities along the chain alignment direction and anisotropic charge transport. Bao group reported that highly aligned small-molecular organic semiconductors of 2,7-oxtyl[1]benzo-thieno[3,2-b][1]benzothiophene (C8-BTBT) blended with polystyrene resulting in mobility up to 43 cm2V-1 s-1. [9] S. G. Bucella et al. also reported an increase in field-effect mobility in the aligned thin film of poly{[N,N0-bis(2-octyldodecyl)-naphthalene-1,4,5,8-bis(dicarboximide)-2,6-diyl]-alt-5,50-(2,20-bithiophene)} P(NDI2OD-T2), with a maximum value of 5 cm2 V-1 s-1.[10] This increase is quite significant when compared to the mobility of thin films formed using conventional spin coating in the range of 0.1 - 0.6 $cm^2$ $V^{-1}$ $s^{-1}$.[11]

### 1.3 Orientation of Semiconducting polymer

In the last two decades, various solution-based methods have been reported to control the molecular arrangement and macroscopic orientation of semiconducting polymer in their thin films and their correlation with device performance and anisotropic charge transport in OFETs. A detailed discussion of the mobility achievements of OFET devices and their anisotropic properties of each solution-based method used to fabricate oriented thin films can

be seen in the report published by Pandey *et al.* [12] In addition; they also presented a discussion regarding the advantages and disadvantages of each and the opportunity to be applied to make electronic devices.

Due to the quasi-1-dimensional nature of the semiconducting polymers, their charge transport properties can be easily improved by orienting the main-backbone along the one direction that is along the charge transport direction. The polymer backbone can exist in three different conformations on a substrate: edge-on, face-on, and end-on, as shown in **Figure 1.1**. In edge-on orientation, the conjugated backbone axis and the π-stacking axis lie in parallel to the substrate plane, and alkyl lamellar stacking lies normal to the substrate plane. Whereas in the face-on orientation, the direction of the π-π stacking axis is perpendicular to the substrate plane, while the direction of the conjugated backbone axis and the alkyl stacking axis is parallel to the substrate plane. In the end-on orientation, π-π stacking and alkyl lamellar stacking lie in parallel to the substrate plane, while the direction of the conjugated backbone axis is perpendicular to the substrate plane.

It is known that the maximum charge transport occurs through the conjugated backbone direction, followed by the π–π stacking direction, and in general they differ by an order of magnitude. However, in the alkyl stacking direction, the carrier mobility is extremely low because the alkyl side chains act as an insulating barrier.[13] Based on this fact, the edge-on orientation is preferred for planar devices such as OFETs where charge transport takes place in plane of the substrate in few nanometers thickness of semiconductor layer near the gate-dielectric interface. Meanwhile, the face-on and end-on orientations are particularly suitable for vertical devices such as PV and OLEDs where they require high carrier transport in the out-of-plane direction.[14–16]

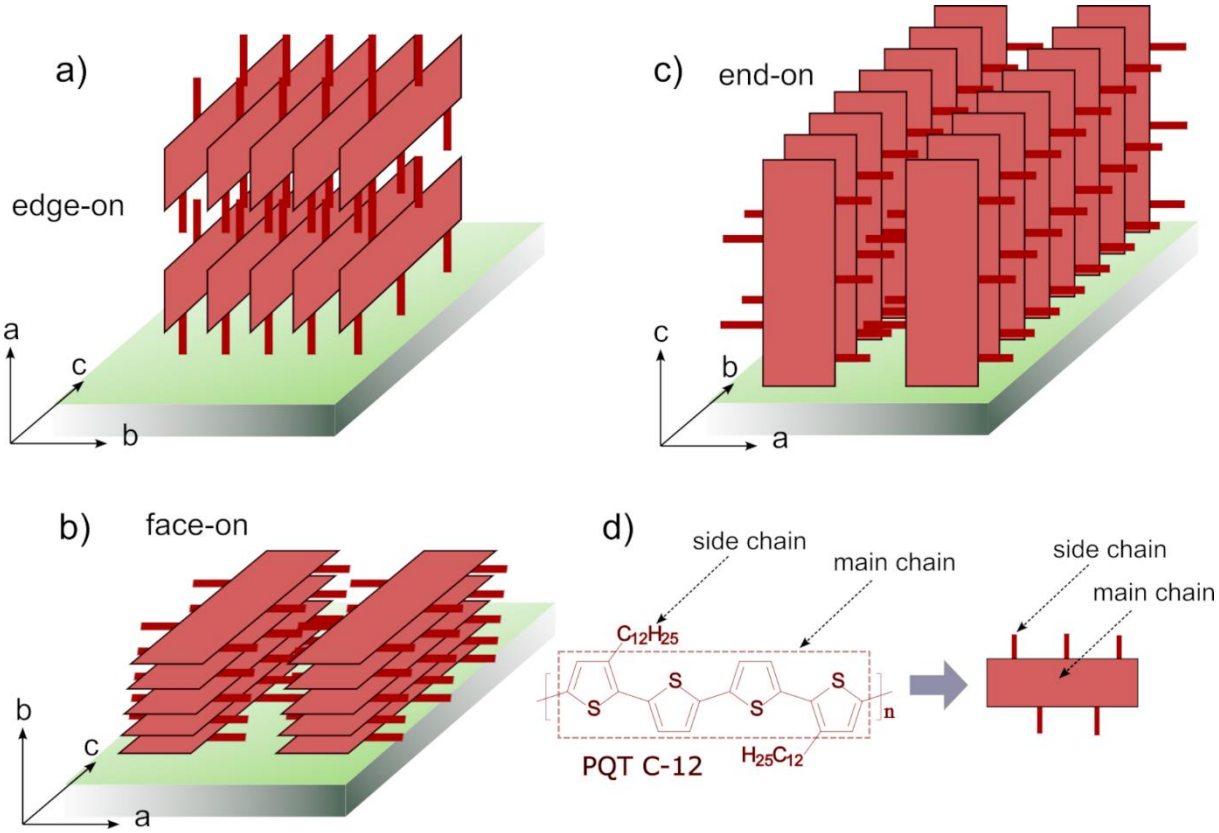


**Figure 1.1. Schematic illustration of three different kind of polymer orientation on the substrate. (a) edge-on, (b) face-on, (c) end-on. Chemical structure of PQT C-12 representing in two dimensions polymer model is shown (d) to understand the visvual representation.**

When the conjugated polymers macroscopically oriented, their orientation can be identified using the naked eye under the polarizer sheet. When the oriented polymer is illuminated by light, the electric field component of the light interacts with the electron cloud in the π-orbitals along the direction of the conjugated polymer chain. The maximum interaction occurs when the electric field component is parallel with the polymer chain orientation, which causes electrons to oscillate in this direction, or a lot of light energy will be absorbed. On the other hand, the minimum interaction occurs when the electric field components are perpendicular to the orientation of the polymer chains. Thus, when the polarizer is parallel to the orientation of the polymer, less light will reach the eye so that the color of the film will

appear dark. On the other hand, much of the light reaches the eye when the polarizer is perpendicular to the orientation of the polymer.

To characterize the polymer orientation quantitatively, polarized ultraviolet-visible (UV-vis) electronic absorption spectroscopy and polarized photoluminescence spectroscopy are sufficient methods to reveal such characteristics. Others techniques such as polarized Raman spectroscopy, polarized Fourier transform infrared spectroscopy can also be used. These measurements provide an adequate approach to calculate the degree of molecular orientation or optical dichroic ratio (DR).[12,17–19] However, to study in detail the microstructure of thin films such as crystallinity, molecular packing, orientation, and defects, the X-Ray diffraction (XRD) technique is a proper technique to obtain such information.[20–22] However, the limitations of the XRD technique are its low spatial resolution and do not provide sufficient information regarding the amorphous regions in the thin film. Another technique that can be used to obtain qualitative information from oriented thin films is the near-edge X-ray absorption fine structure spectroscopy (NEXAFS) method. This method can provide precise information regarding the semiconductor polymer backbone orientation to the substrate and/or perform surface investigations covering only the top few layers.[23]

Conjugated polymers are quasi-one-dimensional in nature, and charge transport in polymers are maximum along the pi-conjugation direction that is polymer backbone. Therefore, orienting them in one direction gives efficient charge transport (field-effect mobility) along orientation direction. On the other hand, we get in low field-effect mobility perpendicular to orientation direction as charge transport is suppressed due to high resistance arising from the presence of only $\pi$- $\pi$ stacking and few tie chains or amorphous lying polymers. Moreover, using multiple oriented floating films layer-by-layer for vertical integration of the device can be good provided the directional charge transport is required. It is worth noticing that such

layer-by-layer geometry is challenging to fabricate using any solution-processable method due to the lack of orthogonal solvents for the majority of the semiconducting polymers.

### 1.4 Organic Field Effect Transistor

The concept of the thin-film transistor (TFT) was first introduced by Weimer in 1962.[24] Later, in 1986, A. Tsumura *et al*. from Materials and Electronic Devices Laboratory, Mitsubishi Electric Corporation, Japan first introduced a field-effect transistor using polythiophene as an organic semiconductor with mobility was ~$10^{-5}$ $cm^2/Vs$.[25] The performance of organic field-effect transistors (OFETs) continues to improve, and, in 2016, Heeger's group reported the OFET mobility of the organic semiconductor material poly[4-(4,4-dihexadecyl-4H-cyclopenta[1,2-b:5,4-b]dithiophen-2-yl)-alt-[1,2,5]thiadia-zolo-[3,4-c]pyridine] (PCDTPT) was 56.1 $cm^2/Vs$ which was obtained after iodine vapor doping treatments.[26] Detailed information on the progress made in OFET mobility over the period 1985 to 2018 can be found in the report published by Paterson *et al*.[27] From **Figure 1.2**; it can be seen that the mobility achievement of *p*-channel OFETs is higher than that of n-channel. Interestingly, the mobilities achievement of solution-processed OFETs is comparable with that of single-crystal and vacuum-processed OFETs.

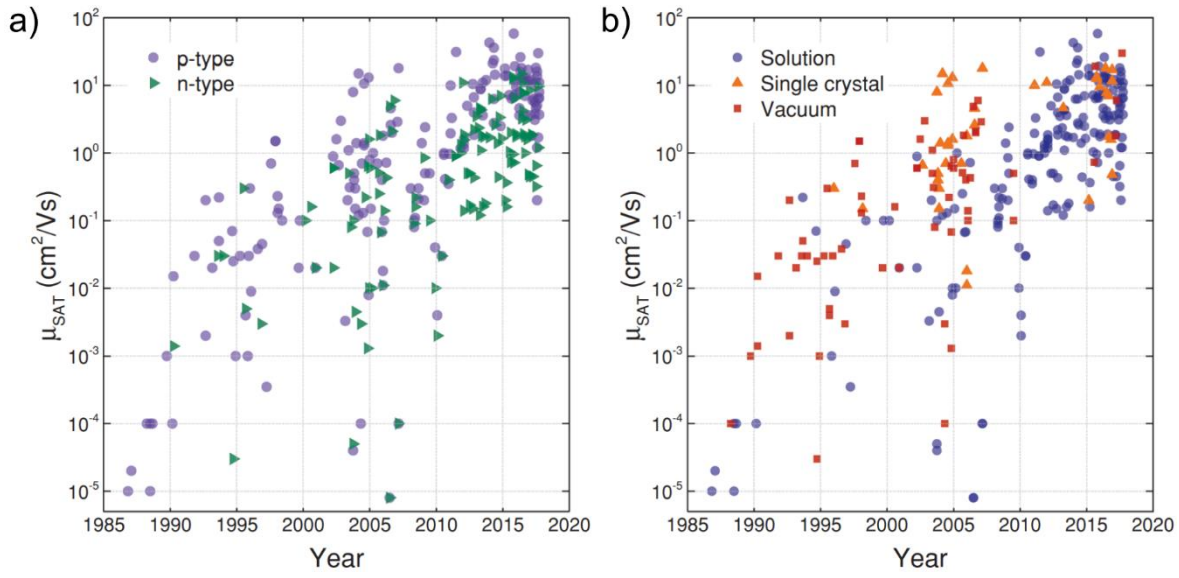

**Figure 1.2. Plots of field-effect carrier mobility values over time. The data has been separated into the following categories: a) Charge carrier type: p-channel and n-channel. b) Processing technique: solution processed, single crystal, and vacuum. Reproduced with permission.[27] Copyright 2018 Wiley-VCH Verlag GmbH**

OFETs are a main device of flexible and/or plastic electronics. Many of these devices are early-stage prototypes, which is certainly a challenge that scientists and engineers must overcome before prototypes can become real-world products. However, some of them have become commercial products and are part of today's modern electronic devices. One of the advantages of using OFETs is that they can be used as basic circuit elements to build integrated circuits with specific functions. For example, the OFET can be used as a "driver" transistor which can act as a signal amplifier or on/off switch of a device. To this day, most OLED-based displays are driven by a back-plane of OFETs.

The configuration of OFETs varies according to fabrication method. In general, there are four possible configurations of OFETs available, as shown in the **Figure 1.3**. Among them, the bottomgated configuration is the most reported. This configuration usually utilizes a doped silicon wafers substrate having $SiO_2$ on its top layer. The top-gated structure configuration provides another advantage: an encapsulation of the semiconductor layer by a dielectric layer. As a result, the semiconductor layer is protected from air and humidity in the environment.

The dielectric layer plays an important role in OFETs because this layer serves to accumulate charge carriers on the semiconductor/dielectric interfaces. Its permittivity and thickness determine the capacitance of the dielectric layer. The value of the capacitance, together with the operating voltage of the device, determines the number of charge carriers generated in the semiconductor. Several new organic dielectric layers to meet the requirements of low voltage operation, are solution-processable, transparent, and can be used on flexible substrates, have been reported by several researchers.[28–30]

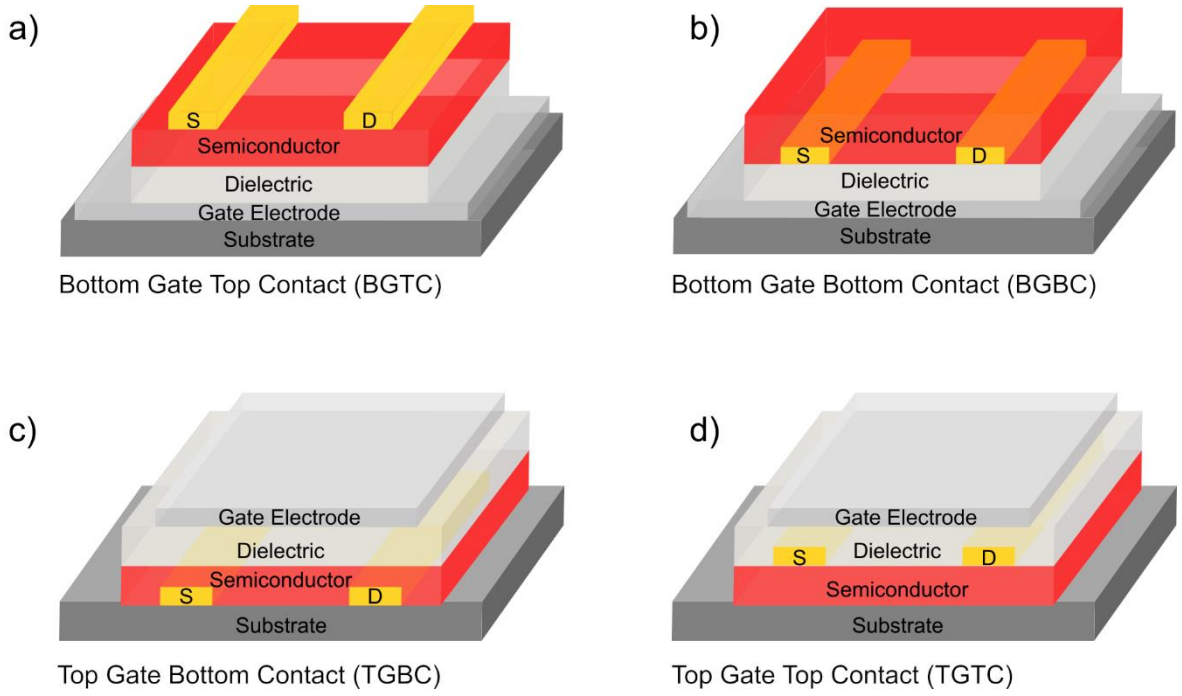


**Figure 1.3. Schematic illustration of OFETs device configuration for (a) bottom gate top contact, (b) bottom gate bottom contact, (c) top gate bottom contact, (d) top gate top contact.**

The operating principle of OFETs can be explained as follows: When a negative (positive) voltage difference ($V_{GS}$) between the gate and source terminals is applied, holes (electrons) in the OSC accumulate at the OSC/dielectric interface, and then Fermi energy shifts towards HOMO (LUMO) in the case of p-type (n-type) OSC. This accumulation of charge carriers forms a conduction path between the source and drain electrodes. This conduction path has a low resistivity that allows charge carriers to be transported. Therefore, by applying the voltage difference negative (positive) between the drain terminal to the source terminal, holes (electrons) can be transported through the conduction path; this condition causes the transistor in the ON state.

Several parameters determine the OFET operation, i.e., the width of the source-drain area or channel width ($W$), the distance between the source- and channel-terminals or the length of the channel ($L$), the capacitance per unit dielectric gate area ($C_i$), the voltage applied to the

gate terminal ($V_{GS}$), the voltage difference between the source and drain terminals ($V_{DS}$), and the minimum $V_{GS}$ required to create a conduction path between the source and drain terminals, this voltage is known as the threshold voltage ($V_{TH}$). The current-voltage (*I*-*V*) characteristic of the OFET can be studied by applying a constant $V_{GS}$, along with applying a continuously increasing voltage $V_D$. Initially, $I_D$ will increase linearly with $V_{DS}$, but at certain $V_{DS}$ conditions, $I_D$ will saturate. The variation of $I_D$ with the voltage in the channel at some position *x* can be written as:

$$I_D = WC_i\mu[V_{GS} - V_{TH} - V(x)\,]\frac{\partial V}{\partial x} \qquad \textbf{(1.1)}$$

where $\mu$ is the intrinsic channel mobility of charge carrier. **Equation. (** 2.1**)** can also written as **Equation. (1.2)**

$$I_D\partial x = WC_i\mu[V_{GS} - V_{TH} - V(x)]\partial V \qquad \textbf{(1.2)}$$

Since $I_D$ is constant, by integrating $x = 0$ to $x = L$,

$$I_D\int_0^L \partial x = WC_i\mu\int_{V(0)}^{V(L)}[V_{GS} - V_{TH} - V(x)]\,\partial V \qquad \textbf{(1.3)}$$

Since $V\,(0) = 0$ and $V\,(L) = V_{DS}$, on solving the **Equation. (1.3)**, we get **Equation. (1.4)**.

$$I_D = \frac{W}{L}C_i\mu\left[(V_{GS} - V_{TH})V_{DS} - \frac{V_{DS}^2}{2}\right] \qquad \textbf{(1.4)}$$

And,

This **Equation. (1.4)** is valid under two assumptions. First, the electric field perpendicular to the channel plane induced by $V_{GS}$ is much larger than the electric field along the channel due to $V_{DS}$. This is also called the Shockley's gradual channel approximation of the junction field-effect transistor. This approach remains valid if the dielectric thickness is much smaller than the channel length so that edge effects due to the gate can be ignored. Therefore,

the assumption that gate field is independent of position in the channel will remains valid. The second assumption is that mobility is constant across the channel.

In linear regime $V_{DS} \ll (V_{GS} - V_{TH})$ and $\frac{V_{DS}^2}{2}$ in **Equation. (1.4)** will be very small, and will make negligible contribution in $I_{DS}$. Therefore, $I_{DS}$ in the linear region $I_{DS}^{lin}$ can be simplified as **Equation. (1.5)**

$$I_{DS}^{lin} = \frac{W}{L} C_i \mu (V_{GS} - V_{TH}) V_{DS} \quad \textbf{(1.5)}$$

Similarly, in saturation where $V_{DS} \gg (V_{GS} - V_{TH})$, and $I_{DS}$ in the saturation region $I_{DS}^{sat}$ can be described by **Equation. (1.6).**

$$I_{DS}^{sat} = \frac{W}{2L} C_i \mu (V_{GS} - V_{TH})^2 \quad \textbf{(1.6)}$$

### 1.5 Research Motivations

Semiconducting polymers have attracted much interest in developing electronic devices based on organic field-effect transistors (OFETs). Polymers-based OFET devices offer exclusive advantages such as mechanical flexibility and tunable optoelectronic properties compared with traditional silicon electronics. In terms of fabrication, most of the semiconducting polymers can solution-processed in a normal laboratory atmosphere or glove box. Therefore, they are compatible for roll-to-roll processing of large-area films and devices, resulting in low manufacturing costs. High mobility in semiconductor polymer-based devices can be realized by optimizing the intra- and inter-molecular charge transport by molecular engineering of the polymers itself or by device and film fabrication techniques. At the semiconductor level, optimizing the molecular weight, coplanarity of the polymer backbone, polymer chain orientation, and intermolecular interactions between neighboring molecules. There are several well-established methods for the orientation of semiconducting polymer films.

However, each method has some demerits associated with the feasibility of overall device performance and fabricating devices by large-area hetero-structured fabrication.[12,31]

The unidirectional floating film transfer method (UFTM) is one of the effective methods that can be used to form large-area-oriented semiconducting polymer thin films. [12,32–34] Oriented thin films from many different semiconducting polymers such as P3HT, PQTC-12, PBTTT-C14, F8T2, and PTB7 can be formed using this method.[33,34] The obtained oriented thin films were then applied to electronic devices exhibiting anisotropy in OFETs and organic light-emitting diodes. In this method, the film is made by dropping one drop of polymer solution on a hydrophobic liquid substrate. The side-walls and slanted bottom of a slider assist the dropped polymer solution spread in one direction over the liquid substrate and simultaneously form a highly oriented solid thin floating film.

These resulting films are ribbon-shaped in nature. The length "longer axis" of these films is along the polymer film expansion direction. However, no reports are investigating large-area characteristics of these films to realize their applicability in large-area flexible electronics, as most of the reports stated only small-area characteristics transferred from the center region of the ribbon-shaped film. However, to reveal the suitability of a method for fabrication of a large flexible electronic device, an in-depth investigation was essential. Therefore, orientation mechanism during film formation, the opto-electrical characteristics of the formed film for a large-area, its suitability for a flexible electronic device, and charge transport anisotropic properties of the floating film interfacial (interfaces of the liquid substrate and air) was certainly required. Furthermore, it is well known that template-assisted alignment using pre-patterned substrates has been widely used to assist the orientation of various polymers. In this regard, it was also necessary to examine the versatility of UFTM in assisting the orientation of the guest semiconducting polymer in a well-oriented host polymer semiconductor

matrix. Discussion of these studies and related topics is logically presented in subsequent chapters.

### 1.6 Thesis Outline

This thesis focuses on the fabrication and characterization of large-area oriented thin films of semiconducting polymers using a recently developed solution processable technique named Unidirectional Floating Film Transfer Method (UFTM). This thesis consists of six chapters which contain a detailed description of the results obtained for this thesis.

The first chapter of this thesis contains brief information regarding the current state-of-art of development of organic electronics over conventional electronics, the theory of basic knowledge of organic semiconductors and working principles of organic field-effect transistors, background issues related to thin-film fabrication techniques for conjugated polymers, and the objectives of this thesis work.

The second chapter provides information regarding the materials were utilized in each of the experiments covered in this thesis. Where the material is obtained, and their chemical structure is given. The types of substrates and the treatment performed on them are also presented. This chapter also briefly describes the thin film deposition technique and thin film characterization carried out in the research reported in this thesis.

The third chapter presented the investigation results on the orientation mechanism, uniformity of film thickness, uniformity of polymer orientation, and carrier mobility in large-area films. In addition, the film resistance to bending has not also been investigated. Thus, in this work, we explore such things to study the versatility of this method for large-area flexible electronics.

In the fourth chapter, a detailed investigation of the growth mechanism and charge transport anisotropy in UFTM films at the liquid and air interface is presented. Anisotropy of

charge transport mobility is studied through OFET fabrication with TGBC and BGTC structures.

Chapter 5 discusses the versatility of UFTM in assisting the orientation of the guest semiconductor polymer in a well-oriented host semiconductor polymer matrix. In this experiment, two different semiconductor polymers were blended with PQT to form a thin film using UFTM.

The last chapter is the sixth chapter, where a general and summarized conclusion of all the work in this thesis is presented. In addition, future work to develop this method for the organic electronic devices is also presented.

# Chapter 2. Experimental Section

## 2.1 Materials

Conjugated polymers which used in this report were poly(3,3‴-didodecyl-quaterthiophene) (PQT-C12), poly[2,5-(2-octyldodecyl)-3,6-diketopyrrolopyrrole-alt-5,5-(2,5-di(thien-2-yl)thieno[3,2-b]thiophene)] (DPPT-TT), and poly(9,9-di-n-octylfluorenyl-2,7-diyl) (PFO). PQT conjugated polymer was purchased from Sigma Aldrich and was used without any further purification. DPPT-TT was synthesized following the previous report.[35] PFO was synthesized by Suzuki-Miyaura coupling as reported.[36,37] The dielectric layer for the OFETs were fabricated with CYTOP$^{TM}$ CTL-809M (CT-Solv. 180 as the solvent), which was supplied by Asahi Glass, Japan. Chemical structure of each conjugated polymers and CYTOP$^{TM}$ shown in **Figure 2.1**.

For different type of self-assembled monolayer (SAM) treatment, the chemicals were purchased from different sources, and they were trichloro(octadecyl)silane (OTS) with purity ≥ 90% (from Sigma Aldrich), trichloro(octadecyl)silane (>99.0%) (from TCI), 1-octadecene technical grade 90% (from Sigma Aldrich). The solvents used in the SAM treatment were super dehydrated toluene (supplied by FUJIFILM Wako), super dehydrated chloroform (supplied by FUJIFILM Wako), and super dehydrated cyclohexane (supplied by FUJIFILM Wako). The chemical structure of all these chemicals are attached in **Figure 2.2**.

Different solvents, such as anhydrous chloroform, anhydrous 1,2-dichlorobenzene, were used to dissolve polymers depending on the case/experimental requirements, and they were purchased from Sigma Aldrich and were used without any further purification. The chemical structure of these solvents shown in **Figure 2.3**.

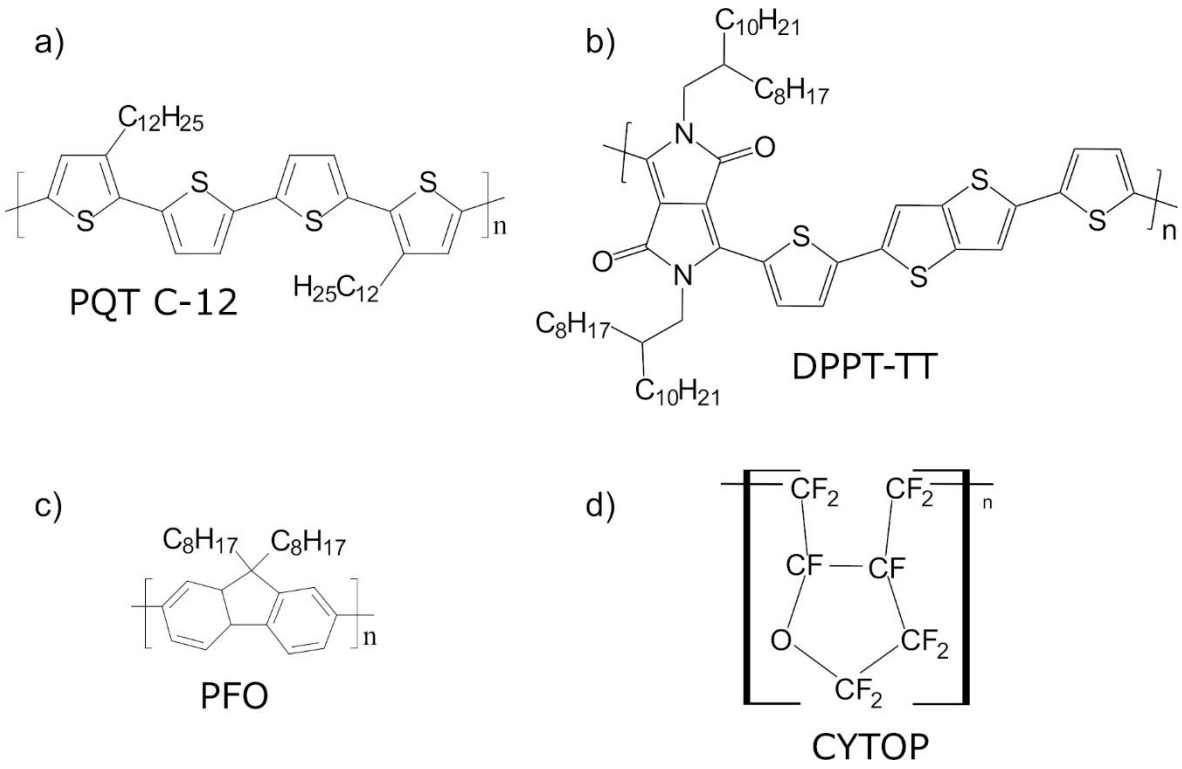


**Figure 2.1. Chemical structure of conjugated semiconducting polymers of PQT-C12 (a), DPPT-TT (b), PFO (c), and CYTOPTM (d).**

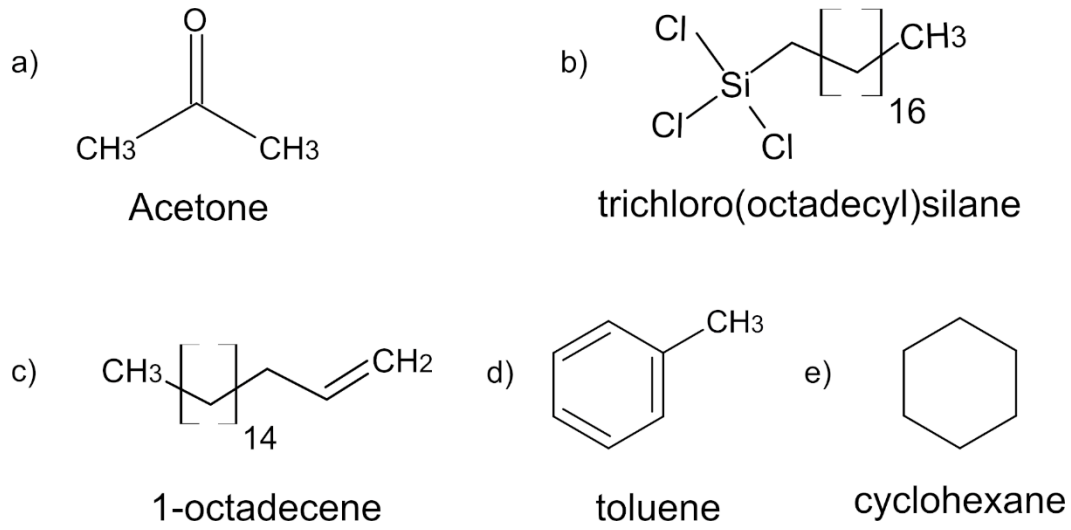


**Figure 2.2. Chemical structure of acetone (a), trichloro(octadecyl)silane (b), 1-octadecene (c), toluene (d), and cyclohexane (e).**

The liquid substrate, for fabrication of the polymer films via Floating film transfer method (FTM), the mixture of glycerol and ethylene glycol was used. After fabricating the FTM film on liquid substrate, they were transferred on the other substrates and adhered liquid substrate was washed off with methanol. The chemicals for liquid substrate and for washing the films, were purchased from Sigma Aldrich. Their chemical structure of them presented in **Figure 2.4.**

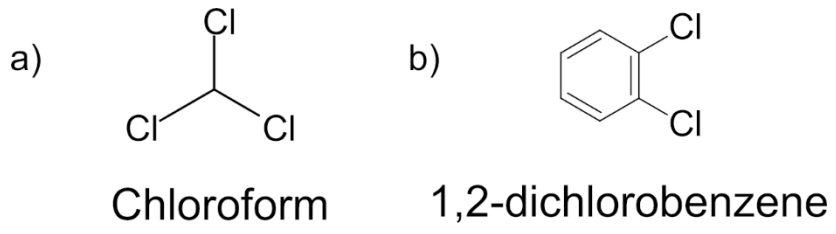


**Figure 2.3. Chemical structure of chloroform (a) and 1,2-dichlorobenzene (b).**

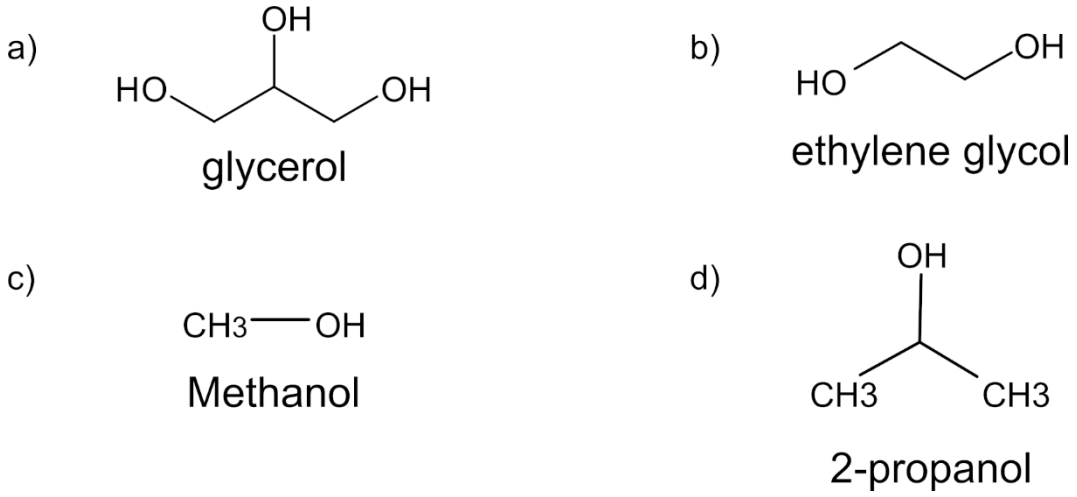


**Figure 2.4. chemical structure of glycerol (a) ethylene glycol (b) 2-propanol (c), and methanol (d).**

## 2.2 Substrate preparation

Substrate type and surface treatment of substrate in this thesis work varied depending on the experimental requirements. The typical substrates were normal glass, device-grade glass, and $SiO_2/Si(n^{++})$. The substrates were cut in desired size through a diamond cutter. They were thoroughly cleaned in an ultra-sonic bath of acetone for 10 minutes and then rinsed with hot acetone followed by irradiation under $UV/O_3$ for 15 minutes to ensure the surface was clean from any invisible particle and organics contamination. Further the SAM layer or a thin layer of CYTOP$^{TM}$ deposited to increase surface hydrophobicity. For the purpose of evaluating the optical anisotropy in thin films, the normal glass slides after SAM layer deposition were used. To fabricate OFETs, the device-grade glass or $SiO_2/Si(n^{++})$ were preferred.

For SAM layer deposition, the clean substrates were immersed in a container filled with the solution of 160 $\mu$l OTS into 40 ml of octadecene under a nitrogen atmosphere for 3 hours, followed by washing twice in an ultrasonic bath of a mixture of super-dehydrated chloroform and cyclohexene in 1:1 ratio, and then once ultrasonic bath of super-dehydrated chloroform for 10 minutes each. Then the substrates were dried at 150 ℃ for 15 minutes before using them further. For the preparation of thin layer of CYTOP$^{TM}$ on the substrates, solution of the CYTOP CTL-809M in the CT-Solv. 180 solvent with ratio (1:30) was poured on the substrate then spun at 1000 rpm for 45 seconds followed by immediately annealing at 100 ℃ for 1 hour under normal laboratory conditions.

## 2.3 Deposition methods

Thin film deposition technique significantly influences the modern era of technology because it is the backbone of advanced technology in various fields such as optical devices,

environment-related applications, telecommunications devices, and energy storage devices. At the application stage, the main issue is related to the morphology and stability of a thin film, strongly dependent on the deposition technique. Generally, there are two well-known techniques to fabricate a thin film with top quality: chemical and physical deposition techniques. This dissertation will present two chemical and one physical deposition technique to create thin films. Unidirectional floating film transfer method (UFTM) and spin coating are the two chemical deposition techniques to obtain polymer thin films, and thermal evaporation is the one physical deposition technique to deposit metal electrodes for fabricating the organic devices.

### 2.3.1 Film fabrication via unidirectional floating film transfer method (UFTM)

FTM was initially reported in 2009, and thereafter extensively worked upon by Takashima and co-workers. [12,38] This method offers convenience in fabricating a thin film as well as aligning a backbone chains of $\pi$-conjugated polymers.[12,38,39] Later, A. Tripathi *et al.* modified the FTM, which in addition to offering the advantages of the previous method, also provides the ability to create large areas of thin films.[32] In the modified FTM, film expansion direction is restricted by placing a custom-made slider, which leads to unidirectional expansion of the oriented film, therefore, it was termed as unidirectional FTM (UFTM).

To fabricate a thin film via UFTM, around 10 ~ 20 $\mu$l of polymer solution in a low boiling point solvent such as chloroform is dropped on the hydrophilic liquid substrate. The solution spreads on the liquid substrate to form the floating film. During expansion, an effective shear force from the liquid substrate acts on the conjugated polymers at the liquid-substrate/solution interface, which led to an alignment of the polymer backbones perpendicular to the expansion direction. The film formation on the liquid substrate provides free movement of polymer molecules to self-alignment, covering the entire film thickness. A discussion of the regulatory characteristics of polymers on liquid substrates and air surfaces is given in **Chapter**

**4**. Moreover, the volatile solvent evaporates simultaneously, and the polymer backbones also undergo self-assembly. Several parameters such as polymer solution concentration, liquid substrate temperature, and viscosity of the liquid substrate determine the film-growth speed and optoelectronic properties of the floating film formed.

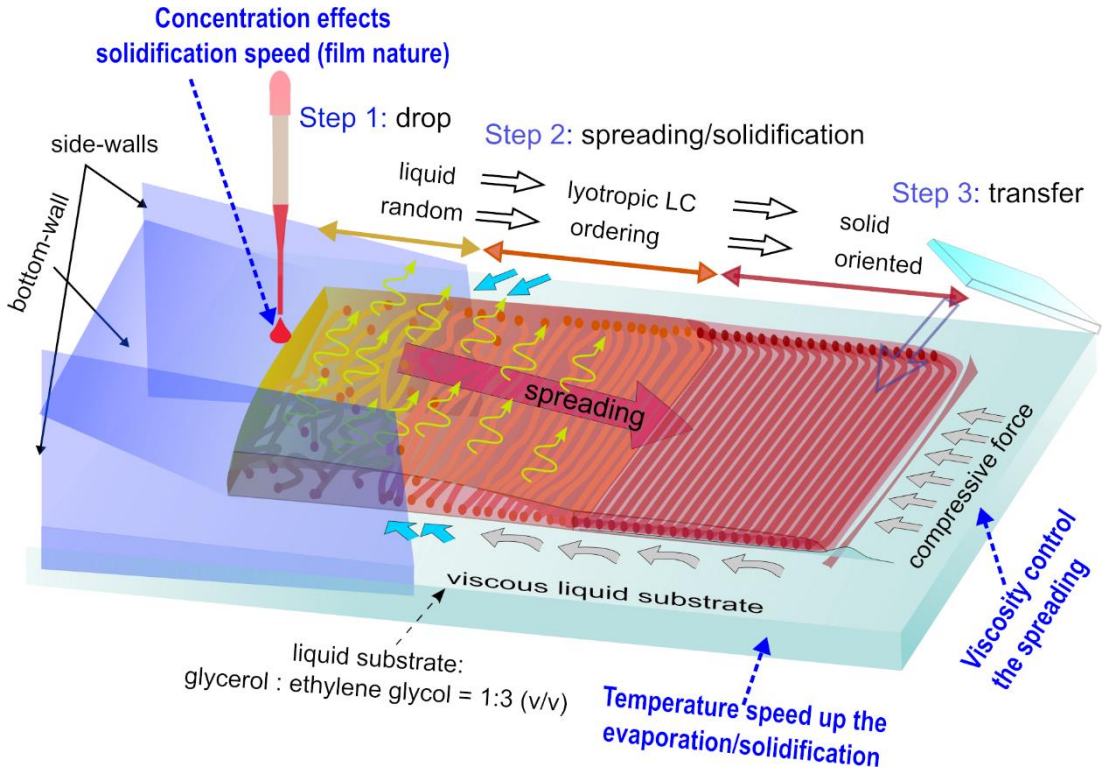


**Figure 2.5. Schematic illustration of floating film transfer method and related mechanism.**

The floating film is easily stamped on the desired substrate. Moreover, due to hydrophobic nature of the polymer films, the film casting becomes more convenient on relatively hydrophobic surface, i.e., CYTOP$^{TM}$ coated or SAM treated substrates. An in-depth discussion accompanied by supporting data related to the mechanism and characteristics of the thin films produced by the UFTM method will be given in **Chapter 3**

Reasonably priced and unsophisticated equipment is required to make thin films using the UFTM method. A Plastic tray in size ~30 × 10 × 2.5 cm$^3$ filled with the liquid substrate,

i.e., mixture of glycerol and ethylene glycol in ratio 1:3 was taken. The slider was made of PTFE sheet (thickness ~ 1 mm) and it was kept near one side of the tray, while keeping the slant surface directed towards the opposite side of the tray. The amount of the liquid substrate is taken such that it reaches up to almost half of the slant surface of the slider.

To fabricate the film, a drop of the polymer solution is placed at the contact line of the liquid substrate and the slant surface of the slider. Temperature controlling of the liquid substrate was done by placing the tray on the hot plate which was equipped with temperature control. Orientation of polymer backbone chain was easily observed by naked eyes with the help of polarizer sheet while light of the lamp was shinned on the floating film. Photograph of experiment set-up and schematic illustration of the UFTM method can be shown in **Figure 2.5** and **Figure 2.6**, respectively.

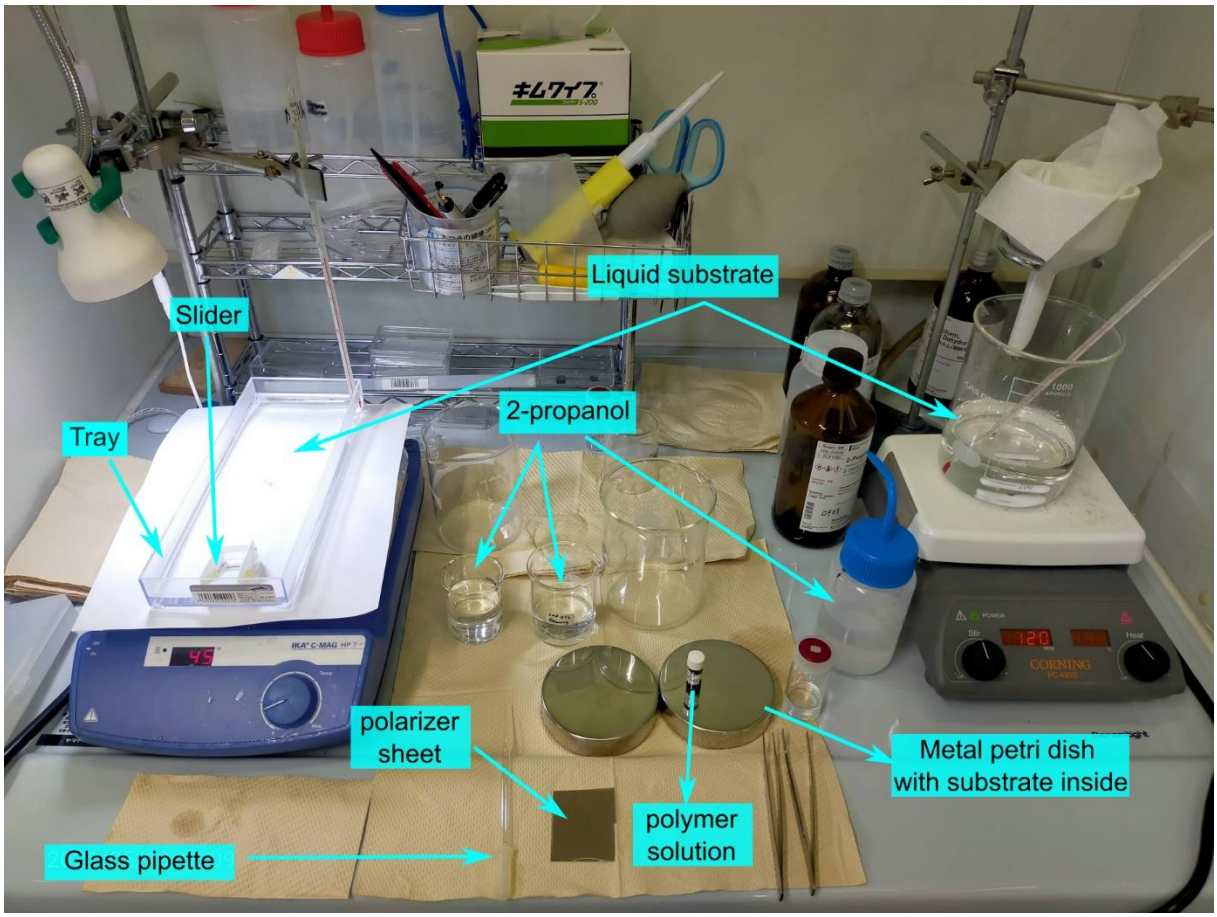


**Figure 2.6. Photograph of experiment set-up in UFTM method inside a fume hood.**

2.3.2 Film fabrication via Spin coating

One of the simple and widely used techniques in organic electronics and nanotechnology to produce a thin film of organic materials in academic institutions and industries through a solution-based process is spin coating.[9,40–45]. This technique offers uniform film thickness with thickness variations of less than 1% due to its self-leveling nature. In general, the thickness of a produced thin film is determined by the inverse of the spin speed square, following the **Equation ( 2.1 ).**

$$h_f \propto \frac{1}{\sqrt{\omega}} \qquad \textbf{( 2.1 )}$$

Where $h_f$ and $\omega$ are the final film thickness and angular velocity/spin speed, respectively, however, the true film thickness also depends on solution concentration and solvent evaporation rate.

In general, spin coating is conducted in three steps; solution dropping, spin up, spin-off and drying. In the first step, a solution is dropped on the substrate to cover the entire substrate's surface completely and then spin-up and spin-off in order. A centrifugal force is applied to the solution during the spin-up while evaporating the solvent for obtaining a thin layer. The highly volatile parts of the solution are easily removed; however, the lowly volatile part remains on the surface, which requires further drying. A spin coater which was used to fabricate a thin film in this dissertation is shown in **Figure 2.7**, while the schematic to describe a spin coating process is shown is **Figure 2.8**.

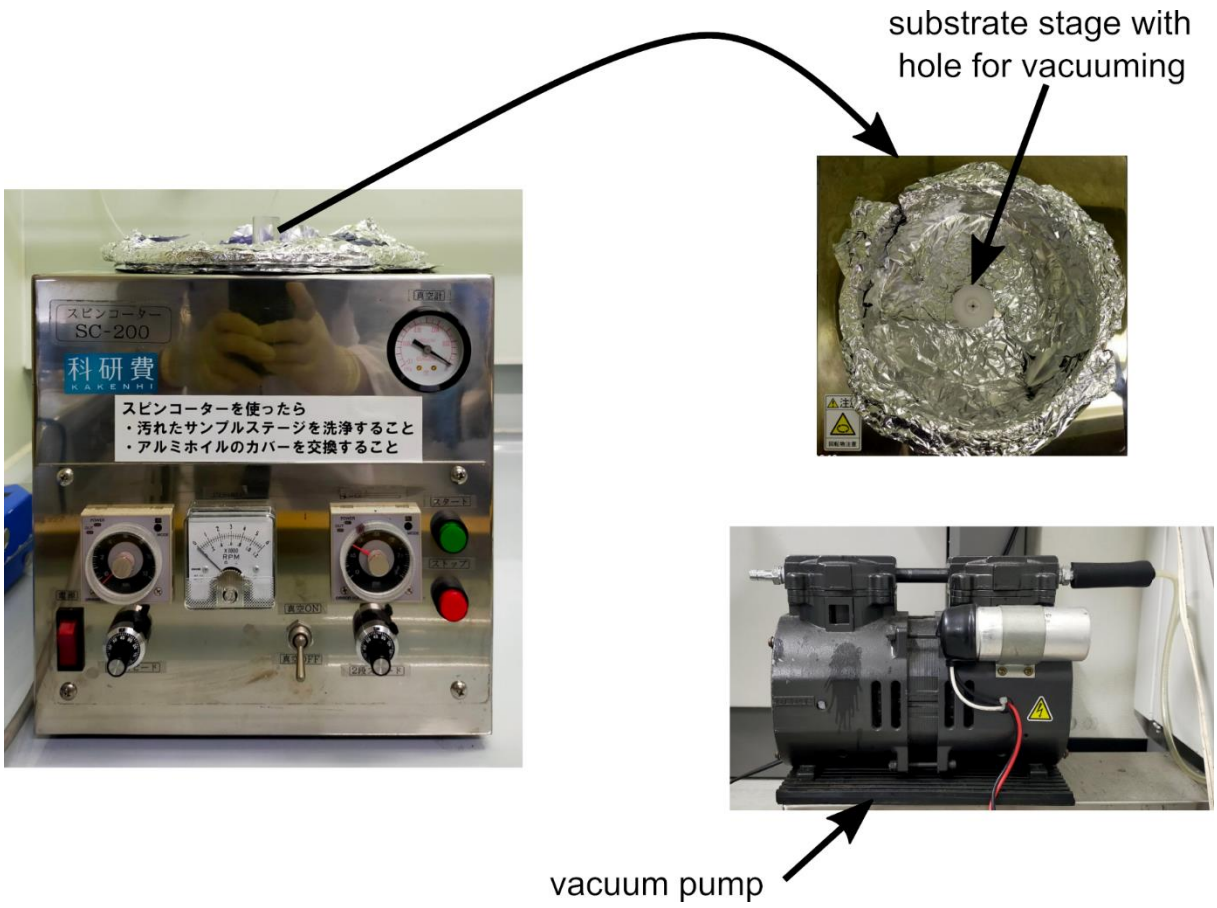


**Figure 2.7. Photograph of the spin coater instrument which used in this dissertation.**

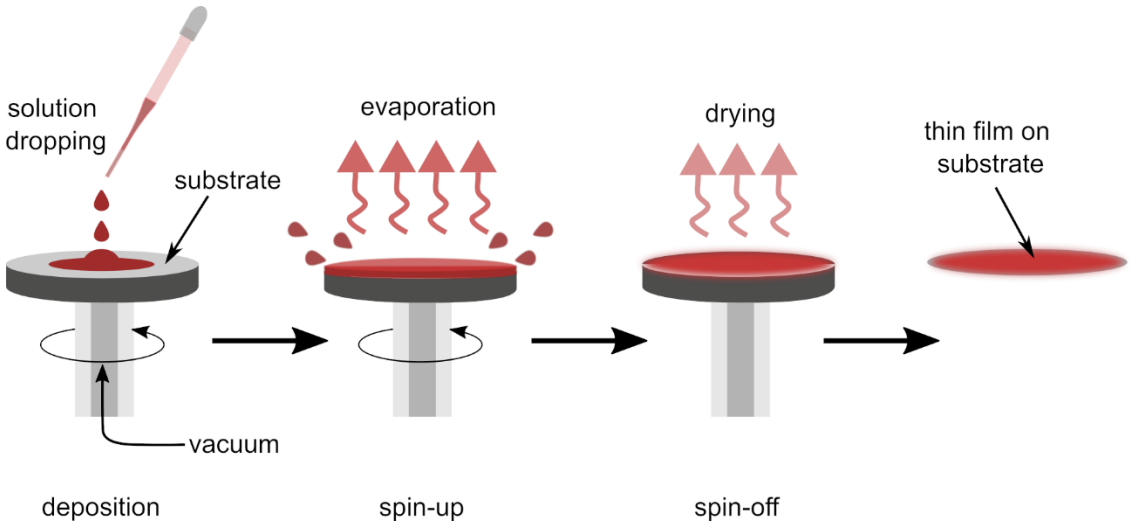


**Figure 2.8. Schematic illustration of stages to create a thin film in the spin coating method.**

Although spin coating is a simple technique and results in a uniform film thickness, this technique faces a limitation such as a substrate size, very low material efficiency, and difficulty creating a multilayer thin-film structure. Increasing substrate size causes difficulty in film thinning due to difficulty in high-speed spinning. Generally, in terms of efficiency, 95% - 98% of a solution dropped on the substrate is wasted, then only 2% - 5% portion of solution adheres to the substrate [46].

### 2.3.3 Thermal evaporation

Thermal evaporation is a technique to form a thin layer on a particular substrate by evaporating source materials. The high-temperature heating of the metals, inside a chamber to facilitate the vapor particles to move directly and reach to the substrate and condenses to form a thin film, very low air pressures is preferred, in order to avoid the undesired oxidation of the electrodes. Evaporating a source material requires resistive heating, which exists in different shapes such as boats, baskets, filaments, and coated roads, fabricated from tungsten, tantalum, or molybdenum that having a high melting point.

Preventing film oxidation and reducing a contamination density during the evaporation process can be achieved in the low pressure of the evaporation chamber, around ~10-4 Pascal. At this pressure, the mean free path of gas in the chamber is approximately 8 meters, so these vapor particles travel in straight lines from the resistive heating point to the target substrate due to less scattering. The mean free path $\lambda_m$ of gas was determined by various physical parameters as described in the **Equation ( 2.2 )**.

$$\lambda_m = \frac{RT}{\sqrt{2}\pi d^2 N_A P} \qquad \textbf{( 2.2 )}$$

2.3Where *P* is the pressure of chamber, R is the gas constant, T is the temperature of chamber, NA is the Avogadro's number, and d is diameter of the gas particles in meters. From this equation, increasing temperature or decreasing the pressure of the vacuum chamber leads to an increase in the mean free path.

In this work, the thermal evaporation technique was mainly used to vaporize Au or Cr and Au to prepare a source- and drain-electrode or vaporize Al to create a gate electrode, a photograph of the thermal evaporation system shown in **Figure 2.9**. Evaporation of Au was always carried out when the chamber pressure was below ~5 × 10-4 Pascal, while for Al evaporation it was always ensured that the chamber pressure was below ~5 × 10-5 Pascal. Chamber pressure for evaporating Al was one order less than Au to ensure no oxidation process occurs during the evaporation; because Al vapors have a very high oxygen affinity to form the aluminum oxide.

Tungsten in a boat-like shape was used for a resistive heating element of source materials because this metal has a melting point of 3,400 ℃ that applicable for high-temperature in the range of 1,600 ℃ to 2,000 ℃ considering the melting point of Cr, Au, and Al is 1888 ℃, 1065 ℃, and 660 ℃, respectively. Using the crystal detector, the deposition rate and thickness were monitored and displayed on the small screen display. In addition, in order to control the deposition rate and thickness, the thermal evaporation system is equipped with current control for adjusting the current flow in the tungsten boat and shutter for hindering the source material vapor from reaching the target substrate when the required thickness achieved.

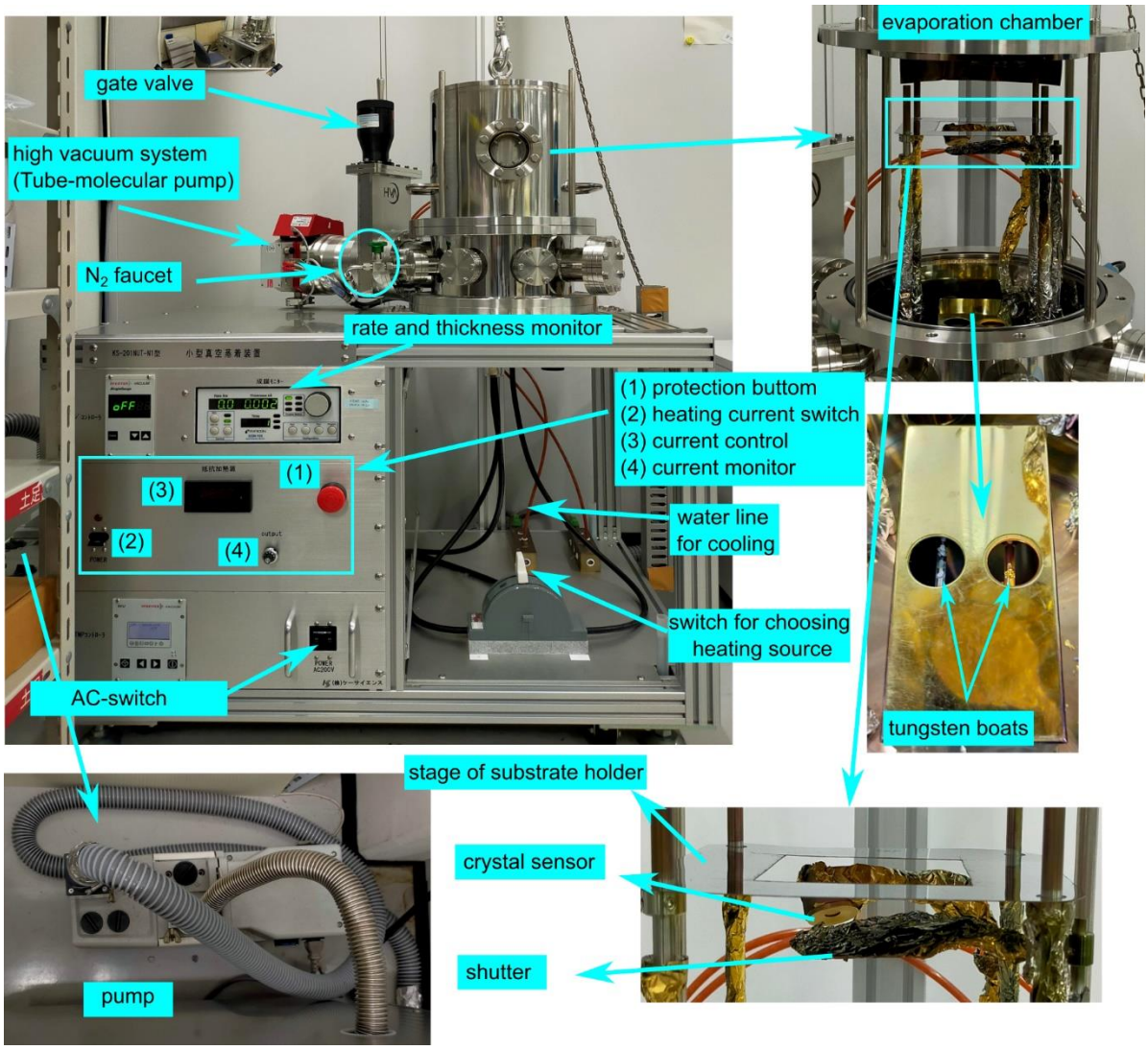


**Figure 2.9. Photograph of thermal evaporation system for metals electrode deposition.**

## 2.4 OFETs Fabrication and Characterization

### 2.4.1 Preparation of OFET substrates

In order to fabricate OFETs, device-grade glass or $SiO_2/Si(n^{++})$ with ~200 nm thermally grown $SiO_2$ layer which have the capacitance ($C_i$) value of 17.9 nF/cm$^2$, was utilized. The device-grade substrate was chosen for top gated bottom contact (TGBC) device structure. However, for fabricating bottom gated top contact (BGTC) OFETs, $SiO_2/Si(n^{++})$ were preferred.

In both the cases, before semiconductor deposition, on the surface of the substrate, either SAM layer or CYTOP$^{TM}$ layer was deposited, as discussed above.

### 2.4.2 Polymer-based dielectric and semiconductor deposition

For fabrication of TGBC OFETs, pure CYTOP CTL-809M was deposited on the OTS treated device-grade glass substrate with pre-patterned source- and drain-electrodes Au (~18 nm)/Cr (~2 nm) to form gated dielectric layer. The coating conditions of CYTOPTM layer, i.e., spinning at 4000 rpm for 45 seconds followed by instantly annealed at 100 $^{\circ}$C for 1 hour in the air atmosphere, the thickness of the CYTOP layer was ~ 650 nm with Ci of 2.77 nF/cm$^2$.

Spin coating and UFTM techniques were used for depositing semiconducting polymer layers depending on the experiment requirements. UFTM method was utilized when purposes of an experiment to examine the anisotropic properties of an oriented thin-film polymer. However, films were spin coated to form a non-oriented film with isotropic properties. Moreover, the thin spin coated films were also utilized as the supporting layer (to avoid cracking near the edge of electrodes) in TGBC OFET fabricated with UFTM coated films.

Considering hydrophobicity on the substrate surface, film fabrication via spin coating of polymer solution was difficult due to less wettability of polymer solution on the substrate. Therefore, at the edges of the substrate fine boundary was created using polyimide tape, which helped to hold the solution on the substrate during spin-up of substrates. In addition, spin-coating was conducted in two steps, at first at 500 rpm for 5 seconds followed by 2500 rpm for 75 seconds, in order to deposited the polymer layer properly. For removing any remaining solution on the substrate, a final step conducted spin-up at high speed (~6000 rpm) for 60s. Set-up for UFTM experiment is shown in **Figure 2.6**, while the digital image of the instrument used for of spin coating is shown in **Figure 2.7**.

### 2.4.3 Electrode deposition

The electrodes were deposited by patterning the thermally evaporated metal. For patterning the source and drain electrodes, a nickel shadow mask was placed on the substrate/polymer thin film before evaporating vaporizing the gold inside the vacuum chamber shown in the **Figure 2.9**. In some OFETs, the gate electrode was also fabricated by patenting the evaporated gold or aluminum. The digital image and schematic for masking, and electrode deposition are shown in **Figure 2.10**.

The mask was designed in such a way that, the channel length and width of the OFET was 20 μm and 2 mm, respectively. Moreover, since the substrate size was larger than the size of the mask, gold layer was also got deposited on the edges of the substrate, which was not desirable for preventing the current leakage in the OFETs. Therefore, it was removed the using a fine wooden tip and/or cotton bud. To deposit the aluminum for the gated-electrode, pieces of nickel sheet were utilized to cover substrate/films and leaving a small portion of the area near the source and drain electrodes exposed.

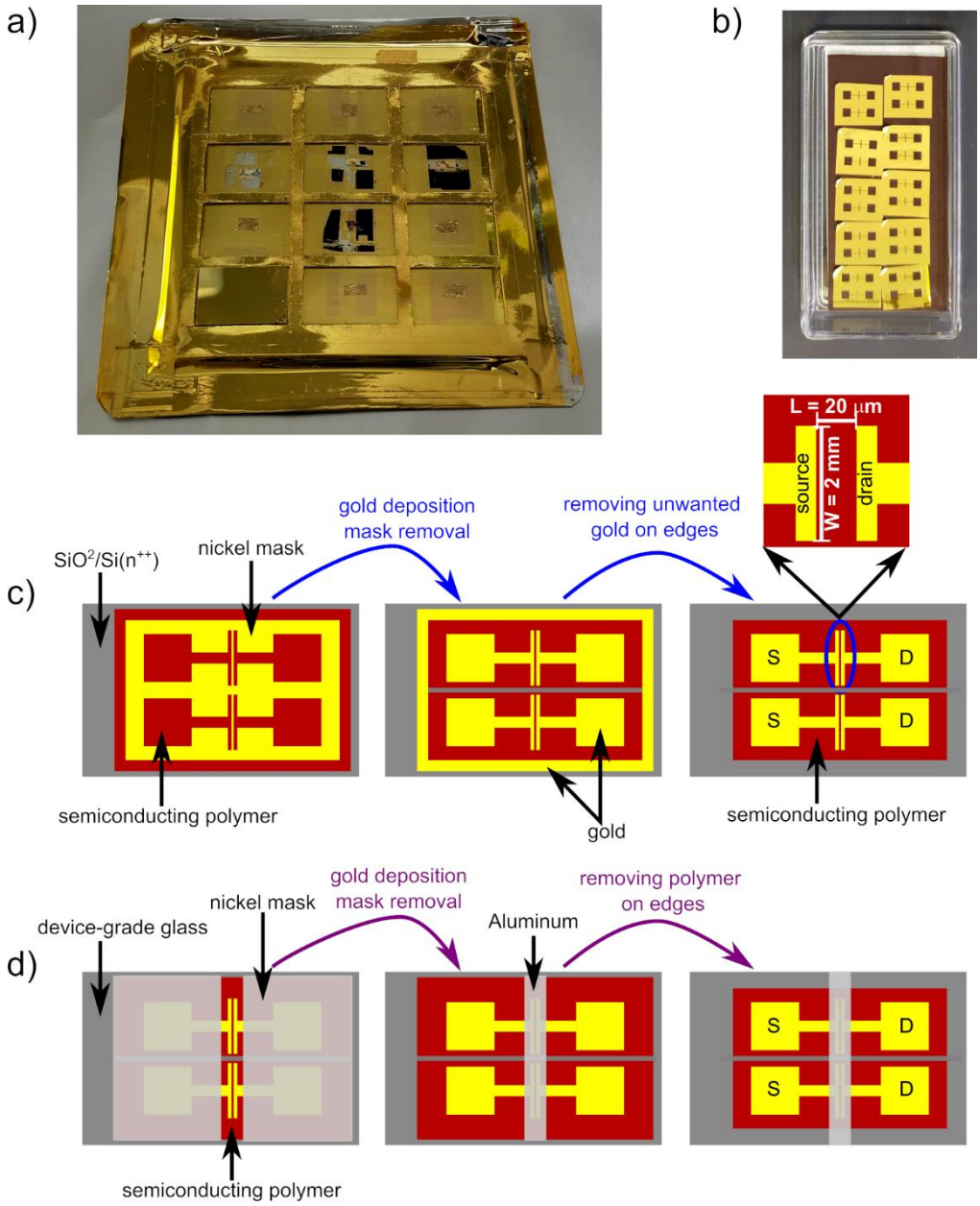


**Figure 2.10. Photograph of nickel shadow mask (a), substrate holder (b), and schematic flow diagram of the steps for creating metals contact of OFETs devices; for source-drain electrode (c), and for gate electrode (d).**

### 2.4.4 Device characterization

The performance of OFETs is probed by measuring their transfer and output characteristics. Here, these measurements were conducted using a semiconductor parameter analyzer (Agilent E5272A) interfaced with a computer, the image of the set-up is shown in

**Figure 2.11.** Before measurement, the source-, drain-, and the gate-electrodes of the OFETs were connected with copper wires (diameter of 0.1 mm and length of ~3 cm) using indium and fixed on a solid base for the ease of handling. After fixing the OFET it was transferred to a vacuum chamber and after evacuating for ~ 2 minutes (using rotary pump) the OFET measurements were performed.

The transfer characteristics of the OFET was obtained by applying the constant drain-source voltage, while the gate voltage was varied from the minimum voltage to the maximum voltage (maximum gate voltage is not greater than the drain-source voltage); i.e., measuring $I_D$-$V_{GS}$ at fixed $V_{DD}$. For output characteristic, the OFETs were supplied with source-drain voltage that varies from low to high voltage, while the gate voltage was kept at different values; i.e., measuring $I_D$-$V_{DD}$ at different $V_{GS}$. Both of these measurements were carried out cyclically.

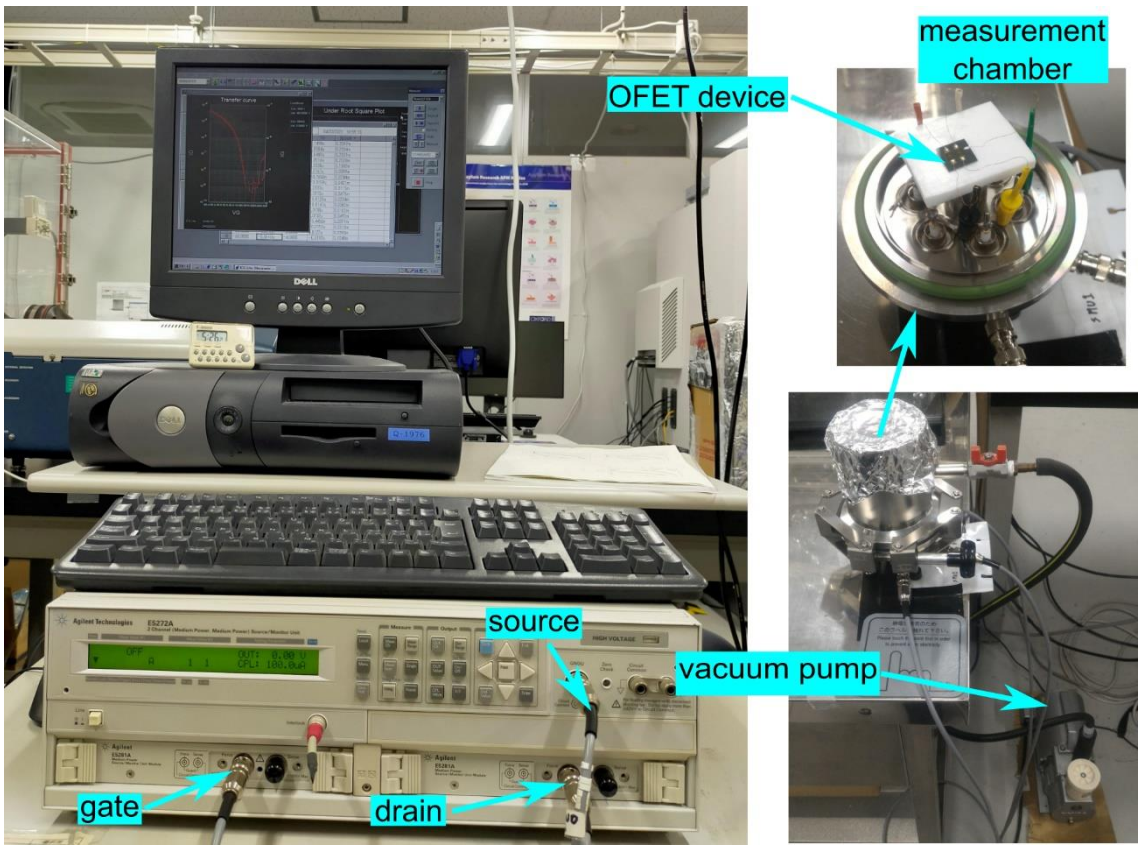


**Figure 2.11. Photograph of semiconductor parameter analyzer Agilent E5272A for measuring I-V characteristics of fabricated OFETs.**

From the transfer characteristics of OFETs in saturation regime, i.e., from the plot of $\sqrt{I_D}$ vs $V_{GS}$. The value of carrier mobility and threshold voltage were estimated by following **Equation ( 2.3** ), and further simplification, i.e., **Equations ( 2.4 ) – ( 2.6 ).**

$$I_{DS}^{sat} = \frac{C_i \mu W}{2L} (V_{GS} - V_{TH})^2 \quad \textbf{( 2.3 )}$$

$$\sqrt{I_{DS}^{sat}} = \sqrt{\frac{C_i \mu W}{2L}} (V_{GS} - V_{TH}) \quad \textbf{( 2.4 )}$$

$$k = \sqrt{\frac{C_i \mu W}{2L}} \quad \textbf{( 2.5 )}$$

$$\mu = \frac{2k^2}{C_i \frac{W}{L}} \quad \textbf{( 2.6 )}$$

## 2.5 Characterization of the Thin Films

### 2.5.1 Ultraviolet – Visible Spectroscopy

The principle of UV-Visible Spectroscopy is based on the absorption of ultraviolet light or visible light by molecules containing bonding and non-bonding electrons (ground state) to excite these electrons to anti-bonding molecular orbitals that having higher energy (excited state). The different energies between the ground state and the excited state of the electron are equivalent to the total absorption of ultraviolet radiation or visible radiation. The wavelength of the UV-Visible region covers around 800 – 200 nm, which is equivalent to the energy range 1.5 – 6.2 eV.

UV-Visible spectroscopic data provide quantitative and qualitative information of characterized molecules or compounds. In this work, UV-Vis-NIR spectrophotometer (JASCO V-770DS) equipped with a polarizer (Model GPH-506) was utilized to characterize the

fabricated polymer thin films. By analyzing the obtained spectra, the optical properties of the films, such as increasing/decreasing effective conjugation length, increasing/decreasing inter-molecular interactions, and optical anisotropic properties, were unveiled.

In order to characterize the optical anisotropic properties related to the degree of orientation of the polymer chains, a polarizer lens (which resulted in linear polarization of the light) was placed between the sample and the light source because the transition dipole moment of the optically induced π–π* transition is aligned along conjugation direction of the semiconducting polymers [47]. Thus, the absorbance was higher when the light polarization direction was aligned parallel (||) to the polymer chain orientation direction, it further decreased by moving the polarization direction away from the polymer chain orientation direction. Subsequently the minimum value of absorbance was obtained when they were orthogonal (⊥) to each other. The optical anisotropy was estimated in terms of the dichroic ratio (DR), following **Equation ( 2.7 )**. Schematic representative of the UV-Visible spectroscopy and digital image of the UV-Vis spectrophotometer used in this work are shown in **Figure 2.12.**

$$DR = \frac{Maximum\ Absorbption_{\parallel}\ at\ (\lambda_{\max\parallel})}{Absorbption_{\perp}\ at\ (\lambda_{\max\parallel})} \qquad \textbf{( 2.7 )}$$

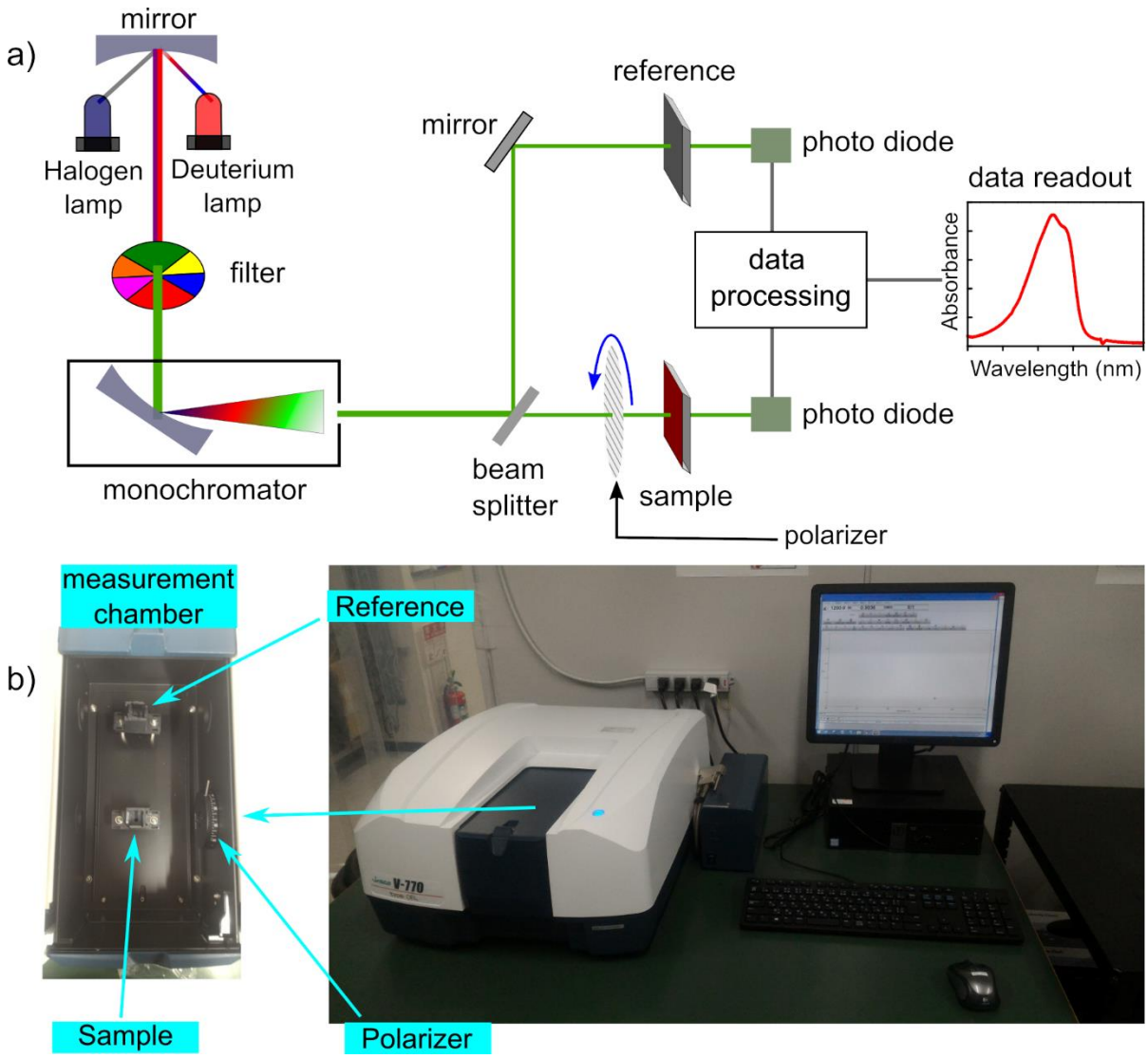


**Figure 2.12. Schematic representation of the processes involved in absorption spectroscopy and (b) Photograph of the UV-Vis spectrophotometer (JASCO V-770DS).**

2.5.2 2D position mapping

Basic principles in 2D position mapping are similar to UV-Visible spectroscopy; however, mapping systems was equipped with a moving stage providing it the capability of probing the distribution in thickness and molecular orientation in thin films. For conducting the measurements, the instrumental setup established at Kyushu Institute of Technology, Japan was accessed.

The schematic representation of the 2D position mapping system is shown in **Figure 2.13**. For thin film characterization, the film coted on a transparent glass was mounted on a 2D moving stage. Then the sample was irradiated with a white light source and the transmitted light was received through the optical fiber cable connected to the photonic multichannel analyzer (PMA, 7473-36, Hamamatsu Photonics). The PMA consists of a Czerny–Turner type spectrograph where the light beam is collimated and dispersed in constituent wavelengths followed by receiving of all the dispersed beams at different channels simultaneously. Since all dispersed rays of all the wave lengths are received simultaneously, whole absorption spectra for the irradiated area are obtained in a single instant.

For the measurement of polarized spectra, a polarizer film is placed between the incident light and the sample. Further by moving the stage the spectra at different positions of the film is measured and their integration leads to the characterization of thickness or orientation variation in the film. The parameters for controlling the resolution of the mapping measurement are mask diameter, stage speed, and the shutter operating frequency inside the PMA.[18] For optimum resolution and ease of measurement, the mask of diameter 0.5 mm, stage speed of 1 mm/s, and the shutter operating frequency of 2 Hz with 4% duty cycle were selected. The spectra for continuous array of points, with diameter of 0.5 mm, were measured along the ribbon width. At every point area, the absorption spectrum was taken with a spectral resolution of 2 nm, and to improve the S/N ratio five spectra were averaged out.

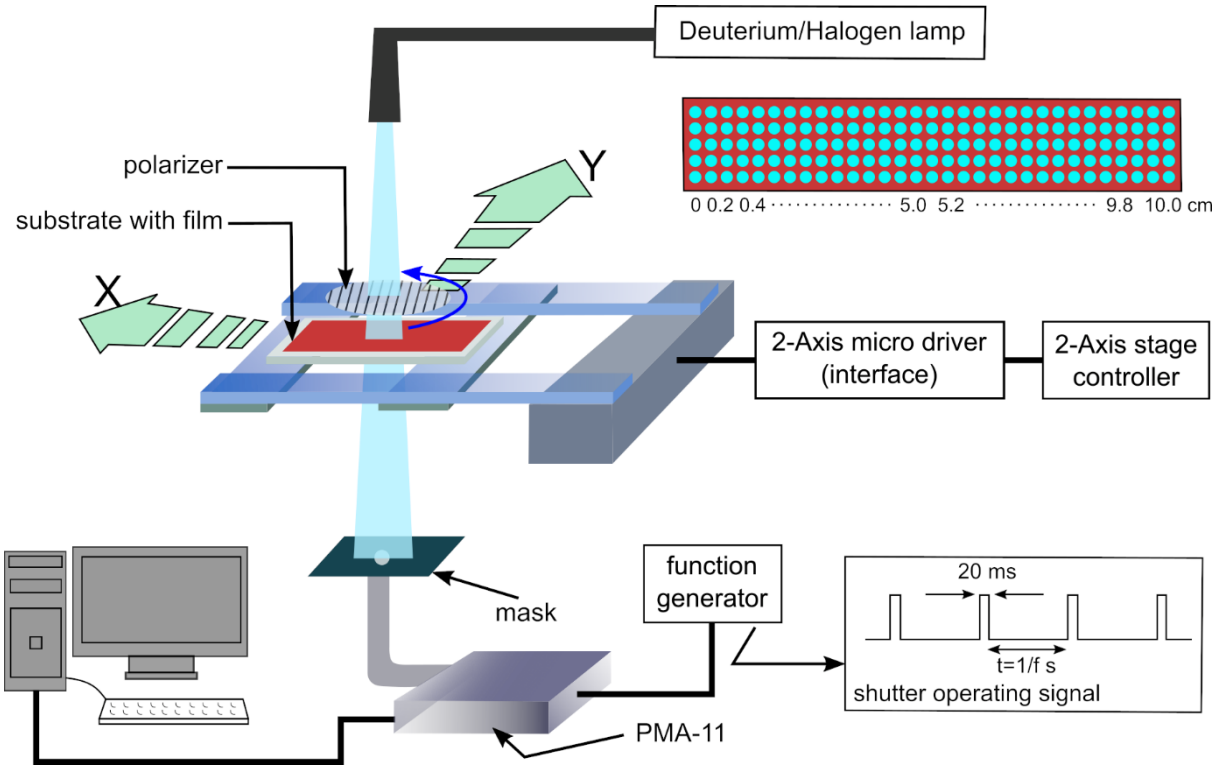


**Figure 2.13. Schematic illustration of 2D positional mapping set-up**

2.5.3 X-ray diffraction

X-ray diffraction (XRD) is a well-known technique to study solid-state structural properties. This technique has been widely utilized to analyze molecular and crystal structure, identify quantitatively various compounds related to their chemical species, determining the crystallinity degree, and measuring the particle size. X-ray diffraction patterns resulted from the reflection of X-ray light from a solid-state corresponding to the physical and chemical properties of its solid-state.

In order to characterize the organic thin films, the angle of incoming X-ray to the sample has to below the critical angle of the surface from several nm up to typically several 100 nm. Therefore, Bragg reflections are only coming from the surface structure of the sample. This technique is called Grazing Incidence X-ray Diffraction (GIXD). This technique gives the

ability to unveil the sample structures within 10 nm from the surface to provide a clear picture of the structure at the atomic and/or molecular level.

The equation to understand the X-ray diffraction is the Bragg equation, it given in the **Equation ( 2.8 )**.

$$n\lambda = 2d\ sin\theta \qquad \textbf{( 2.8 )}$$

Where $n$ is an integer, $\lambda$ is the wavelength of the X-rays, $d$ is the interplanar spacing between the atoms, and $\theta$ is the angle between the X-ray beam and surface normal. From this equation, interplanar spacing between the atoms can be calculated using respective $\theta$

In this work, out-of-plane and in-plane GIXD technique was utilized to determine the conformation of oriented thin films on substrates. In-plane measurement was conducted at the Division of Green Electronics, Graduate School of Life Science and Systems Engineering, Kyushu Institute of Technology, Japan. While out-of-plane measurement was carried out at Division Materials Science, Graduate School of Science and Technology, Nara Institute of Science and Technology. The measurements were conducted using Rigaku smart lab X-ray diffractometer with a radiation source of Cu-Kα (1.5418 Å) and operated at 45 kV (200 mA).

During the in-plane GIXD measurements, the sample and the detector were moved along an arc with angles of $\varphi$ and $2\theta\chi$, respectively. Here $\chi$ represents the angle between the scattering vector ($Q$) and polymer orientation direction.[48,49] In order to characterize the anisotropic macromolecular arrangement in the film, the measurement was taken in two conditions, i.e., when $\chi = 0°$ and when $\chi = 90°$ The incident angle ($\omega$) and the scattered angles of X-ray with respect to the sample plane was kept at 0.14 and 0.28, respectively. The schematic geometry of out-of-plane and in-plane GIXD measurement shown in **Figure 2.14.**

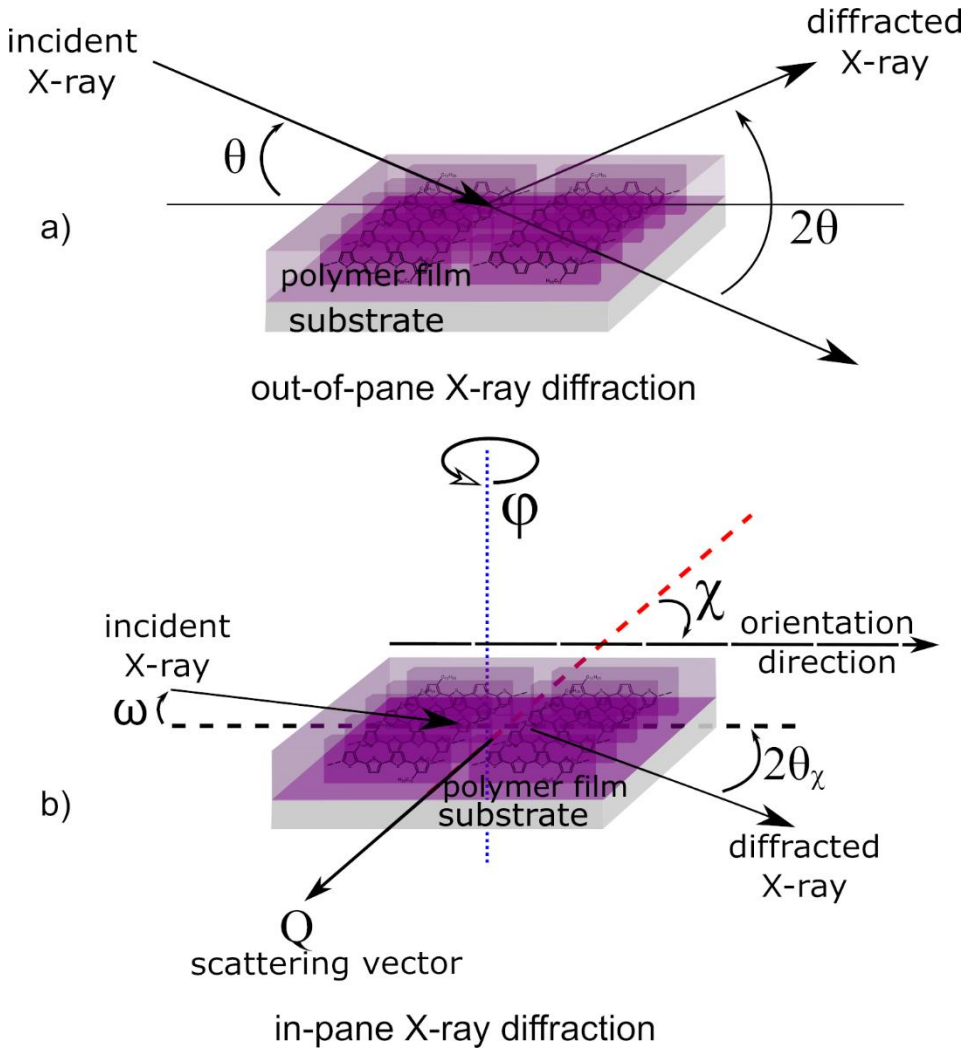


**Figure 2.14. Schematic geometry of out-of-plane and in-plane GIXD**

2.5.4 Atomic force microscopy

A powerful technique to study materials at the surface level is atomic force microscopy (AFM). This technique is able to obtain a clear surface image of many kinds of surfaces such as composites material, ceramic, polymer, and even biological samples. The basic principle of this technique is mapping interaction between a flexible cantilever and the surface of a sample during scanning. The integrated profile of interactions in the form of a deflection of the cantilever results in the characteristics of the samples. Recent progress of this technique is its

capability for investigating properties such as topography, adhesion, and other characteristics of surfaces with resolution in the range of tens of microns to even few nanometers.

In general, the AFM can be operated in contact mode or non-contact mode. In contact mode, the cantilever is kept physically in contact with the sample surface during the scanning along the surface. In this mode, the cantilever gets a vertical deflection due to sample topography. In Contrast to contact mode, in the non-contact mode, the cantilever oscillates near the sample surface with the frequency close to the resonance frequency. The distance between the cantilever and the surface is controlled by using feedback circuit to keep the amplitude and phase of the oscillation unchanged.

In this thesis work both AFM modes were utilized to study the morphology of polymer thin-films. Contact mode AFM were utilized for measuring the thickness of polymer thin films and surface morphology. While the non-contact mode AFM was needed when the phase separation in the polymer blend films were probed. In this work the AFM measurements were conducted by an atomic force microscope (SPM-9700, Shimadzu). A digital image the instrumental setup is shown in **Figure 2.15**.

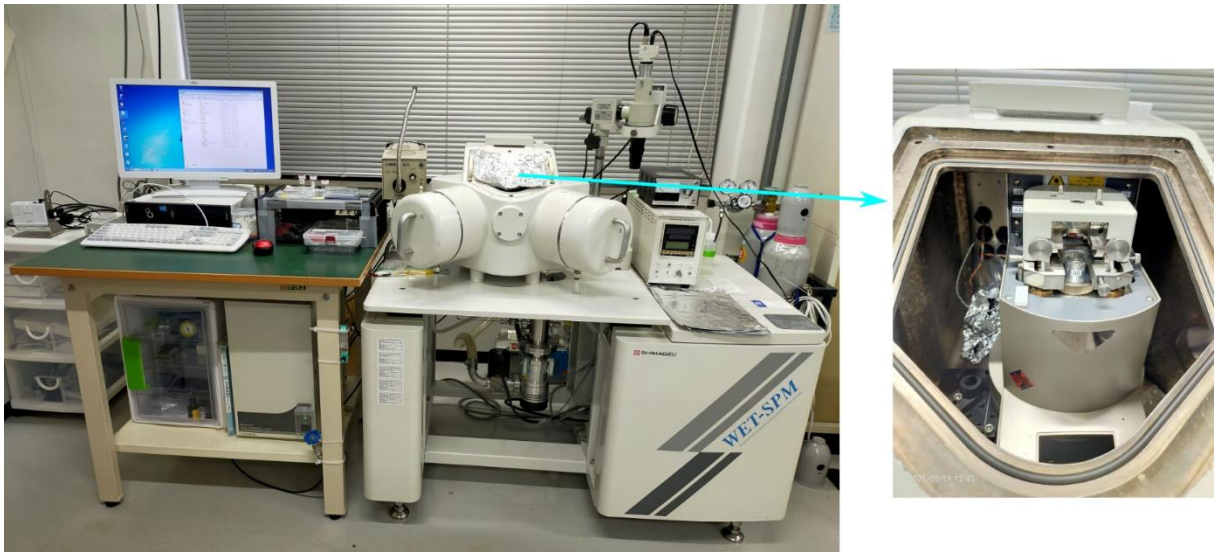


**Figure 2.15. Digital image of AFM instrument.**

# Chapter 3. Unidirectional Floating Films Transfer Method for Large-Area Floating Films

## 3.1 Introduction

Thin films of large-area semiconductor polymers that can be solution-processed with high-throughput are one of the main challenges for the realization of large-area organic electronic circuits for a wide range of practical applications from phototransistors, biological sensors to organic electronic circuits. [12,50,51] Semiconductor polymers have excellent resistance in terms of flexibility and stretch-ability, which offer them to coat on complex surfaces, which expands the range of microelectronic devices for applications in wide-area display circuits, and a wide variety of sensors and actuators.[52,53]

The increase in charge transport in semiconductor polymers can be enhanced by the uniaxial orientation of the polymer main chains along the channel direction of organic field-effect transistors (OFETs). [10,39,51,54–56] Various methods for orienting semiconductor polymers at a macroscopic scale using shear forces during/post-film fabrication have been developed and established. However, its application in wide-area flexible electronics is somewhat limited for various reasons described in detail elsewhere. [12,57]

In general, polymer orientation techniques depend on mechanical shear forces, which are sensitive to the hydrophobic nature of the surface and are not suitable for flexible substrates.[48,58,59] Therefore, the preparation of the film separately with the coating process on the substrate is important to obtain complex heterostructures through layer-by-layer transfer and provides control over the morphology of the film, which is independent of the surface morphology of the substrate.[12] The UFTM method provides this capability and is also capable of preparing large-area-oriented films from multiple polymers.[39,54,60]

In the UFTM method, the orientation of the backbone is precisely controlled in one direction. However, uniformity of film thickness, uniformity of polymer orientation, and carrier mobility in large-area films has not been reported. In addition, the film resistance to bending has not also been investigated. Thus, in this work, we explore such things to study the versatility of this method for large-area flexible electronics. The film prepared from poly(3,3'''-dialkylquaterthiophene) (PQT) formed by using UFTM method.

## 3.2 Experiment Details

### 3.2.1 Materials and films preparation

*Polymer material and solvent:* poly(3,3‴-didodecyl-quaterthiophene) (PQT-C12) and anhydrous chloroform were purchased from Sigma Aldrich without any further purification.

*Chemicals for liquid substrate in UFTM:* Ethylene glycol (EG) and glycerol (GL) were purchased from Fujifilm Wako Pure Chemical Corporation, Japan. Both chemicals were mixed with a ratio of EG and GL was 3:1. The temperature of this liquid substrate was maintained at 45 ℃ before used for film casting.

*Chemicals for SAM treatment:* Octadecyl(trichloro)silane (OTS) with purity >99%, and toluene super-dehydrated were purchased from TCI, Japan and FUJIFILM Wako, Japan. CYTOP CTL-809M and CT-Solv.180 were purchased from Asahi Glass Co., Ltd., Japan.

*Substrates*: Glass substrates for optical characterization of thin films. $SiO_2$/Si ($n^{++}$) substrates with $SiO_2$ thickness of 200 nm and flexible polyethylene naphthalate (PEN) substrates for OFETs device fabrication. PEN substrates also are used to transfer a completely large area of floating film. Glass substrates were washed in ultrasonication bath of acetone for 10 minutes, followed by rinsing in hot acetone. Improving the surface hydrophobicity was

conducted by immersing them in 10 mM OTS solution was prepared in super dehydrated toluene for 3 h in an $N_2$ atmosphere.

*Polymer solutions:* For orientation mapping using polarized absorbance and angular dependence OFETs, PQT was dissolved in anhydrous chloroform with a concentration of 2% (w/w). In order to investigate thickness-dependent performance in OFETs, PQT solution concentration was varied from 0.5 to 4% (w/w) to increase the thickness of floating films.

*Polymer films:* Approximately 10 $\mu$l of PQT solution was dropped near the edge of the center of the tilted bottom slider wall and liquid substrate interface. The droplet solution will spread unidirectional to form a large area of the thin film. The substrate was held with tweezers, then, carefully placed on the floating film to transfer it to the substrate.

### 3.2.2 Devices Fabrication

Self-assembled monolayer (SAM) on $SiO_2$/Si ($n^{++}$) substrates with $SiO_2$ thickness of 200 nm prepared by immersing substrates in 10 mM OTS solution was prepared in super dehydrated toluene for 3 h in an $N_2$ atmosphere. Then, wash them using an ultrasonic bath of a mixture of chloroform and cyclohexane (3:1) for 10 min with repetition 3 times and using fresh solvents. As a final step, substrates were left for drying at 100 °C on a hotplate for 15 min in the air atmosphere.

For preparing a thin film of CYTOP on $SiO_2$/Si (n++), substrates were washed in an ultrasonic bath of acetone for 10 min followed by dipping in hot acetone and cleaned using $N_2$ flow. Later, the solution of CYTOP CTL-809M and CT-Solv.180 (1:30) dropped on the substrate, then spun at 1000 rpm for 45 s followed by annealing at 100 °C on a hotplate for 1 h, then cooled down to room temperature. Floating films were transferred on these substrates and washed with isopropanol to remove any adhered residual liquid substrate to the semiconductor (PQT) film. For flexible devices, PEN substrates were cleaned and mounted on rigid substrates,

as reported earlier. [61] Aluminum (Al) was evaporated for gate electrodes using a shadow mask. The cleaned substrate with Al electrode on the top was treated with UV-ozone for 5 minutes before coated CYTOP CTL-809M using a spin coating (4000 rpm: 45 s) as a dielectric.

For the source and drain electrode, 50 nm of gold was thermally evaporated at a rate of ~1 Å/s at a pressure of $10^{-5}$ pa, and the electrode was patterned using a nickel shadow mask. Channel length ($L$) and channel width ($W$) was 20 μm and 2 mm, respectively. Spin coating of PQT was done with 0.2% (w/w) solution in 2 steps 500 rpm for 5 s followed by 1500 rpm for 75 s.

### 3.2.3 Characterization

To revealing the conformation of oriented thin films on substrates, out-of-plane and in-plane GIXD measurement was conducted using Rigaku smart lab X-ray diffractometer with a radiation source of Cu-Kα (1.5418 Å) and operated at 45 kV (200 mA). During the in-plane GIXD measurements, the sample and the detector were rotated with angle angles of $\varphi$ and $2\theta\chi$, respectively. The $\chi$ represents the angle between the scattering vector ($Q$) and polymer orientation direction.[48,49] In order to characterize the anisotropic macromolecular arrangement in the film, the measurement was taken in two conditions, i.e., when $\chi = 0°$ and when $\chi = 90°$.

Polarized absorption spectra measurements were conducted by using UV-vis-NIR spectrophotometer (JASCO V-770DS) be equipped with polarizer. Thickness measurement and surface topography were measured via atomic force microscope (AFM) using SPM-9600 Shimadzu, Japan. Semiconductor parameter analyzer Agilent E5272A was utilized for current-voltage ($I$-$V$) characterization of OFETs. Capacitance/Area ($C_i$) was measured using an LCR meter (ZM2375, NF Corporation) for parallel plate capacitor structure fabricated similar to transistor geometry, it was 17.9 nF/cm$^2$ and 15.38 nF/cm$^2$ for SAM coated $SiO_2$ or CYTOP

coated $SiO_2$, respectively. Field-effect mobility ($\mu$) was extracted from the transfer curves in the saturation region using equation below.

$$I_{DS} = \frac{\mu C_i W}{2L}(V_{GS} - V_{DS})^2 \quad \textbf{(3.1)}$$

Where $I_{DS}$ is the drain to source current, $V_{GS}$ is the gate to source voltage and $V_{DS}$ is the drain to source voltage.

Orientation degree/DR was calculated from the polarized UV-vis absorption spectra using **Equation ( 2.7 ) in Chapter 2**. The film with size 35 × 18 $mm^2$ prepared and characterized through a 2D positional mapping technique for evaluating the thickness and orientation variation of UFTM films, as reported.[18] For better resolution and ease of measurement, optimum parameters with a mask of diameter 0.5 mm, shutter operating frequency of 2 Hz with 4% duty cycle, and stage speed of 1 mm/s were used. A continuous array of point areas (diameter: 0.5 mm) were scanned along the ribbon width. At every point area, the absorption spectrum was taken with a spectral resolution of 2 nm, and five spectra were taken and averaged to improve the S/N ratio.

### 3.3 Results and Discussions

In the UFTM method, thin films are prepared by dripping the PQT solution at the slider interface and a specially fabricated liquid substrate, as shown in **Figure 3.1 (a)**. Due to the unique design, the slider allows the spreading of the film in unidirectional, and the film was solidified simultaneously during expansion due to the low boiling point of the solvent. It was easy to confirm the orientation direction, just placing a transparent polarizing film on top of the floating film the orientation direction could be confirmed. In most areas of the film, the orientation direction was found to be parallel to the width and perpendicular to the direction of

film expansion, as schematically illustrated in **Figure 3.1 (a)**. But the orientation pattern at the edges of the floating film was different from that in the center.

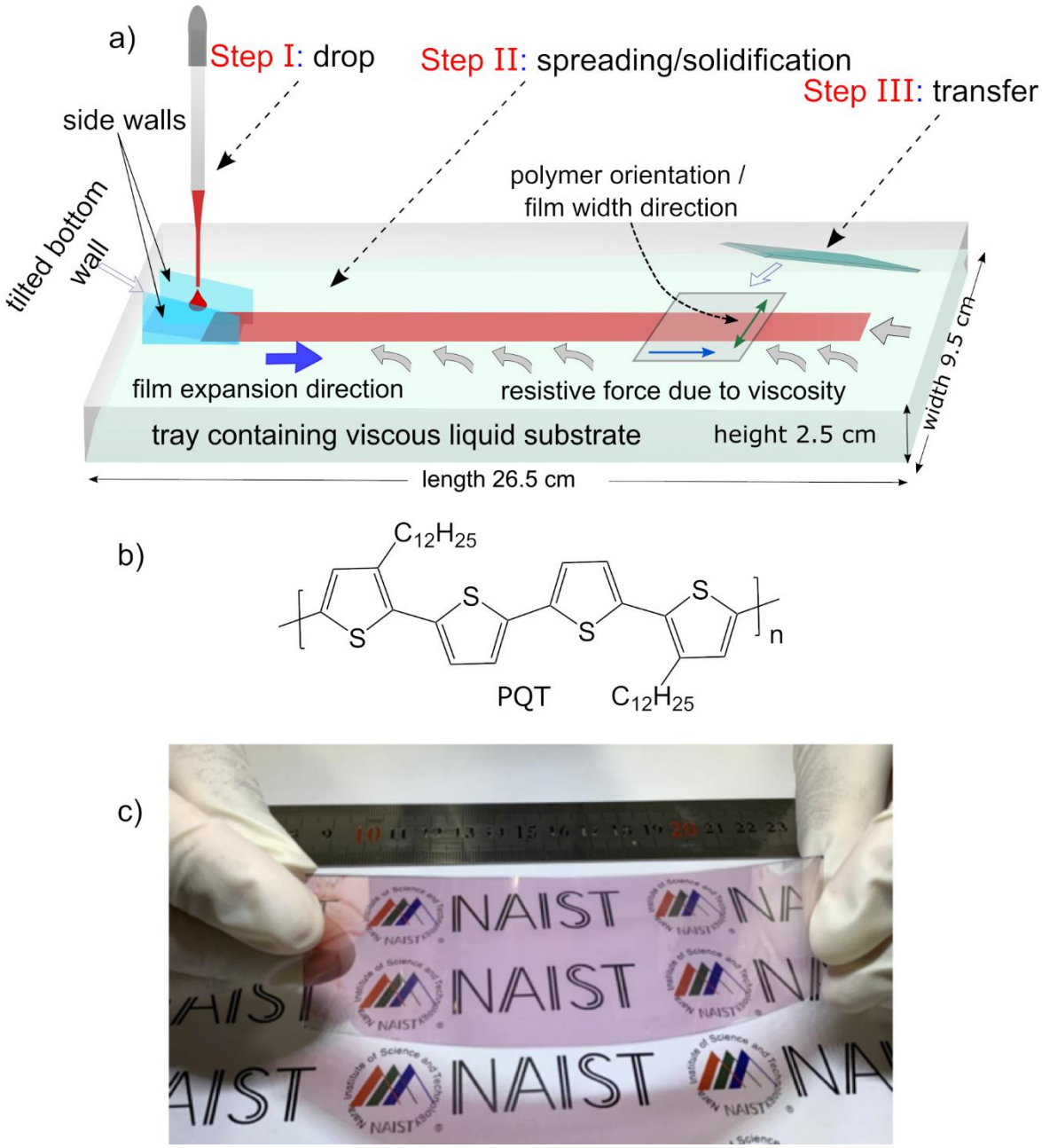


**Figure 3.1. (a) Schematic of the uni-directional floating film transfer method. (b) Chemical Structure of PQT. (c) Photograph of the uniaxially oriented films of PQT 40 cm$^2$ on flexible PEN substrate.**

Uniformly oriented floating film can be transferred to any substrate via simple stamping, ignoring edges having different orientation directions. This method is particularly suitable for preparing large-area-oriented floating films. An example of such films on a flexible PEN substrate with an area of ~40 $cm^2$ is shown in **Figure 3.1 (c)**, with the uniaxial orientation direction shown in **Figure 3.2.** The effective use of the material in this method was understandable because even after neglecting the edges, 40 $cm^2$ of a uniformly oriented film with a thickness of 10 nm can be prepared to produce the required polymer weight per unit area of ~2.5 $g/cm^2$. In particular, the 9 nm spin-coated film required ~138.8 $g/cm^2$.

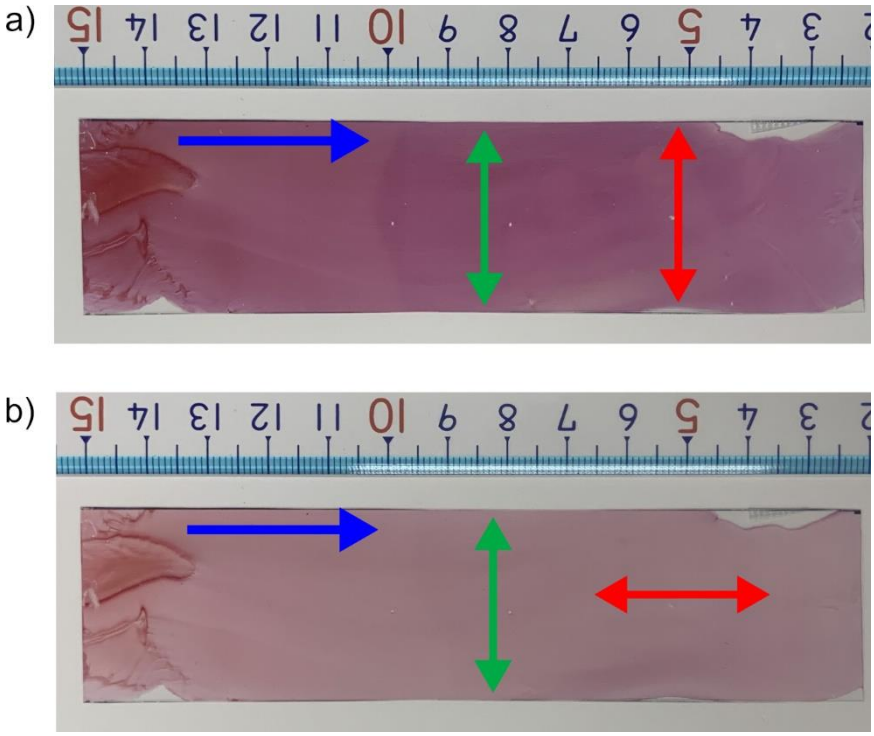


**Figure 3.2. Polarized photograph of the representative 40 $cm^2$ PQT films on PEN substrates prepared using UFTM when the polarizer aligned in parallel (a) and perpendicular (b) with the polymer orientation. Single-sided blue arrows represent the floating film expansion direction, and double-sided green arrows indicate the orientation direction along the width of the floating film. Double-sided red arrows represent the direction of the polarizer.**

**Figure 3.3 (a)** shown the polarized absorption spectra of the center region of the PQT floating film. The DR of the film was 15 with order parameter (S) being >0.8, where S= (DR-1)/(DR+1), which reflect chains backbones of polymer aligned uniaxially along one direction. Well-defined absorption peaks at 545 nm and shoulder at 585 nm were associated with absorption of π–π lamella stacking reflecting strong intermolecular interactions among PQT macromolecules. [62,63] In most areas of the film in UFTM, the PQT films exhibit a strong optical anisotropy, in which light polarized pendicular (⊥) to the direction of film expansion is more strongly absorbed than parallel polarized (||), indicating that the PQT main chains are uniaxially oriented perpendicular to the direction of film expansion ( along the width of the tape-shaped film).

A photograph of a portion of the film taken across the bandwidth through the polarizer film is shown in **Figure 3.3 (b and c).** These images reveal that most of the central regions have maximum absorption with polarized light parallel to the direction of the film width. another thing, the two edges have opposite trends indicating intense absorption with polarized light perpendicular to the film width. To evaluate thickness and DR variation across width, these films were mapped using our 2D position mapping system as previously published. [9]

In general, semiconducting polymer thin films with minimal thickness variations are sensitive to their peak absorbance, directly proportional to thickness (Beer's law). [64,65] Therefore, small variations of the absorption peaks reflected variations in thickness, as shown in **Figure 3.3 (d)**. These results indicate that the film was fairly uniform at 35 mm wide and 18 mm long. The morphology and surface roughness were also investigated using AFM, and the results showed that the film was very uniform with a root mean square of surface roughness <1 nm, as shown in **Figure 3.4**.

Orientation mapping was carried out, taking into account that the polymer was oriented along the film width. The results are shown in **Figure 3.3 (e)**, where the DR ratio appears to be

>10 in most middle regions across the width. In particular, the mapping can only estimate the DR concerning a certain direction as a reference. In this case, the orientation direction of the center region was taken as a reference. Therefore, these measurements do not determine that the polymer was not oriented at the edges because the orientation of the polymer in the region may have a different direction from the direction of the center region.

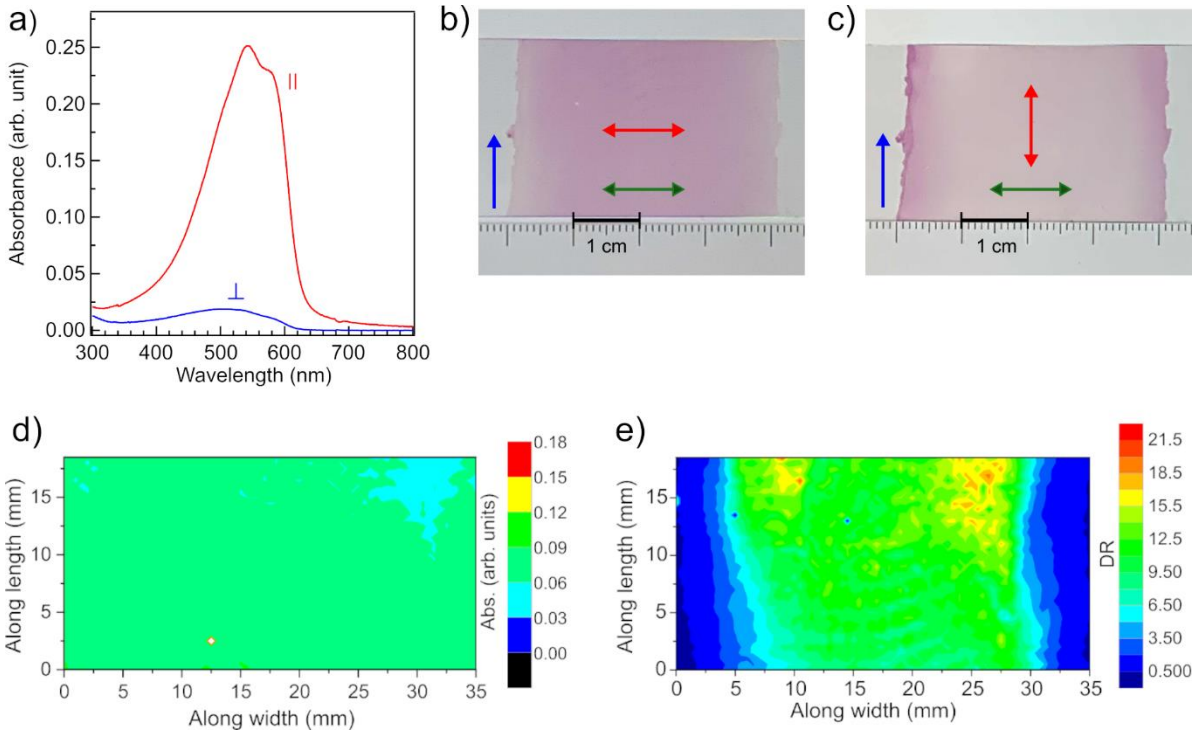


**Figure 3.3. (a) UV-Vis polarized absorption spectra of UFTM film. Photograph of the section of the floating film on a bare-glass substrate with a polarizer in parallel (b) and perpendicular (c) to the width of ribbon-shaped UFTM film. (d) Peak absorption distribution of a section of ribbon-shaped film. (e) DR distribution considering light polarization direction parallel and perpendicular to the width of the ribbon-shaped film. Single-sided blue arrow (b, c) shows the floating film expansion direction in ribbon-shaped UFTM films. Double-sided red arrows in (b, c) show the light polarization direction. A single-sided green arrow shows the polymer orientation direction or width direction of the floating film. For 2-D mapping, the film shown in (b or c) was used.**

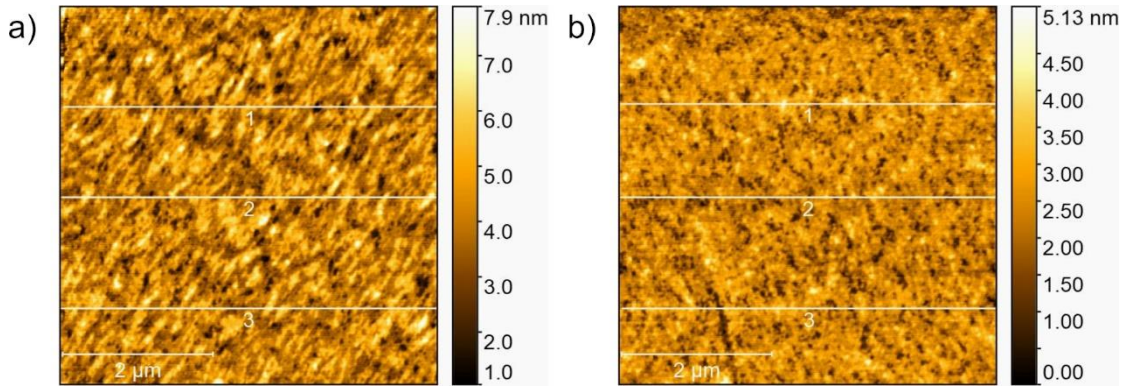


**Figure 3.4**. **AFM topography and surface roughness details of the floating films prepared with PQT concentration (a) 0.5% (w/w) and (b) 1% (w/w).**

A single line scan of the peak absorption intensity as shown in **Figure 3.5 (a)**, with the direction of light polarization parallel (||) and perpendicular ( ⊥ ) to the film width, was conducted to evaluate the orientation distribution along the width. The absorption peak with light polarization parallel to the width has a uniformly high absorption peak in the center region, decreasing towards the edges. On the other hand, the absorption peaks with light polarization perpendicular to the width direction are consistently low compared to the previous case in most central regions and increase at the edges. These results indicate that the polymer was uniformly oriented along the width direction in the middle, and the orientation direction gradually changes towards the edges.

We defined a regime as a boundary region, at the places, where intensity peaks of || and ⊥ absorbance intersects. These results also reflect that the orientation direction of the polymer gradually changes its direction in the boundary region and the degree to which the orientation direction of most polymers at the film edge is somewhat orthogonal. This result in line with the film's polarized image shown in **Figure 3.3 (b and c)** and the DR mapping in **Figure 3.3 (e)**. In order to accurately estimate the orientation and direction of the DR in each

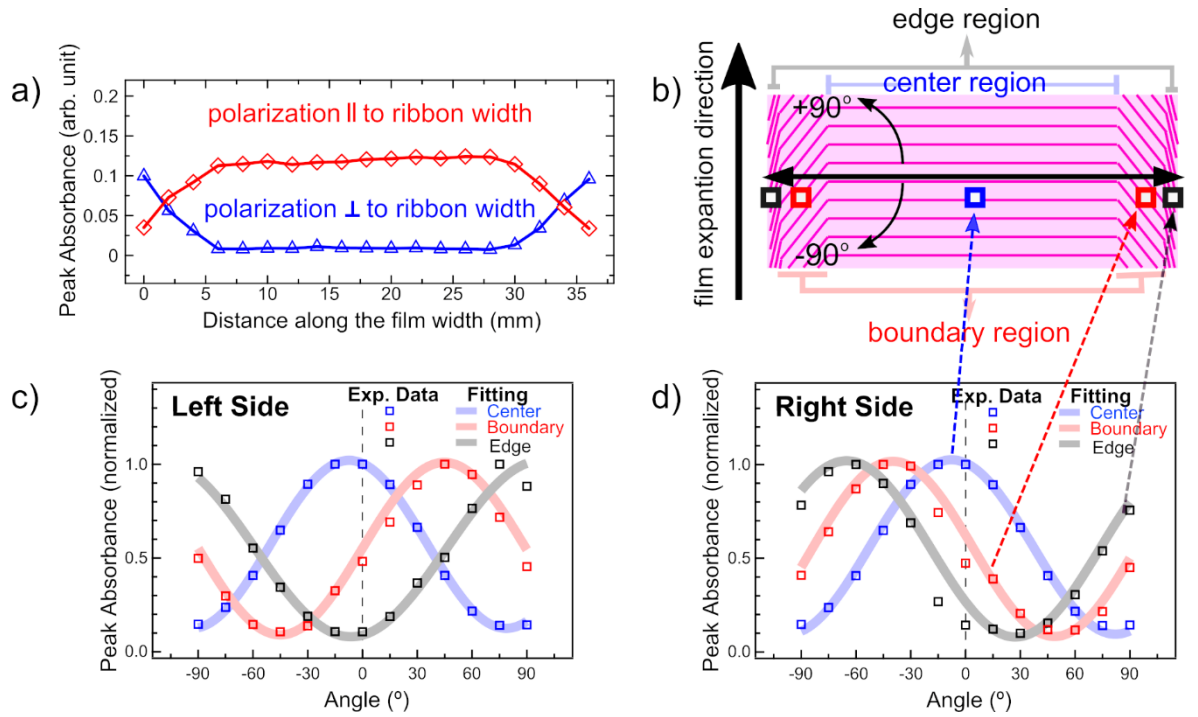


**Figure 3.5. (a) Peak absorption intensity distribution of the film with light polarization direction parallel and perpendicular to the substrate. (b) Schematic representation showing the distribution of the possible orientation direction of polymers in different regions of the films. Normalized peak intensity of angle-dependent spectra taken in different regions for the left side (c) and right side (d) of the film.**

region of the film, i.e., the center, border, and edge regions across the film width, as shown schematically in **Figure 3.5 (b)**, we carried out further investigation.

The angle-dependent polarized absorbance was measured in various regions over the entire width of the film. The peak absorbance of each region from the left side of the film was measured towards +90° to -90° with an interval of 15°. In each case, a polarization direction of 0° was defined with reference to the direction of the center orientation to measure the orientation distribution. The peak intensity of the absorbance value at each angle was normalized by considering the maximum intensity obtained in the area. The results are shown in **Figure 3.5 (c)**. It found the intensity at the center region to be maximum at around 0°, which steadily decreases when rotating the polarizer along with other directions and is in accordance with the mapping results shown in **Figure 3.3 (e)**.

In the boundary region, peak intensity was found to be increasing (decreasing) towards the angles >0° (<0°), and maximum (minimum) intensity were observed at +45° (-45°). For the left edge of the film, peak intensity was found to increasing (decreasing) towards the angles >0° (<0°), and maximum (minimum) intensity was observed at +75° (>-15°). These results suggest that the center region covering most of the film area has orientation perpendicular to the expansion direction of the film, as schematically shown in **Figure 3.5 (b)**; however, across the boundary region to the edges of the film, they tend to be oriented in different directions compared to the film center. A similar trend was observed on the right side of the film, with the orientation of the boundary and the edge region skewed towards the edge of the film, as shown in **Figure 3.5 (d)**.

Despite the different orientation directions across the edges, it should be noted that the DR in each region can be roughly estimated by the ratio of of the peak intensities in this 180° scan, which is ~10, as can be seen from a perusal of **Figure 3.5 (c)**. These results suggest that the orientation intensity of polymers' domain in different regions is similar; however, their orientation direction gradually shifted along the film expansion direction.

The schematic illustration shown in **Figure 3.6** was a possible mechanism for this behavior. We believe the gradual change in orientation direction on both sides of the film results from the shear stress caused by the slider walls designed to expand the film in one direction as the solution begins to flow. Therefore, unlike the circular orientation observed in the floating films fabricated in Petri dishes, [66] polymers in ribbon-shaped FTM were uniformly oriented in center regions that account for more than 70% of the total width.

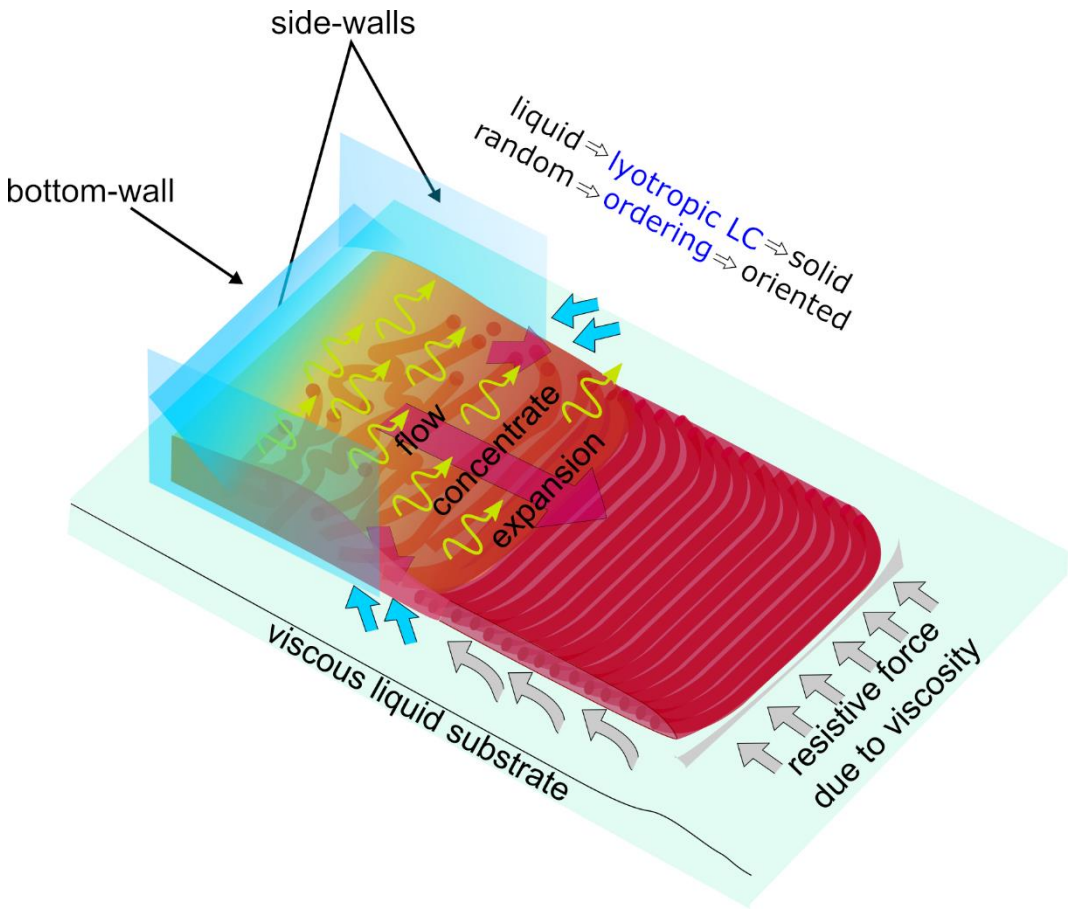


**Figure 3.6. Schematic illustration of proposed orientation mechanism in unidirectional floating film transfer method.**

To confirm the validity of this orientation characteristic in UFTM, we also tested the versatility of this phenomenon with other high mobility Poly[2,5-(2-octyldodecyl)-3,6-diketopyrrolopyrrole-alt-5,5-(2,5-di(thien-2-yl)thieno[3,2-b]thiophene)] polymers, and a similar behavior was observed, as shown in **Figure 3.7**. The polarized photograph in **Figure 3.7** clearly shows that when light was polarized along the width of the film's central region, it is dark. On the other hand, when light polarization was perpendicular to the wide region, most of the center region was light in color. In addition, the color of the edge region was intense.

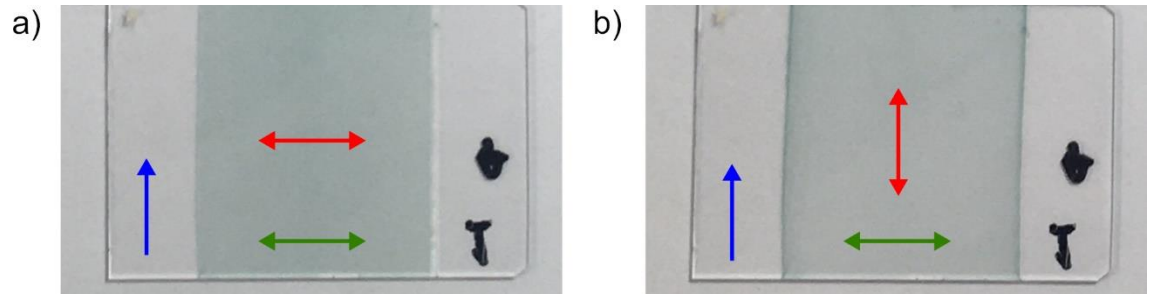


**Figure 3.7. Polarized photograph Poly[2,5-(2-octyldodecyl)-3,6-diketopyrrolopyrrole-alt-5,5-(2,5-di(thien-2-yl)thieno[3,2-b]thiophene)] films prepared using UFTM. Film was transferred on glass substrate across the film width. Light polarization is parallel in (a) and perpendicular in (b) with respect to the film width. Double-sided red arrow shows the light polarization direction. Single-sided blue arrows show the floating film expansion direction in UFTM. Double-sided green arrow shows the polymer orientation or film width direction.**

Orientation conformation of the semiconducting polymer in a thin film is important for understanding the charge transport anisotropy in OFET. Therefore, we prepare the PQT film from the center region then measure out-of-plane and in-plane GIXD. From out-of-plane GIXD measurement results, we observed the diffraction peaks (*h*00) up to 2$^{nd}$ order related to alkyl lamellar stacking, as can be shown in **Figure 3.8 (a)**. *d*-spacing was calculated to be 2.07 nm which shows that alkyl side chains are partially interdigitated and is in good agreement with studies reported by Kline et al.[67] Measurements of in-plane GIXD were conducted along the parallel ($\chi$ = 90°) and perpendicular direction ($\chi$ = 00°), the schematic of measurement setup and results were shown in Error! Reference source not found. **(b)**. A diffraction peak around 2 $\theta_{\chi}$ = 21.2° arising from π–π staking between the polymers was only observed for $\chi$ = 90°, reflecting the unidirectionally aligned polymers. There was no diffraction peak related to the alkyl lamellar stacking in in-plane measurement, which reflect that polymer backbones were aligned uniaxially with the conjugated backbone and π–π staking in-plane of the substrate, so-called edge-on orientation. [32,39].

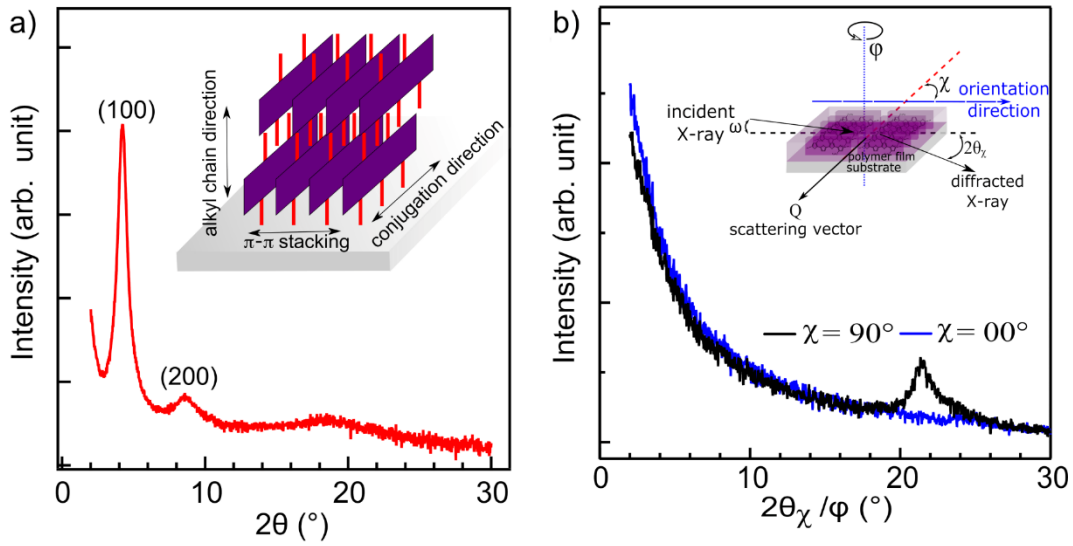


**Figure 3.8. Out-of-plane (a) and in-plane (b) GIXD pattern of PQT films prepared by UFTM. Inset in (a) is a schematic illustration of edge-on oriented conformation. Inset in (b) shows the schematic illustration of in-plane GIXD measurement where scattering vector is parallel (χ = 90°) and perpendicular (χ = 00°) to polymer orientation direction.**

Analysis of both peaks that appeared in the out-of-plane XRD measurement results using the Williamson-Hall equation, which is defined as $\beta\ cos\theta = K\lambda/D + \varepsilon\ 4sin\theta$. Where $D$ is the crystallite size in nm, $K$ is a numerical factor refer to as the crystallite shape factor (0.95), $\lambda$ is the wavelength of X-rays, $\beta$ is the width (full-width at half-maximum) of the X-rays diffraction peak in radians, $\varepsilon$ is a micro-strain and $\theta$ is the Bragg angle in degree. The full width of the diffraction peak at half the maximum of both peaks is the result of the contribution of crystal size and micro-strain, where the contribution of micro-strain is almost the same as the contribution of crystal size as shown in **Figure 3.9**. These results indicate that the resulting thin film has a semi-crystalline structure, which has high long-range order but weak positional order.

Mobility anisotropy in edge-oriented films is smaller (<1 order of magnitude) because of the presence of a conjugated backbone and π–π staking in-plane of the substrate in comparison to face-on-oriented films. [19,58,68]. In-plane charges transport properties of the films were checked by making OFETs in each region. Since the orientation direction in different

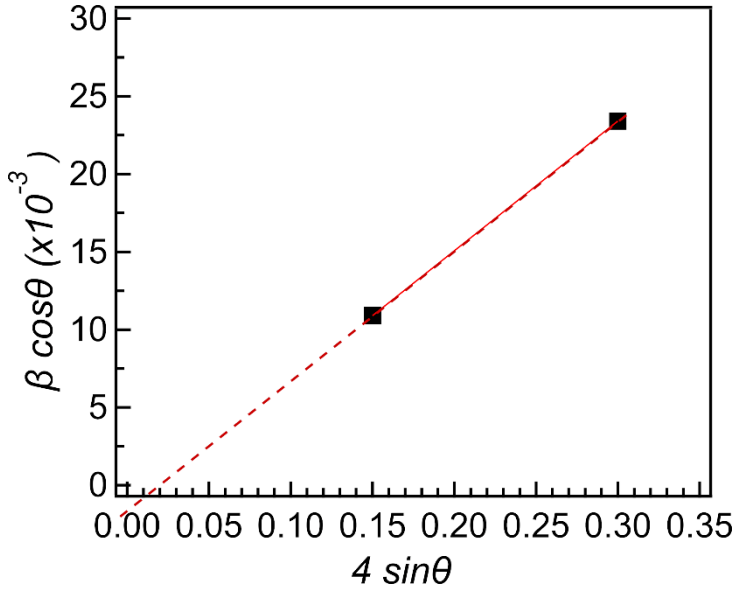


**Figure 3.9. Williamson-Hall plot of out-of-plane X-ray diffraction data in Figure 3.8 (a)**

regions were already known, OFET's channel direction was tuned considering 0° in parallel to the orientation direction of the center region and was set as a reference in each region as shown in **Figure 3.10 (a)**. The mobilities of the angle-dependent field effect in different regions with respect to the orientation direction in the central region was shown in **Figure 3.10 (b)**.

At the center, where polymer orientation direction is at 0° to channel direction, field-effect mobility in parallel (0°) and perpendicular (90°) direction was found to be $5.7\times10^{-3}$ $cm^2/Vs$, and $6.4\times10^{-4}$ $cm^2/Vs$, respectively. Tripathi et al. have reported the dependence of the molecular weight on DR and field-effect mobility of UFTM film.[69] As the SAM layer is similar to that reported, we believed this lower value of field-effect mobility is due to the low molecular weight of the purchased PQT. The mobility anisotropy of 8.9 is in line with polarized UV-vis absorbance and GIXD results, showing high DR and edge-on conformation..[70–72]

Maximum field-effect mobility in the boundary region was found when the channel direction was at 45° with respect to the orientation direction of the central region as shown in **Figure 3.10 (a)**, and was in line with the results of angle-dependent peak absorbance. At the edge region, field-effect mobility was lowest at 0° as the dominant orientation was found for

angle ≈70° (>45°), shown in **Figure 3.10 (b)**. Maximum field-effect mobility in the edge region was also observed at 45°. However, it is worth noticing that field-effect mobility was high for angles >45°, compared to that of center and boundary regions. Since the channel width of OFETs was 2 mm more than the width of edge-region of UFTM films, as can be seen in **Figure 3.3 (b and c)**. Therefore, these field-effect mobilities in the edge region were expected to originate from both the edge and boundary regions. The lowest mobility at 0° and higher mobility at angles >45° reflect that the polymers in the edge region were almost orthogonally oriented towards the center.

For comparison, spin coated devices were also prepared on same substrates and average field-effect mobility was estimated to be $1.42\times10^{-3}$ $cm^2/Vs$. Field-effect mobility of spin coated devices is in well agreement with the results reported by Pingel et al.,[73] where they have reported the effect of molecular weight of PQT on field-effect mobility. Moreover, field-effect mobility spin coated device is between 0° and 90° oriented films as these films are isotropic in nature. Similar results on oriented poly(3-hexyl thiophene) using strain alignment

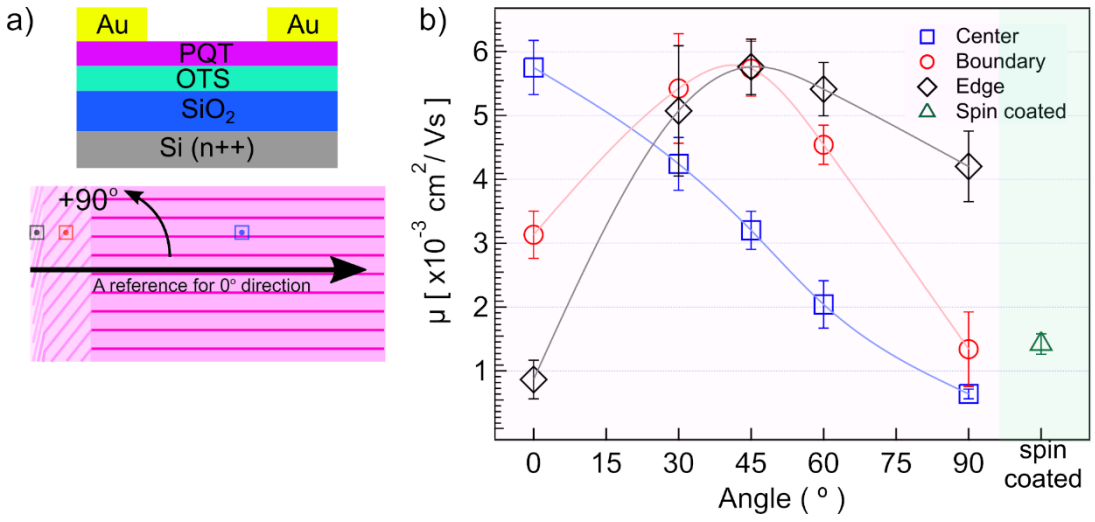


**Figure 3.10. (a) Schematic of OFET and reference angle for measurement of angle-dependent field-effect mobility in different regions of ribbon-shaped films of PQT. (b) Angle-dependent field-effect mobility in different regions of UFTM film and field-effect mobility of spin coated OFETs. Average and standard deviation at each angle was calculated from 5 or more devices.**

have been reported where mobility of isotropic film was in between the mobility along the orientation direction and orthogonal direction.[74]

Large area films, which comprise 70% of the area along the width, can be obtained by transferring floating films at the center region, even though ignoring its boundary and edge regions. For example, one of the large area films with a size of 40 $cm^2$ having a uniaxial orientation shown in **Figure 3.2**. In order to investigate the variation of the field-effect mobility in these large-area films, we fabricated a transistor array by transferring the film along the expansion direction, considering that the channel direction was parallel to the orientation direction (film width). From this large floating film, we can obtain 42 OFETs fabricated in two rows along their length in an area of 15 × 2.5 $cm^2$, as shown in **Figure 3.11 (a)**. In this case, the SAM-layer was replaced with an ultra-thin layer (9 nm) of CYTOP which facilitates better adhesion with the floating film due to its high hydrophobicity. It found that device-to-device variation and hysteresis in OFET performance using high SAM decreased by a considerable amount in the case of CYTOP. [75,76]

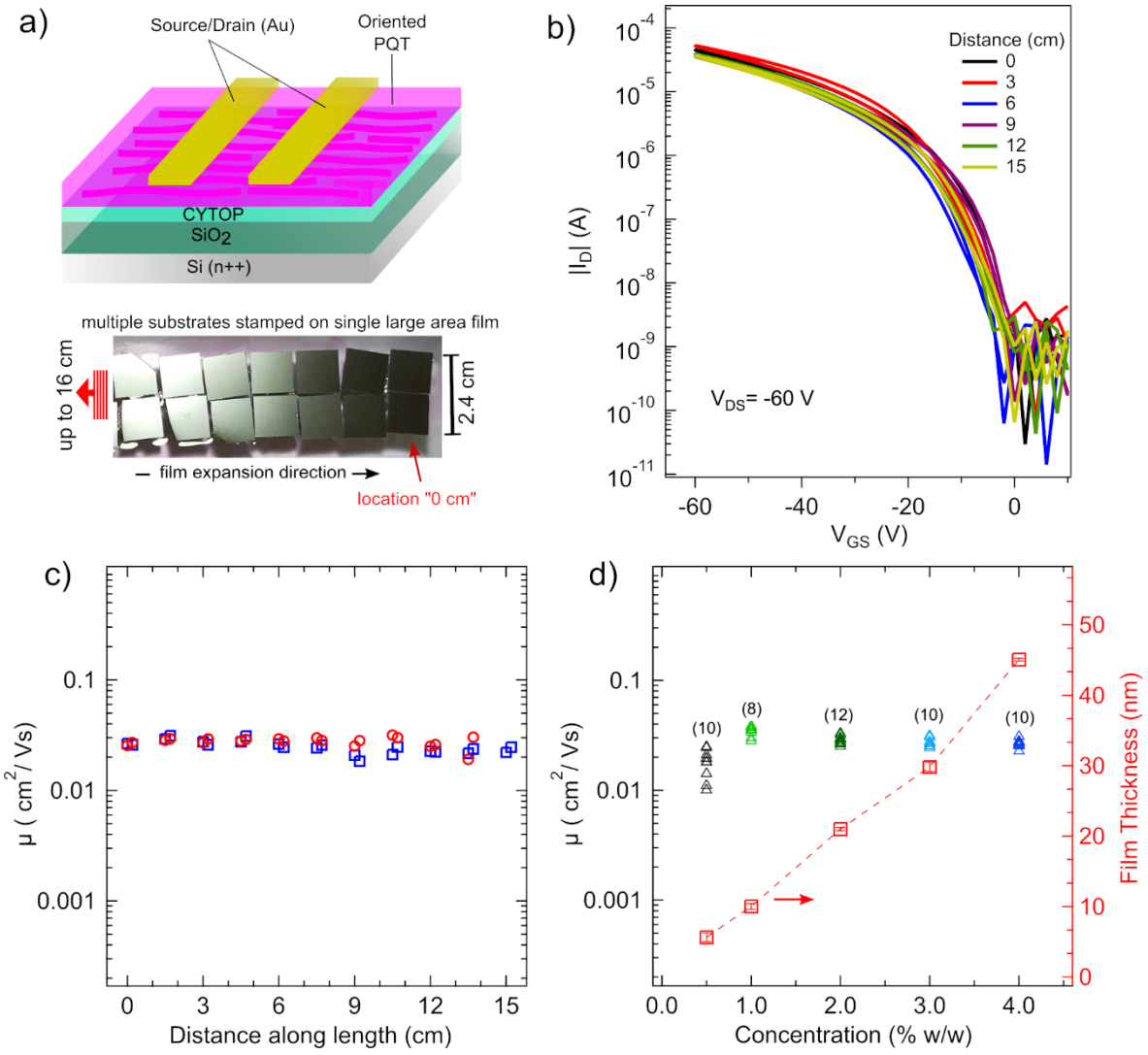


**Figure 3.11. (a) Schematic illustration of fabricated bottom-gated top-contact OFET devices with a photograph showing many CYTOP/$SiO_2$/Si(n++) substrates transferred on single large-area floating films for mobility mapping along the 16 cm length of the ribbon-shaped floating films. (b) Transfer characteristics of OFETs at length 0, 3, 6, 9, 12, 15 cm of the single ribbon-shaped floating film. (c) Variation of field-effect mobilities along the length of the single ribbon-shaped floating film. (d) Variation of field-effect mobility and film thickness with PQT concentration. PQT concentration was 2% (w/w) in (b) and (c). Values in parentheses in (d) are total number of devices fabricated.**

**Figure 3.11 (b)** shown the transfer curve of the OFETs along length at the equidistant interval of 3 cm. This transfer curve clearly showed p-type unipolar behavior with an on-voltage around 0 V and $I_{on}/I_{off}$ ratio of $10^5$. It has been commonly reported that the hysteresis in the FET device was due to the presence of hydrophilic components at the semiconductor and dielectric

interface. [77] Since these floating films were washed with isopropanol and then annealed at 60 °C to evaporate any residual solvents, therefore, negligible hysteresis and well-defined on/off characteristics can be attributed to the absence of any residual solvents or hydrophilic liquid substrates from UFTM procedure. We believe that strong interaction between the CYTOP interface and PQT films, highly hydrophobic CYTOP surface with water contact angle of ~ 112°, and subsequent washing with isopropanol prevented any hysteresis, as many researchers have reported.[78–83]

**Figure 3.11 (c)** shown the variation of field-effect mobilities for two rows along the length, and the average field-effect mobility of these OFETs was 0.0262±0.0033 $cm^2/Vs$. Interestingly we did not find any malfunctioning devices, and all of the 42/42 transistors fabricated were working. Moreover, the standard deviation of mobility in these large-area films was negligible, comparable to or better than many other solution-based procedures for the fabricating of isotropic and anisotropic large-area films for OFETs and circuits. [84–87]

Only by changing the concentration of the polymer solution, the thickness of the film formed by UFTM will change. To investigate the effects of semiconducting polymer film thickness on the FET devices, we varied the solution concentration from 0.5 to 4% (w/w), resulting in a film thickness of 5.6 to 45 nm. Results of the field-effect mobilities and film thickness regarding PQT concentration are shown in **Figure 3.11 (d)**. Interestingly, field-effect mobilities were in the same order even if increased the thickness by ≈9 times. However, maximum mobility and higher reproducibility were obtained with 10 nm thick films prepared with 1% (w/w) concentration. These results confirm that UFTM offers large-area films with oriented semiconducting polymers and enables minimal compromise in performance uniformity.

Floating film prepared by 0.5% (w/w) was 5.6 nm thick, which means film merely consisted of 2-3 layers of edge-on stacked polymers on the substrate considering the lamellar

stacking distance of ~2.1 nm. These results reveal that even 2-3 layers could construct charge pathways as film maintain considerable performance >0.01 $cm^2$/Vs. However, we believe that slightly low value and device-to-device variation were due to the film's relatively high surface roughness, as confirmed by AFM images (**Figure 3.4**). Many researchers have studied thickness-dependent performance in OFETs, and the relation between thickness and field-effect mobility depends on several parameters, as already reported.[85,88,89] Therefore, thickness/concentration-dependent growth mechanism in UFTM and their influence of film morphology using various semiconducting polymers is important.

Flexible OFETs were fabricated in bottom-gated top-contact geometry on 100 µm thick PEN substrates using Al gate electrode and CYTOP dielectric ($C_i$ = 2.54 nF/$cm^2$) shown in **Figure 3.12 (a)**. Measurement was first conducted with flat devices such that the bending radius of curvature ($r$) is ∞. Average field-effect mobility of flexible devices was 0.0181 ± 0.006 $cm^2$/Vs (maximum 0.026 $cm^2$/Vs). These results on flexible devices are comparable to devices on rigid substrates with a CYTOP interface. We also examined mechanical flexibility by bending the devices across the channel direction sequentially across cylindrical rods of different radii ($r$= 10 mm, 6.5 mm, 3 mm).

Transfer curves of flexible OFETs are shown against the different bending radius shown no considerable difference, as shown in **Figure 3.12 (b).** Evolution of field-effect mobility and threshold voltages with respect to bending radius is shown in **Figure 3.12 (c)** and **(d)**. The mobility and threshold show no significant change even when bent at radii of 3 mm, suggesting the absence of significant film cracking or layer delamination during flexing of the substrate. We noticed that connection to drain and source pads via silver paste were delaminated as bending 100 µm thick PEN substrates was difficult; such aggressive flexing can cause deformation the flexible substrate. Nevertheless, this process depends not only on the quality

of the semiconductor layer but also on the mechanical compatibility between the other device layers and the intrinsic properties of the other layers and their response to bending.[87,90]

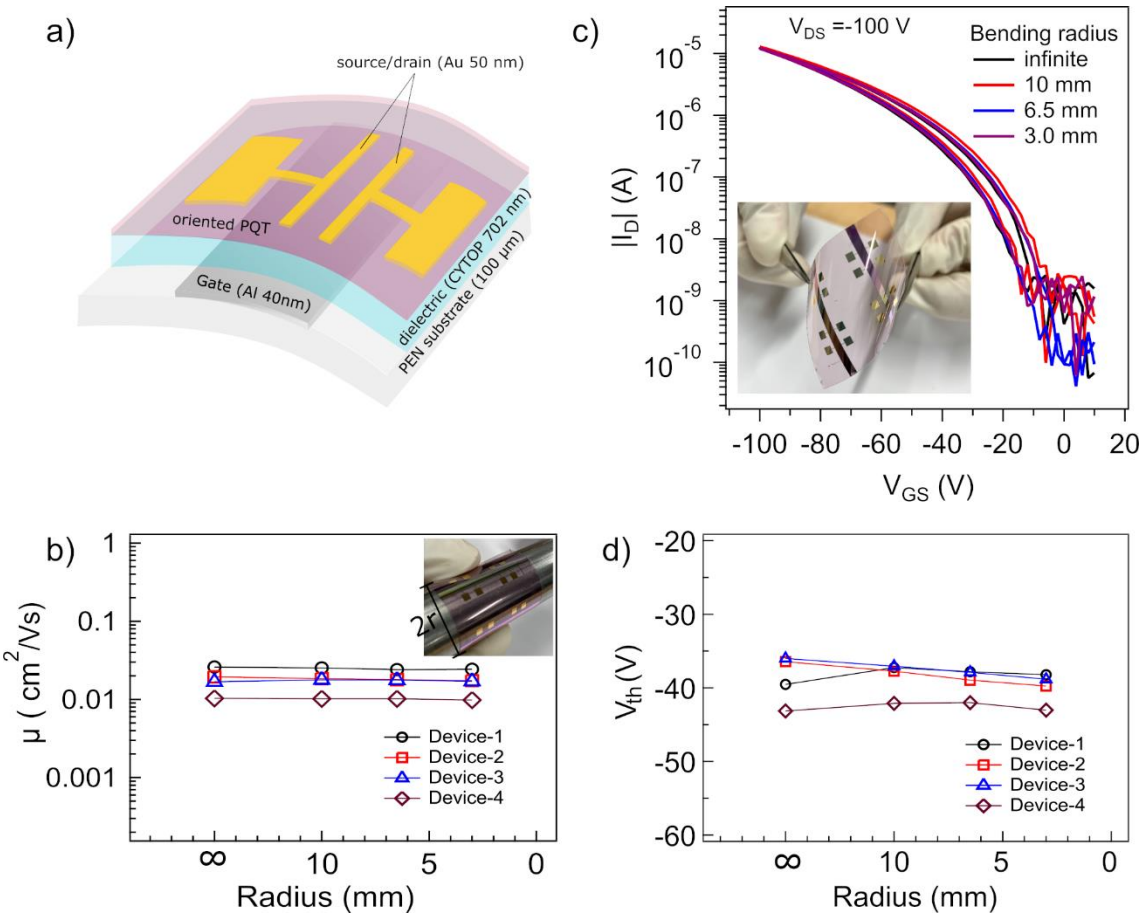


**Figure 3.12. (a) Schematic illustration of the flexible bottom-gated top-contact OFETs. (b) Transfer curve of the flexible OFETs at different bending radii. Evolution of field-effect mobility (c) and threshold voltage (d) with *r*. Inset in (b) is the photograph of the flexible OFETs.**

### 3.4 Conclusions

The UFTM capability to prepared large-area (~40 $cm^2$) uniformly oriented PQT thin films has been demonstrated. Its high uniformity has been revealed using 2-D positional mapping and AFM measurement. Using angle-dependent absorbance measurement, we confirmed orientation characteristics in the majority of the center region covering 70% of the

entire width of the film was highly uniform. The orientation of the polymer crosses the edges nearly orthogonal to the center. Mapping angle-dependent field-effect mobilities were in line with the angle-dependent peak absorbance of UV-vis absorbance spectra measurements. The average field-effect mobility of many OFETs fabricated from two rows along the length of a single film with an area of ≈15×2.5 $cm^2$ was 0.0262±0.0033 $cm^2$/Vs. Film thickness variations in field-effect mobility shown no appreciable difference in performance, and even 10 nm thick films offer highly reproducible results in terms of device performance. Flexible OFETs with bottom-gated geometry on PEN substrates using CYTOP dielectrics had average field-effect mobility of 0.0181 $cm^2$/Vs and no considerable change in mobility after bending the flexible devices at different radii (10, 6.5, and 3 mm). In addition to multilayer film fabrication capability, we believe these key features of UFTM are expected to contribute towards novel hetero-structured devices and next-generation flexible circuits.

# Chapter 4. Anisotropic Properties of Floating Films at Different Interfaces

## 4.1 Introduction

Semiconducting polymers are widely investigated for various technological applications such as flexible electronics, devices for conversion alternative energy, and sensing and imaging devices. [62,91,92] The main advantage of conjugated polymers is that they can be solution-processed, offering inexpensive and uncomplicated device manufacturing. Their one-dimensional *p*-orbital result in optical and electronic anisotropic properties. These properties can be achieved in device applications when the backbone chains are aligned. [12,32,34] In addition, the alignment of the backbone chains in polymer thin films can increase the mobility by more than an order of magnitude, as has been widely reported.[12,58,93,94] The majority of the orientation techniques to align conjugated polymers are suitable for practical large-area flexible circuits due to the possibility of damaging the bottom films or substrate chemically or mechanically. The floating film transfer (FTM) method is one method for aligning conjugated polymers, so that the performance of OFET devices can be improved, as shown in some of the previous reports. [12,32–34,55] Later, by modified form of the FTM method, as shown in **Figure 2.5,** unidirectional expansion of a polymer resulting in oriented and large-area of floating films can be achieved, then we called unidirectional floating film transfer method (UFTM).

Molecular alignment in UFTM and their optical and charge transport anisotropy have been extensively investigated. However, there are no detailed reports on the molecular alignment at the liquid and air interface. Therefore, investigation pertaining to the orientation at both the interface, or in other sense, how orientation (or degree of orientation) varies with the thickness have not been investigated yet. It is well known that the charge transport in OFET occurs within few nanometers or few monolayers near the gate-dielectric/semiconductor

interface. Therefore, the charge transport anisotropy also depends on the alignment of polymers near the interface. However, it is important to investigate the molecular-alignment characteristics of floating films at both liquid interface and air-interface in UFTM as these characteristics also determine the performance and anisotropy of OFETs when considering a bottom-/top-gated geometry. These characteristics are investigated through the anisotropy of the charge carrier in both OFET structures.

This chapter presents a detailed investigation of the growth mechanism and charge transport anisotropy in UFTM films at liquid interface and the air interface. Anisotropy of field-effect mobility was studied through OFET fabrication with TGBC and BGTC structures. In the TGBC OFET, the air interface of floating film will be used for semiconductor/dielectric interfaces. While in BGTC OFET, the liquid interface of floating film was studied. To fully understand the effect of film thickness on charge transport anisotropy at both interfaces, we also varied the film thickness by varying the casting of the polymer solution in UFTM. Further results and discussion related to these investigations is made in the result section of the this chapter.

## 4.2 Experiment Details

### 4.2.1 Materials and films preparation

*Polymer material and solvent:* poly(3,3‴-didodecyl-quaterthiophene) (PQT-C12) and anhydrous chloroform were purchased from Sigma Aldrich without any further purification.

*Chemicals for liquid substrate in UFTM:* Ethylene glycol (EG) and glycerol (GL) were purchased from Fujifilm Wako Pure Chemical Corporation, Japan. Both chemicals were mixed with a ratio of EG and GL was 3:1. The temperature of this liquid substrate was maintained at 45 ℃ before used for film casting.

*Chemicals for SAM treatment:* Octadecyl(trichloro)silane (OTS) with purity >90%, and toluene super-dehydrated were purchased from TCI, Japan and FUJIFILM Wako, Japan. CYTOP CTL-809M and CT-Solv.180 were purchased from Asahi Glass Co., Ltd., Japan.

*Substrates*: Normal glass substrates for optical characterization of thin films, while device-grade glass substrate and $SiO_2$/Si ($n^{++}$) substrates with $SiO_2$ thickness of 200 nm for OFETs device with structure BGTC and TGBC. Before SAM treatment and CYTOP deposition, substrates were washed in an ultrasonication bath of acetone for 10 minutes, followed by rinsing in hot acetone and drying under nitrogen flow.

To improve the surface hydrophobicity of normal glass for optical characterization, the substrates were immersed in 160 ul of OTS solution prepared in 40 ml super dehydrated toluene for 3 h in the air atmosphere. However, for OFETs fabrication purposes, SAM treatment and CYTOP deposition were presented in detail in the device fabrication section.

*Polymer solutions:* PQT was dissolved in anhydrous chloroform with various concentration because the concentration of polymer solution is an important parameter to decide the thickness of thin-film.[39,93,12] In this study, variations in the concentration of PQT were 0.5, 1, 2, and 3% (w/w) to vary the film thickness.

*Polymer films:* Approximately 10 μl of PQT solution was dropped near the edge of the center of the tilted bottom slider wall and liquid substrate interface. The droplet solution will spread unidirectional to form a large area of the thin film. The substrate was held with tweezers, then, carefully placed on the floating film to transfer it to the substrate.

### 4.2.2 Devices Fabrication

For BGTC OFETs fabrication, clean $SiO_2$/Si(n++) substrates were coated by CYTOP$^{TM}$ using spin coating at 1000 rpm for 45 s, then annealed just after coating at 100°C

for 1 h in the air atmosphere, resulting in the thickness of ~10.44 nm. The CYTOP solution was prepared by dissolving CYTOP CTL-809M in CT-Solv. 180 in the ratio of ~1:30. The PQT floating film then transferred on these $SiO_2$/Si(n++) coated CYTOP. The source-drain electrode with the channel length of 20 μm and width of 2 mm was formed by evaporating the gold under the nickel shadow mask. The gold was evaporated resulted in thickness up to ~50 nm.

SAM coated on clean device-grade glass substrates for fabrication of TGBC OFETs device. Clean substrates were immersed in a container with 160 $\mu$l of OTS solution prepared in 40 ml super dehydrated toluene which was placed on a hot plate (80 ℃ for 2 h) in the air atmosphere. Substrates was cleaned in ultrasonication bath of toluene for 10 minutes with repetition 3 times using fresh solvents. As a final step, substrates were left for drying at 100 °C on a hotplate for 15 min in the air atmosphere. Later, source and drain electrodes were formed by placing a nickel shadow mask on the substrate before vaporizing the chromium and gold. The chromium was vaporized firstly, then gold, which resulted in thickness of ~2 nm and ~18 nm, respectively.

The PQT floating film was transferred on that substrate, followed by proper washing with 2-propanol to remove the liquid substrate adhering to the film; then dried at 60 ℃ for 30 minutes under nitrogen atmosphere. Later, pure CYTOP CTL-809M was coated using spin coating with a speed of 4000 rpm for 45 seconds, obtaining the CYTOP thickness ~650 nm, then dried at 60 ℃ for 1 h in air atmosphere, immediately after coating. As a gated electrode, the aluminum was evaporated under the nickel sheet mask with a thickness of ~40 nm.

In any case, since the thickness of source-drain of TGBC FETs was ~20 nm, for PQT films with the thickness 5.6 and 10 nm obtained from PQT solution of 0.5 and 1 % (w/w), diluted PQT solution with concentration 0.2 % (w/w) in 1,2-Dichlorobenzene deposited using 2 steps spin coating (1st step of 500 rpm for 5 s and 2nd step of 1500 rpm for 75 s) resulted in

thickness of (8.7±0.1) nm as supporting layer to avoid cracking of films at the edge of both sources and drain electrodes.

### 4.2.3 Characterization

Polarized absorption spectra measurements were conducted by using UV-vis-NIR spectrophotometer (JASCO V-770DS) be equipped with polarizer. Thickness measurement and surface topography were measured via atomic force microscope (AFM) using SPM-9600 Shimadzu, Japan. Semiconductor parameter analyzer Agilent E5272A was utilized for current-voltage (*I-V*) characterization of OFETs. Capacitance/Area ($C_i$) was measured using an LCR meter (ZM2375, NF Corporation) for parallel plate capacitor structure fabricated similar to transistor geometry, it was 2.77 nF/cm$^2$ and 15.38 nF/cm$^2$ for pure CYTOP coated device-grade glass and CYTOP coated $SiO_2$, respectively. Field-effect mobility ($\mu$) was extracted from the transfer curves in the saturation region using below.

$$I_{DS} = \frac{\mu C_i W}{2L}(V_{GS} - V_{DS})^2 \qquad \textbf{(4.1)}$$

Where $I_{DS}$ is the drain to source current, $V_{GS}$ is the gate to source voltage and $V_{DS}$ is the drain to source voltage. Orientation degree/DR was calculated from the polarized UV-vis absorption spectra using **Equation 2.7 in Chapter 2**.

## 4.3 Results and Discussions

UV-Vis polarized absorption spectra of films with variation solution concentration shown in **Figure 4.1 (a).** It is clearly shown that all the fabricated films have clear optical dichroism with high DR with main peak at $\lambda_{max}$ around 537 nm in parallel absorption spectra.[93] Absorption spectra in parallel show a low energy feature around 580 nm, suggesting a vibronic band associated with the (0-0) transition spectra corresponding to structural ordering formation

in the solid-state and π-π lamella stacking which is absent in perpendicular absorption spectra is attributed to random distribution of polymer chains. [32,39,95]

Obviously observed in **Figure 4.1 (b)**, the main peak of normalized nonpolarized absorption spectra at around 540 nm was unchanged even though the solution concentration increased. However, the ratio $A_{0-0}/A_{0-1}$ increases when the solution concentration more than 0.5 % (w/w), which reveals the PQT macromolecule enhances their interchain interactions. Increasing the polymer concentration to 2 and 3% (w/w) causes a shoulder peak of about 500 nm to be clearly seen, addressing the presence of an amorphous polymer chain. This is also confirmed by the appearance of a weak absorption peak at around 680 nm, which shows a transition between amorphous and crystalline phases. [17,96]

In concentration 0.5 % (w/w), the PQT macromolecules have a high degree of freedom of movement in the solution phase; once it dropped on the liquid substrate, droplet solution spread out on the liquid substrate before it solidified that provide non-uniform floating-film and low interchain interaction. However, when using concentrations 1, 2, and 3 % (w/w), the number of polymer macromolecules in one polymer droplet enhances, restricting their free movement while they are going from solution to solid-state. Therefore, solidification will be faster polymer solidification and solvent evaporation, preventing rapid dispersal resulting in a uniform floating-film and high interchain interaction, which indicated by increasing the ratio $A_{0-0}/A_{0-1}$.

The evolution of the number of aligned polymers contributing to the electronic transition in the polarized absorption spectrum is shown in **Figure 4.1 (c)**. It was clearly observed that the absorption intensity in parallel enhancing with increasing the concentration of the solution. Interestingly, adding the concentration from 0.5 to 1% (w / w) did not change the absorption intensity perpendicularly, suggesting that the contributions of unaligned polymer in both films were similar. However, using a more concentrated polymer would slightly

increase the absorption intensity perpendicularly due to increasing content of randomly lying polymer as a result of decrease in DR.

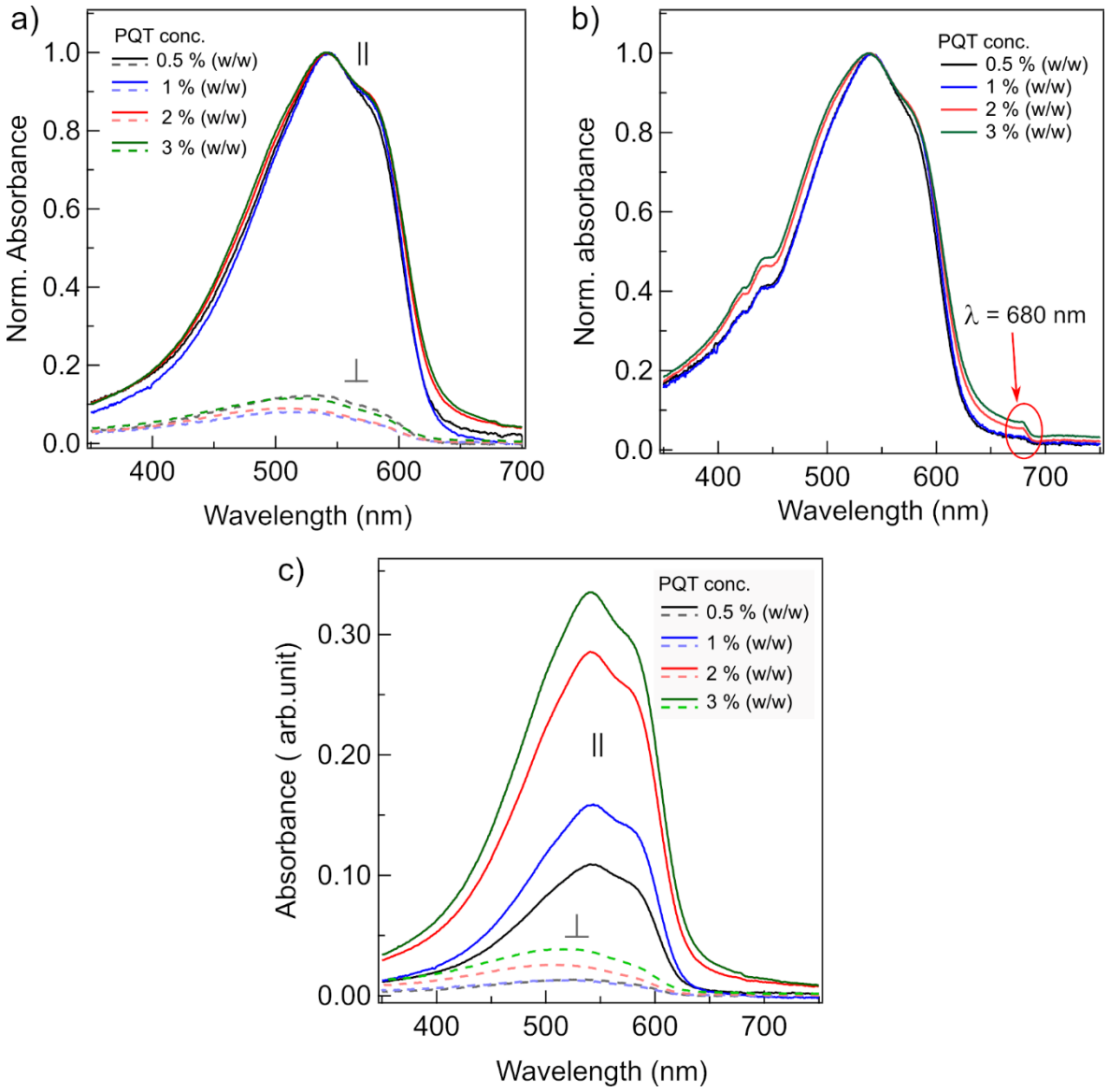


**Figure 4.1. Absorption spectra of PQT C-12 films with different concentration. (a) Polarized (normalized), (b) Non-polarized (normalized), and (c) Polarized.**

The change in film thickness due to different concentrations is presented in **Figure 4.2 (a)**, and increasing the polymer concentration every 1% (w/w) resulted in a rise in film thickness of about ~ 10 nm. This result shows that a favorable way to tune the film thickness in solution-based processing of fabricating a thin film, especially in the UFTM, is possible by controlling polymer solution concentration. For each solution concentration 0.5, 1, 2, and 3 % (w/w)

resulted in the PQT film thickness of (5.6±0.6), (10.0±0.4), (21.0±0.2), (29.8±0.6) nm, respectively.

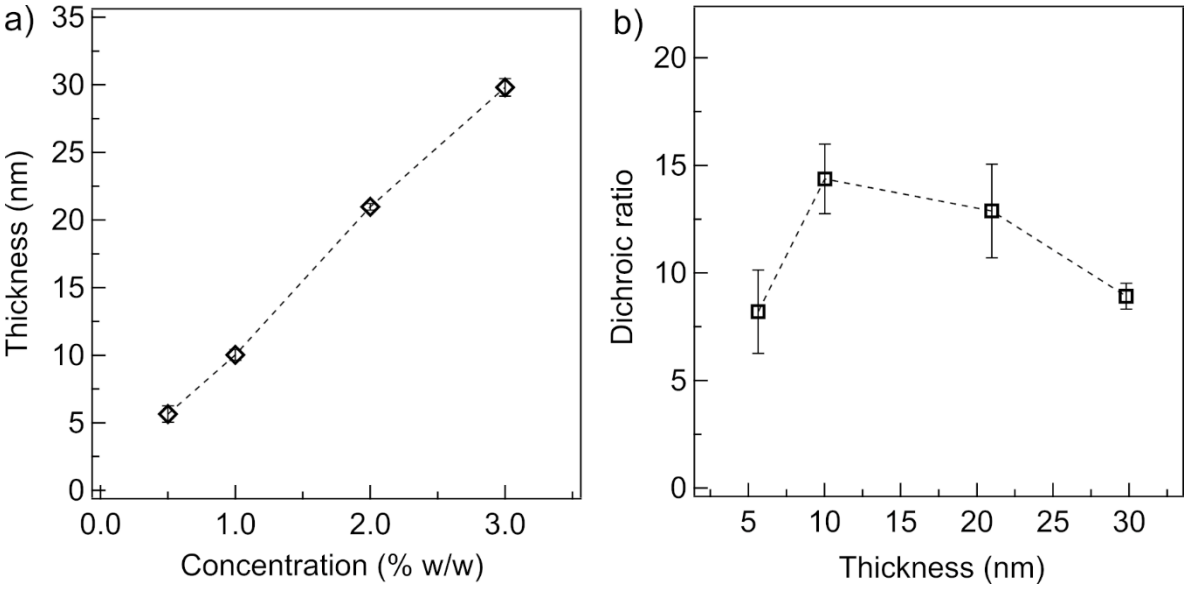


**Figure 4.2. (a) Films thickness of the oriented film with different polymer solution concentration. (b) Variation in the film's dichroic ratio in respect to the film thickness**

**Figure 4.2 (b)** presents the DR of films as a function of film thickness due to different polymer solution concentration casting of UFTM. At a certain range of thickness, the DR tends to increase; however, increasing the concentration more than 1% (w/w) reduces the DR together with the appearance of increased amorphous polymer content in the film. It shows that the maximum DR achieved at the film thickness of 10.02 nm for solution concentration 1 % (w/w).

The AFM images in **Figure 4.3** disclose the evolution of the interfacial morphology at liquid-and air-interface of floating film with respect to concentration or film thickness. The AFM images exhibited a similar surface morphology of both interfacial at the same solution concentration where observed the noodle-like structure, this structure more pronounced when increased the concentration. Surface morphology of the film prepared using solution concentration 0.5 % (w/w) with thickness 5.64 nm resulted in the root mean square (RMS) roughness ($S_q$) 0.865 nm and 0.867 nm for liquid- and air-interface, respectively. The $S_q$ of the

film prepared from 0.5% (w/w) was relatively larger and we believe that low polymer concentration decreases the solidification speed, giving more time to polymers assemble by themselves and grow by the static mode, as explained elsewhere.[54] The increasing polymer concentration in the solution at a certain concentration results in uniform polymer distribution in a large area because expansion and solidification of polymer in the droplet were in balance which was approved by decreasing $S_q$.

At a certain concentration/film thickness, the rms roughness of both interfacial morphologies of the floating film was slightly different. The $S_q$ of the air interface was a comparatively less than the $S_q$ of the liquid interface and is attributed the friction force arising from the liquid substrate. Increasing the film thickness offer less influence of friction force from the liquid substrate on the most top layer/air interface of floating film. Since the $S_q$ of all thin films was less than 1 nm, which is sufficient for OFFET devices. Several studies have been established to reveal the effect of the conjugated semiconductor roughness on the device performance, and they found the field-effect mobility will only be effected when the roughness are in the range of 1 to 4 nm. [82,97,98,99]

Another interesting finding of UFTM is its ability to orient the polymer in a thin film with a thickness of up to 29.8 nm, which corresponds to a solution concentration of 3% (w/w). However, to confirm the orientation distribution over the thickness, anisotropy in field-effect mobility using BGTC and TGBC needs to be evaluated with different film thicknesses.

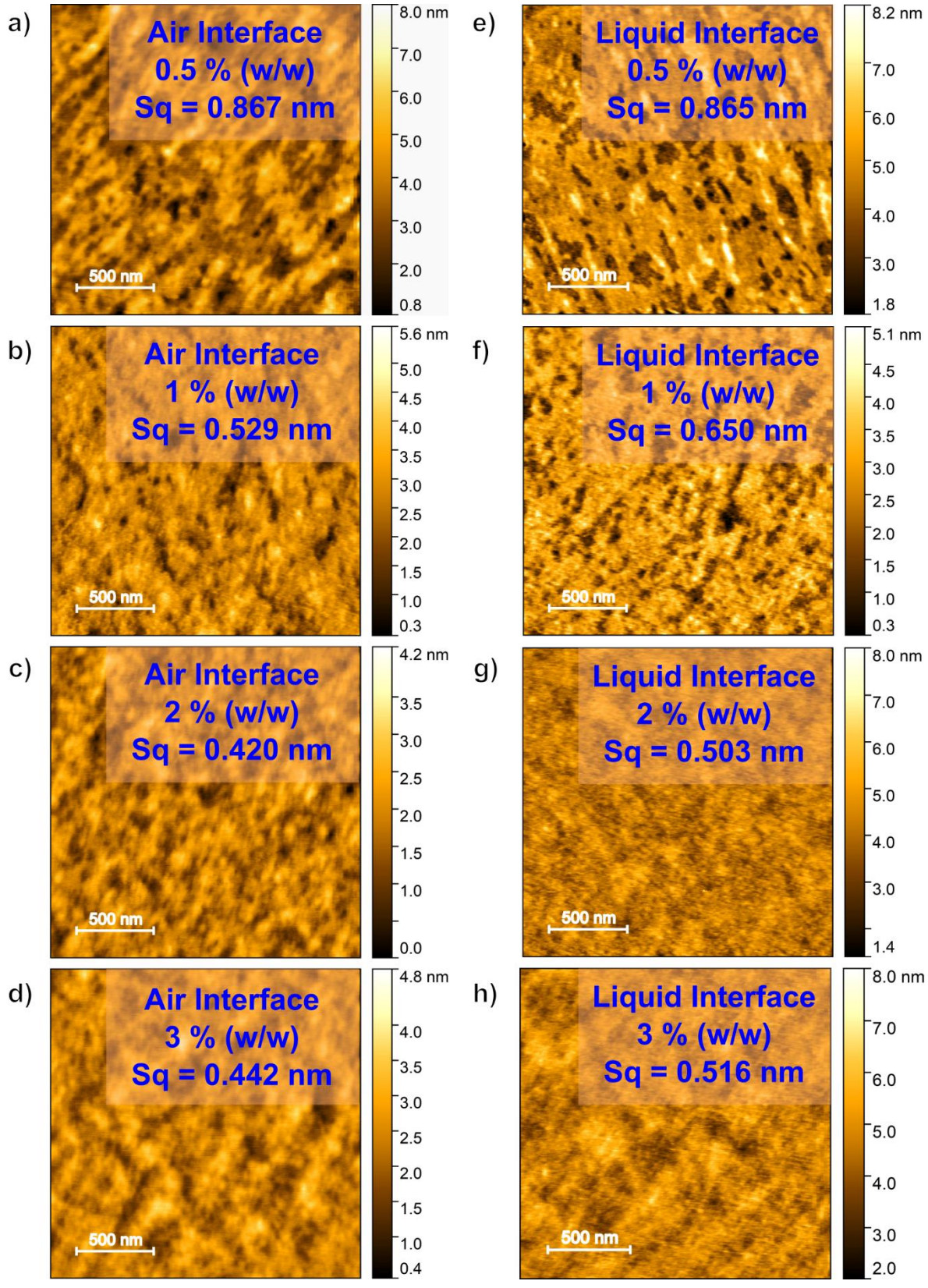


**Figure 4.3. Contact-mode atomic force microscopy image of the liquid interface (a) – (d) and air interface (e) – (h) of the floating film formed with different polymer concentration. From (a) to (b) and (e) to (h) the polymer concentrations were 0.5, 1, 2, and 3 % (w/w), respectively**

**Figure 4.4 (a) and (b)**. show illustration schematic of OFET with structure BGTC and TGBC fabricated with different PQT film thickness clearly exhibited the typical transfer characteristic of a p-type OFET with negligible hysteresis and similar on/off ratios in the order of $10^5$ for the channel aligned in parallel with the polymer orientation, as shown in **Figure 4.5 (a) and (b)**. Field-effect mobility in the saturation regime for PQT films with orientation parallel/perpendicular to the channel direction is presented in **Figure 4.5 (c) and (d)**. Anisotropic charge transport with high field-effect mobility with orientation direction parallel to channel direction can be clearly seen. The highest average mobility achieved in PQT PETs with BGTC and TGBC structure was 0.035 $cm^2/Vs$ and 0.029 $cm^2/Vs$, respectively. In comparison with the benchmark value of PQT-C12 (>0.1 $cm^2/Vs$), relatively low mobility in this report could be related to many other parameters that should optimized; such as molecular weight, polydispersity index, dielectric/semiconductor interface, channel length, and fabrication condition, etc. other than polymer chains orientation, which their optimization is beyond the scope of present study.[100,73]

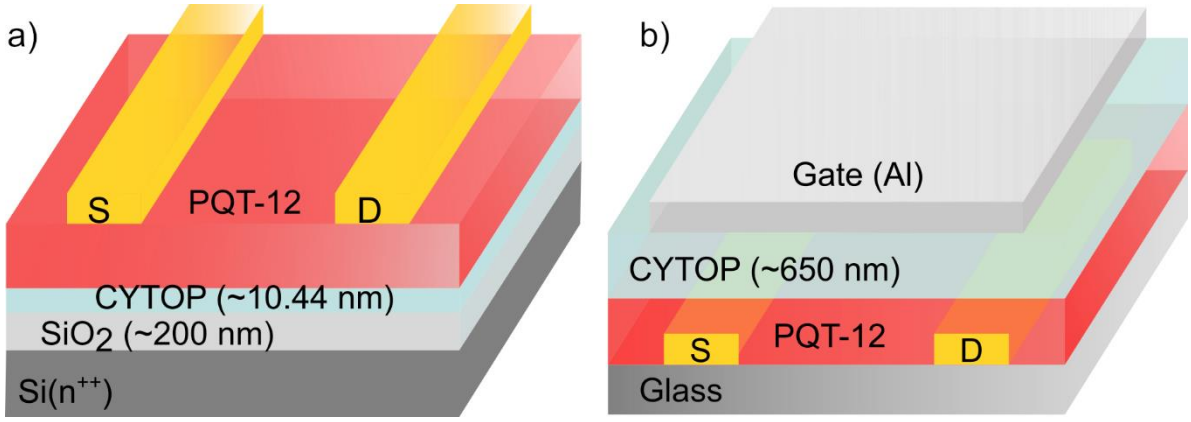


**Figure 4.4. Schematic diagram of fabricated (a) bottom-gated top-contact (BGTC) and (b) top-gated bottom-contact (TGBC) OFET device.**

Result shown in **Figure 4.5** suggests that a charge transport in the OFET occurs in semiconductor near the dielectric/semiconductor interface as only with ~5.6 nm thick film of semiconducting polymer containing 2~3 layers of edge-on stacked interdigitated PQT is sufficient for charge transport as discussed in the previous chapter. **Figure 4.5 (c) and (d)** showed that field-effect mobilities of devices with the channel direction aligned in parallel did not changed significantly even when the DR of the corresponding PQT film changed significantly. This indicates there exist some limitation on the polymer alignment to effect the overall charge transport in an oriented thin film after certain DR is achieved.

**Figure 4.6 (a)** showed the evaluation of anisotropy in field-effect mobility ($\mu_{\parallel}/\mu_{\perp}$) at liquid-interface and air-interfaces with different polymer thickness in BGTC and TGBC OFETs. The $\mu_{\parallel}/\mu_{\perp}$ trend is similar for BGTC and TGBC OFETs at each film thickness. These results indicate that the UFTM method capable of orienting the polymer throughout the film thickness and not only near the liquid substrate and which is maintained even when the film thickness increased up to around ~30 nm.

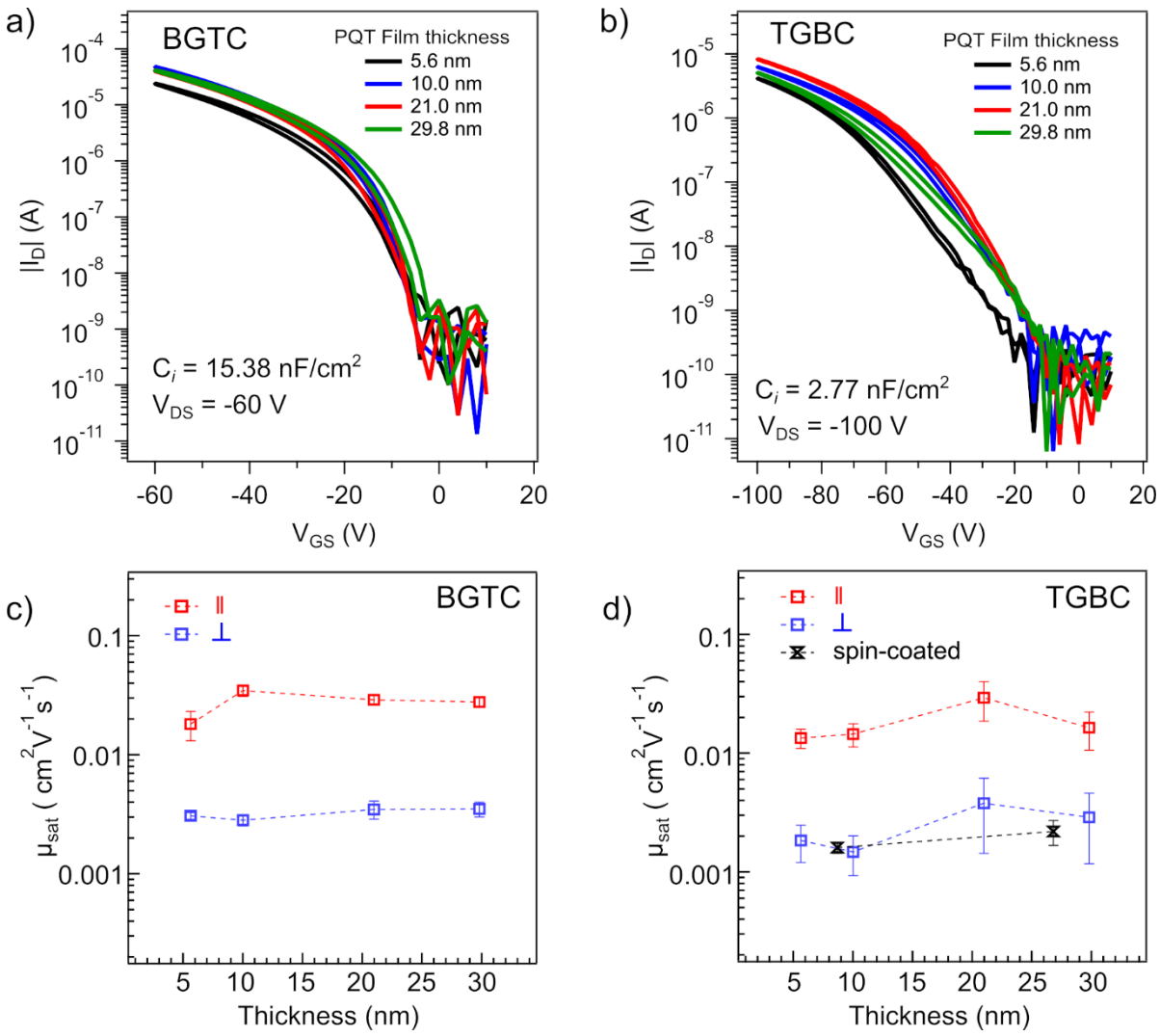


**Figure 4.5. Transfer characteristic of the OFET devices with channel ∥ to the polymer orientation as function of the film thickness for (c) BGTC and (d) TGBC architecture. Average $\mu_{sat}$ of OFET devices with channel ∥ and ⊥ for (e) BGTC and (f) TGBC.**

Many researchers have studied thickness-dependent performance in OFETs, and the relation between thickness and field-effect mobility depends on several parameters. [85,88,89] In this work, we found that the field-effect mobility in PQT channel aligned in parallel with polymer orientation slightly changed with film thickness; meanwhile, the DR changed largely. This finding suggests that after achieving a certain value of DR, the charge transport in the semiconducting polymer will not increase significantly due to a presenting of amorphous

parts/tie chains. These tie chains providing interconnecting transport pathways between crystalline domains in the PQT thin film that facilitates charge transport.[101,102]

**Figure 4.6 (b)** shows the possible charge transport mechanism in the PQT film. When the channel direction was aligned along the orientation direction, we assumed that the charge would be transported through π-conjugations, tie chains, and π-π stackings. The most contribution in charge transport is through π-conjugations that give the fastest transport, and the tie chain facilitates the transporting of charge from one crystalline domain to another. At the same time, the π-π stackings help in charge transport when there is discontinuity of the $\pi$ -conjugations in the crystal domain. This assumption is in line with the observation that a large drop in DR value does not reduce value of $\mu_{\parallel}$ significantly. In any case, the charge will be passed π-π stackings and tie chains when the channel direction is aligned perpendicularly to the orientation direction. Thus, the π-π stackings are the most widely used pathway for charge transport, while tie chains support transporting between crystal domains.

In the FTM method, the film is grown on a liquid substrate, providing more freely moving for the polymer molecule during the film formation. This freedom of movement affords the ability of the polymer chains to uniformly self-assembly with the direction of arrangement of the polymer chains perpendicular to the direction of polymer dispersion and over the entire film thickness. Furthermore, the uniqueness of a growing mechanism of the film on a liquid substrate provides the same degree of orientation at the film on the liquid substrate interface and air interface. Therefore, the orientation characteristics of the UFTM film will provide the same performance to OFET devices with top gate and bottom gate structures.

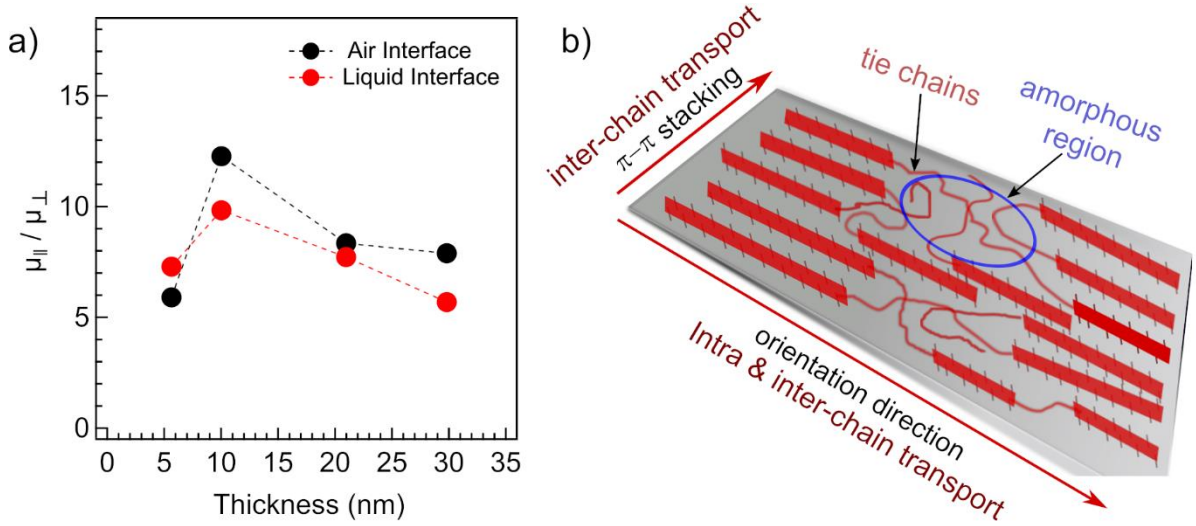


**Figure 4.6. (a) The ratio of $\mu_{\parallel}$ to $\mu\perp$ ($\mu_{\parallel}/\mu\perp$) of PQT FETs in various PQT film thickness with the structure of BGTC (air interface) and TGBC (liquid interface), and (b) schematic illustration of the possible charge transport mechanism in oriented PQT films.**

### 4.4 Conclusions

In summary, we have confirmed that UFTM method could orient the polymer in a thin film for the entire film thickness, which imparts similar anisotropic properties at the liquid-air interface that means throughout the thickness of the film. This method is also suitable for the fabrication of OFET devices with BGTC and TGBC structures. We have also revealed that once the DR of the thin films reach a certain value, the parallel mobility will not increase significantly by increasing the DR further as the existing tie chains also assist in charge transport.

# Chapter 5. Assisting Orientation of Conjugating Polymer Using Polymer Blend

## 5.1 Introduction

In thin films of semiconducting polymers, mostly carrier transport occurs via the π-conjugated backbone and helped by tie chains, inter-chain, and inter-domain hopping. [55,58,103] In the last decade, many tremendous scientific efforts were made to fabricate thin films of oriented polymers for their various applications, which resulted in the development of many different orienting methods. [12,31,104] For that reason, several solution-based oriented film fabrication methods were developed, which offer convenience and cost-effectiveness for high-performance optoelectronic devices. [12,54]

Pre-aggregation in solution is essential for directing the polymer chains in the film. In general, marginal solvents are used to form polymer aggregates in solution, making this process difficult because the solubility of semiconducting polymers is very sensitive to the chemical structure of the conjugated backbone and side chains. Therefore, most reports based on a single semiconducting polymer system orientation are mainly reported. [10,12,51] However, multi-component systems are sometimes important in obtaining various optoelectronic characteristics, which is difficult to do over single materials. [105–107] In addition, several reports have shown an increase in film crystallinity of organic small molecules and semiconducting polymer by blending them with amorphous or insulating polymers to provide a polymer base matrix during film fabrication. [9,108–110]

The floating-film transfer method (FTM) was reported as an easy orientation technique. [38,39] In FTM, a drop of polymer solution is placed on a hydrophilic liquid substrate with high surface tension, and the solution is spread over it. The viscous pull acting against the direction

of film expansion leads to the orientation of the polymer backbone resulting in an oriented floating film. In addition, simultaneous solvent evaporation promotes self-alignment during the transition from solution to solid phase through the lyotropic liquid crystal (LC) phase improving the overall orientation. Semiconducting polymers with LC characteristics have shown better orientation ability in FTM.[60] However, not all CPs exhibit LC phase transition characteristics.

This chapter reported an examination of the versatility of UFTM in assisting the orientation of guest semiconducting polymer in the well-oriented host semiconducting polymer matrix during thin film fabrication. Examination of the backbone orientation degree in the film was conducted via polarized UV-vis-NIR absorption spectroscopy. Therefore, to differentiate the orientation degree in the blends, semiconducting polymers with an absorption spectrum that does not overlap with the visible absorption peaks were chosen. Experiment details and further discussion regarding the obtained results were presented in the next sub-chapters.

## 5.2 Experiment Details

### 5.2.1 Materials and films preparation

*Polymer material and solvent:* poly(3,3‴-didodecyl-quaterthiophene) (PQT-C12) and anhydrous chloroform were purchased from Sigma Aldrich, Japan without any further purification. Poly(9,9-di-n-octylfluorenyl-2,7-diyl) (PFO) was synthesized by Suzuki-Miyaura coupling having the weight-average molecular mass ($M_w$) of 58 Kg/mol and polydispersity index of (PDI) of 3.31 measured using gel permeation chromatography calibrated by Polymethylmethacrylate standard [37]. Poly[2,5-(2-octyldodecyl)-3,6-diketopyrrolopyrrole-alt-5,5-(2,5-di(thien-2-yl)thieno[3,2-b]thiophene)] (DPPT-TT) was synthesized as per the reported literature having the $M_w$ and PDI of 92 Kg/mol and 2.45 [35]

*Chemicals for liquid substrate in UFTM:* Ethylene glycol (EG) and glycerol (GL) were purchased from Fujifilm Wako Pure Chemical Corporation, Japan. Both chemicals were mixed with a ratio of EG and GL was 3:1. The temperature of this liquid substrate was maintained at 55 ℃ before used for film casting.

*Chemicals for SAM treatment:* Octadecyl(trichloro)silane (OTS) with purity >90%, and 1-octadecene technical grade 90% were purchased from Sigma Aldrich, Japan without any further purification. Super dehydrated chloroform and cyclohexane super dehydrated were purchased from FUJIFILM Wako, japan.

*Substrates*: Glass substrates were washed in ultrasonication bath of acetone for 10 minutes, followed by rinsing in hot acetone. Improving the surface hydrophobicity was conducted by immersing them in the solution of 160 $\mu$l OTS into 40 ml of octadecene under a nitrogen atmosphere for 3 hours, followed by properly washing in an ultrasonication bath of a mixture of super-dehydrated chloroform and cyclohexene in ratio 1:1 twice, and one time in super-dehydrated chloroform for 10 minutes in each process. Then the substrates were dried at 150 ℃ for 15 minutes before using them in a further process.

*Polymer solutions:* Polymer solutions were prepared by dissolving in anhydrous chloroform 1 % (w/w) and kept with a magnetic stirrer on a hotplate of 60 °C for 30 minutes to ensure the complete dissolution. Polymer blend was prepared by mixing the polymer solutions in different ratios (%, v/v). A similar method was used to increase the overall concentration of polymers to 2% (w/w).

*Polymer films:* Approximately 10 $\mu$l of solutions were dropped near the edge of the center of the tilted bottom slider wall and liquid substrate interface. The droplet solution will spread unidirectional to form a large area of the thin film. The substrate was held with tweezers, then, carefully placed on the floating film to transfer it to the substrate.

5.2.2 Characterization

Polarized absorption spectra measurements were conducted by using UV-vis-NIR spectrophotometer (JASCO V-770DS) be equipped with polarizer. Thickness measurement, surface topography and phase images were measured via atomic force microscope (AFM) using SPM-9600 Shimadzu, Japan. Orientation degree/DR was calculated from the polarized UV-vis absorption spectra using **Equation 2.7 in Chapter 2**.

## 5.3 Results and Discussions

In this work, thin films were fabricated using the UFTM method, a schematic illustration of the UFTM mechanism shown in **Figure 5.1 (a)**. To examine the ability of the UFTM method to orient the guest polymer through a blending approach, PQT was used as the host polymer, PFO, and DPPT-TT as the guest polymer. Then, by mixing each guest polymer into the host polymer, each guest polymer's degree of orientation or DR value increased. The naked eye confirmed macroscopically oriented film perpendicular to the film spreading direction by placing a polarizer film in front of the film. In addition, the degree of polymer chain alignment was confirmed utilizing polarized UV-vis-NIR absorption spectroscopy. When the direction of polarization of the incident light was parallel to the polymer backbone ($A_{\parallel}$), maximum absorption was observed. on the other hand, the minimum absorption was observed when the direction of the incident light polarization was perpendicular to the polymer backbone ($A_{\perp}$).

**Figure 5.1** shows the absorption spectrum of the PQT films coated by the ribbon-shaped and spin-coated FTM, in which the PQT thin-film highly aligned with DR 11.68 ± 1.26. In addition, a $\lambda_{max}$ at 543 nm with a shoulder of about 602 nm was observed in the UFTM-formed PQT films, whereas the spin-coated PQT films had the $\lambda_{max}$ at the same wavelength

with relatively weak shoulders. The more prominent spectra on the UFTM film were due to highly ordered lamella stacking, which makes the interactions between the chains better. In addition, there was also an increase in the effective conjugate length and an increase in intermolecular interactions, as indicated by a red-shift of the main peak and an increase in shoulder vibration, respectively. [32,39,111]

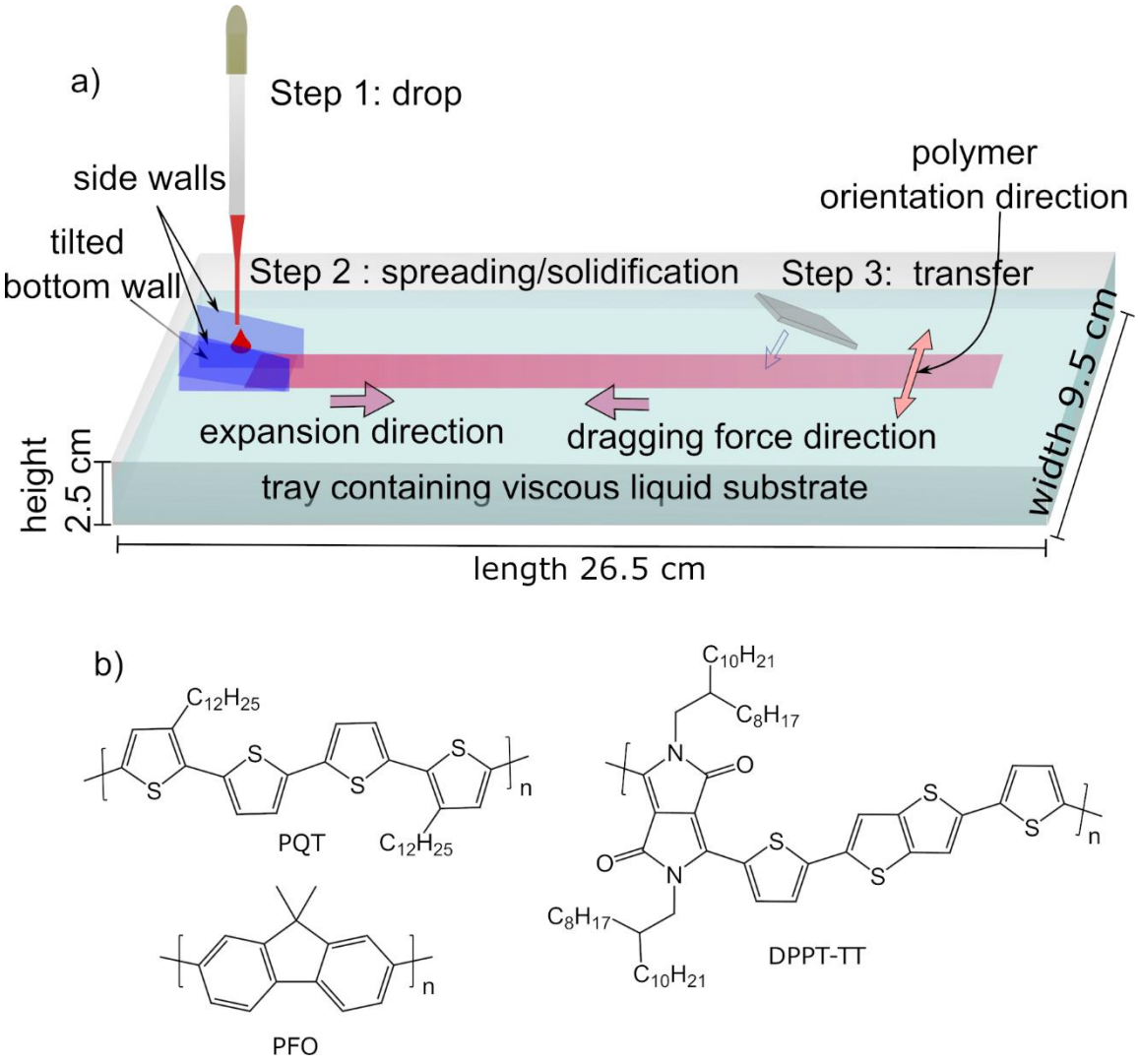


**Figure 5.1. (a) Schematic illustration of floating film transfer method. (b) Chemical structure of the different conjugated polymers utilized in this work.**

For PFO thin film with a similar casting condition resulted in a low DR of 2.94 with $\lambda_{max}$ at ~390 nm; this DR slightly better than the results reported by Arnaud et al. [37] These results agree with the results reported by Arnaud et al., where they performed the FTM procedure using a petri dish. In our case, we failed to observe the presence of the $\beta$-phase in the PFO. [37,112] It should be noted UFTM films are highly reproducible with negligible variations in thickness or DR. [32]

It has been reported that the orientation ability of thiophene-based polymers is highly dependent on two things i) the liquid crystal properties and ii) the interdigitation characteristics of the side chains to provide free movement of the polymer backbone in solution during the simultaneous phenomenon of solution expansion (spreading) and drying processes occurring in the FTM. [111] Analysis of polymer orientation in thin films has been extensively investigated by calculating DR using polarized UV-vis absorption spectroscopy. Therefore, to analyze the orientation of the individual components in an oriented polymer blend, the individual polymers in the blend must have different absorption ranges. As we can see in **Figure 5.2 (a) and (b)**, most of the absorption ranges of PQT and PFO did not overlap and could be used for this study, where the pristine PQT FTM films have high DR, and pristine PQT FTM films have low DR. It has also been reported that PFOs have liquid crystal properties and a tendency to align.

As the absorbance tail of PQT lies below 400 nm (**Figure 5.2 (a)**), therefore, to estimate the DR of PFO in the blend, it was necessary to reduce the contribution of PQT in the absorbance spectrum of the blending. To do this; first, the absorbance peak || or on pure PQT in **Figure 5.2 (a)** normalized according to the absorbance peak || on the PQT PFO blend shown in **Figure 5.2 (c)** and then subtracted to get the absorbance spectrum || of the PFO in the blend, the similar procedure was carried out to obtain the absorbance $\perp$ of the PFO in the blend, the result of this reduction was shown in **Figure 5.2 (d)**.

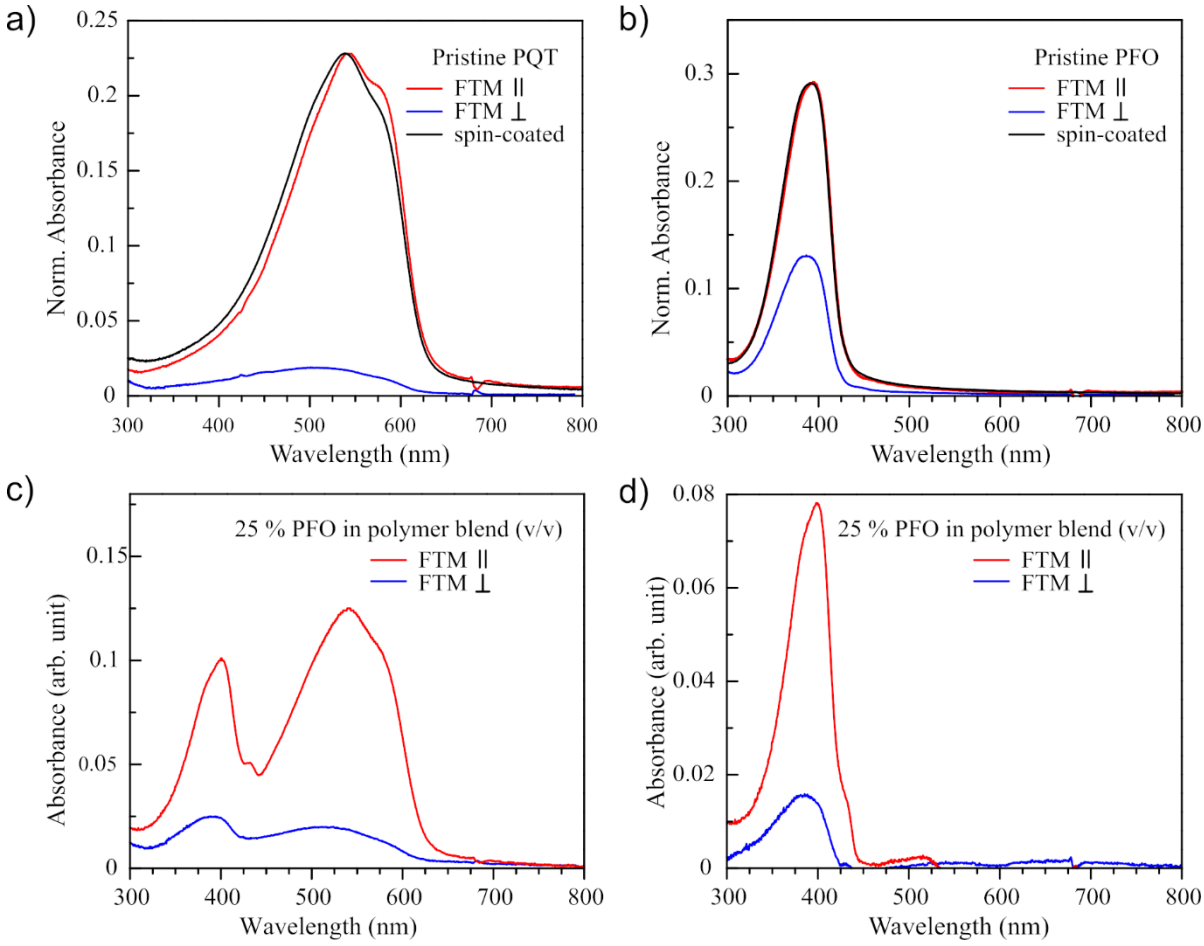


**Figure 5.2. Polarized UV-Vis absorption spectra of FTM and spin-coated pristine PQT (a) and PFO (b) films. (c) Polarized absorption spectra of FTM film of PFO: PQT (1:3) blend. (d) Polarized spectra of PFO extracted from blend obtained after subtraction of PQT contribution in the blend. In each case, || and ⊥ represent light polarization parallel and perpendicular to the polymer orientation direction, respectively.**

**Figure 5.3 (a) and Table 5.1** show the DR of the PFO ($DR_{PFO}$) with various blending ratios of polymer and overall polymer weight in solution. When the PFO amount was ≤25% of the polymer blend, $DR_{PFO}$ was >4. $DR_{PFO}$ was even found to be >8 when the PFO amount was ≤ 10% in the blend. On the contrary, the overall DR of the PQT ($DR_{PQT}$) began to decrease linearly. These results reflect that because PQT has a high self-assembly tendency at the macroscopic scale, it tends to assist the orientation of the guest polymer, namely PFO, by 2−4 times. Moreover, because both polymers were well dissolved in chloroform, we failed to notice any phase separation. For that reason, we believe that PFOs, when added in small amounts, tend

to be between PQT macromolecules, and PQT's orientational ability promotes PFO macromolecular alignment. In any case, for the 40% PFO in the blend, we speculated that the decrease in $DR_{PFO}$ must have been due to the high entanglement between the PFO macromolecules, and consequently, the DRPQT was also decreased.

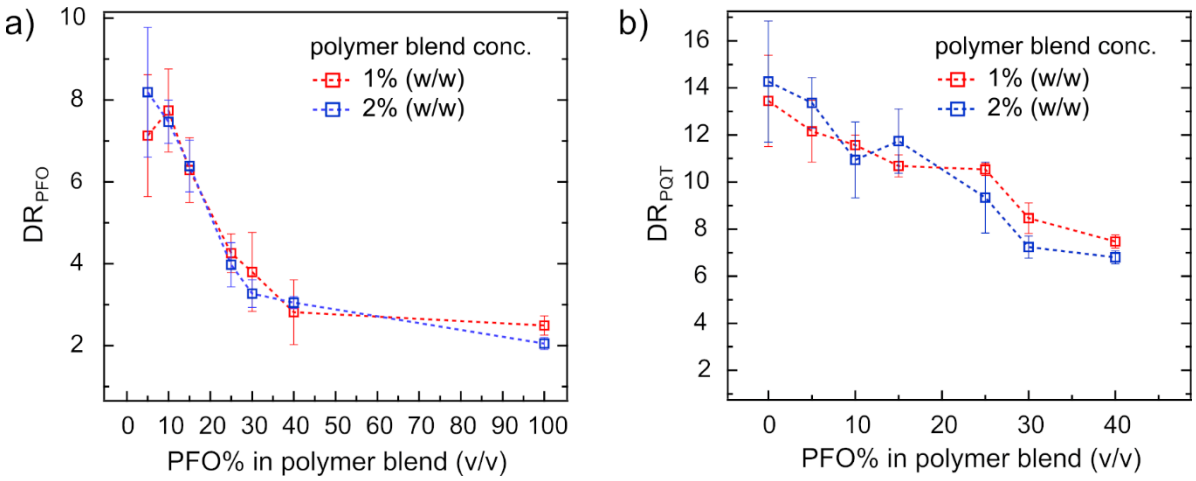


**Figure 5.3. Variation of $DR_{PFO}$ (a) and $DR_{PQT}$ (b) with increasing PFO ratio in PFO:PQT blend.**

**Table 5.1. DR of pristine PFO, PQT, and their blend with the increasing amount of PFO.**

| Polymer Concentration | PFO % in blend[a] | PFO DR[b] | PQT DR[b] |
|---|---|---|---|
| 1 wt% | 0% (Pristine PQT) | - | 13.45 ± 1.94 |
| | 5% | 7.13 ± 1.49 | 12.16 ± 1.31 |
| | 10% | 7.74 ± 1.01 | 11.57 ± 0.43 |
| | 15% | 6.29 ± 0.79 | 10.69 ± 0.47 |
| | 25% | 4.26 ± 0.47 | 10.54 ± 0.26 |
| | 30% | 3.80 ± 0.96 | 8.47 ± 0.65 |
| | 40 | 2.82 ± 0.79 | 7.47 ± 0.28 |
| | 100% (Pristine | 2.49 ± 0.23 | - |

| Polymer Concentration | PFO % in blend[a] | PFO DR[b] | PQT DR[b] |
|---|---|---|---|
| | PFO) | | |
| **2 wt%** | 0% (Pristine PQT) | - | 14.27 ± 2.57 |
| | 5% | 8.19 ± 1.58 | 13.36 ± 1.08 |
| | 10% | 7.47 ± 0.53 | 10.94 ± 1.61 |
| | 15% | 6.39 ± 0.63 | 11.74± 1.37 |
| | 25% | 3.98 ± 0.54 | 9.34 ± 1.50 |
| | 30% | 3.27 ± 0.34 | 7.24 ± 0.47 |
| | 40 | 3.05 ± 0.15 | 6.80 ± 0.42 |
| | 100% (Pristine PFO) | 2.05 ± 0.16 | - |

[a]Individual polymer solution was prepared by dissolving them in the solvent (%, w/w) and then mixed (%, v/v) to prepare the blend. [b]DR was calculated from at least 3-4 films.

Although there have been several reports of blending polymer/polymer and polymer/small molecule, it has shown phase separation and increased interactions between polymer chains. [113,114] Contrary to this, as shown in **Figure 5.4 (a)**, $A_{0-0}/A_{0-1}$ of PQT continued to decrease with the increasing amount of PFO in the blend, which revealed that intermolecular interactions between PQT macromolecules decreased with the addition of PFO in the blend. Therefore, this evidence supports our hypothesis that PFO macromolecules were somehow located in-between PQT macromolecular groups and were not phase separated even when PFO accounts for 40% in the polymer blend.

It has been reported that there was a dependence of polymer concentration on DR NR-P3HT; it found that polymer concentration changes the overall thickness of the film and the solidification rate of the polymer solution when spread on a liquid substrate. [115] The contribution of polymer concentration to film thickness is difficult to measure and can change from one polymer to another. However, in this case, as the overall polymer solution concentration increased, the corresponding thickness increased, as shown in **Figure 5.4 (b)**. It should be noted that this increase in film thickness was possible without major changes in the

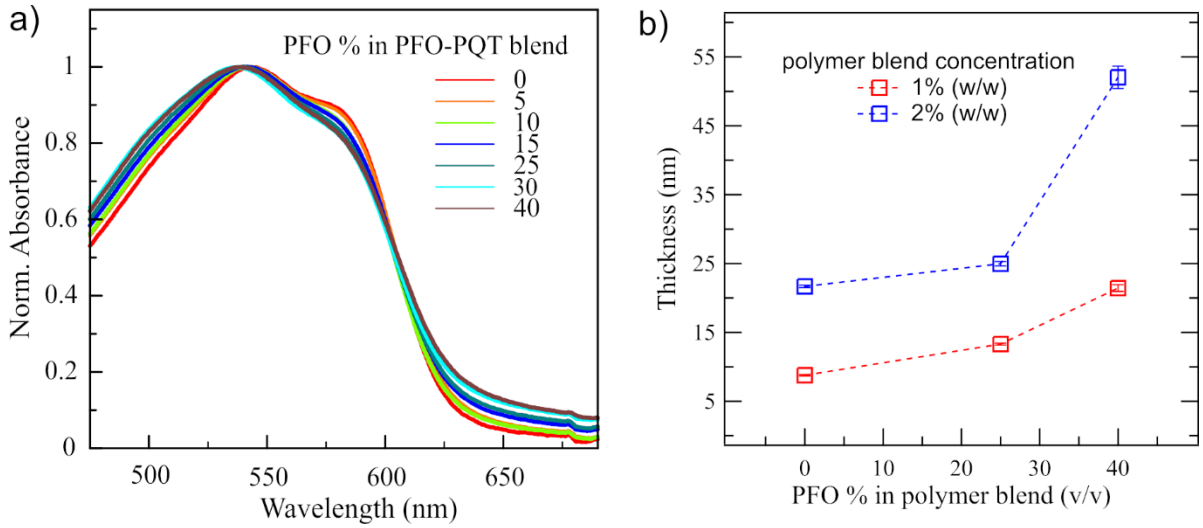


**Figure 5.4. (a) Normalized spectra of PQT for $A_{0-0}/A_{0-1}$ comparison. (b) Variation of film thickness with increasing PFO ratio in PFO:PQT blend.**

overall DR, as shown in **Figure 5.3 and Table 5.1**. Moreover, the film thickness in FTM can also be controlled by layer-by-layer deposition because the film preparation procedure is not dependent on the substrate, as previously reported.[60]

To evaluate the validity of this technique, another polymer DPPT-TT was also mixed in small amounts with PQT; the results are shown in **Figure 5.5**. The maximum DR obtained with DPPT-TT pristine is 1.6. DPPT-TT does not have LC behavior. It has been reported that semiconductor polymers that do not have LC behavior are oriented at a very low extent, such as RR-P3HT and poly[4,8-bis[(2-ethylhexyl)oxy]benzo[1,2-b:4,5-b']dithiophene-2,6-diyl][3-fluoro-2-[(2-ethylhexyl)carbonyl]thieno [3,4-*b*]thiophenediyl].[34,111] Therefore, it is easily understood that the low DR might due to the above considerations.

Similar to PFO, DPPT-TT was also blended with PQT, and the polarized UV-Vis-NIR absorption spectrum was shown in **Fig. 5.5 (b).** DR DPPT-TT increased to 2.6 in the blend with a weight ratio of 10% DPPT-TT in the blend of DPPT-TT and PQT. In addition, there was a redshift from 802 nm to 824 nm in $\lambda_{max}$ of DPPT-TT. The wavelength feature at ~802 nm is associated with the ground state absorption set as 0-0 ($\pi$-$\pi^*$ transition). The low wavelength

feature set for the shoulder as 0-1 aligns with the previous literature for DPPT-TT and many derivatives. [116–118] The increased relative intensity of the 0-0/0-1 absorption feature of DPPT-TT in the mixture compared to the pure film. These results suggest that the increase in the effective conjugation length and highly ordered DPPT-TT macromolecules enhance the intermolecular interactions in the polymer blend. Based on the results obtained for PFO and DPPT-TT, when blended with highly ordered PQT, their features related to the absorption spectrum reflect an increase in effective conjugation and inter-chain interactions.

The cantilever oscillates over the sample surface in AFM tapping mode/dynamic mode without touching. The cantilever oscillates at high frequencies near its resonant frequency. This particular interaction is important for soft materials such as polymers, as they are less damaging to the sample. The advantage of AFM dynamic mode is that it can generate the topographic and phase images simultaneously. The surface morphologies of the thin films prepared by pristine and blended polymers using the UFTM were investigated by AFM tapping mode with scanning size $2 \times 2\ \mu m^2$.

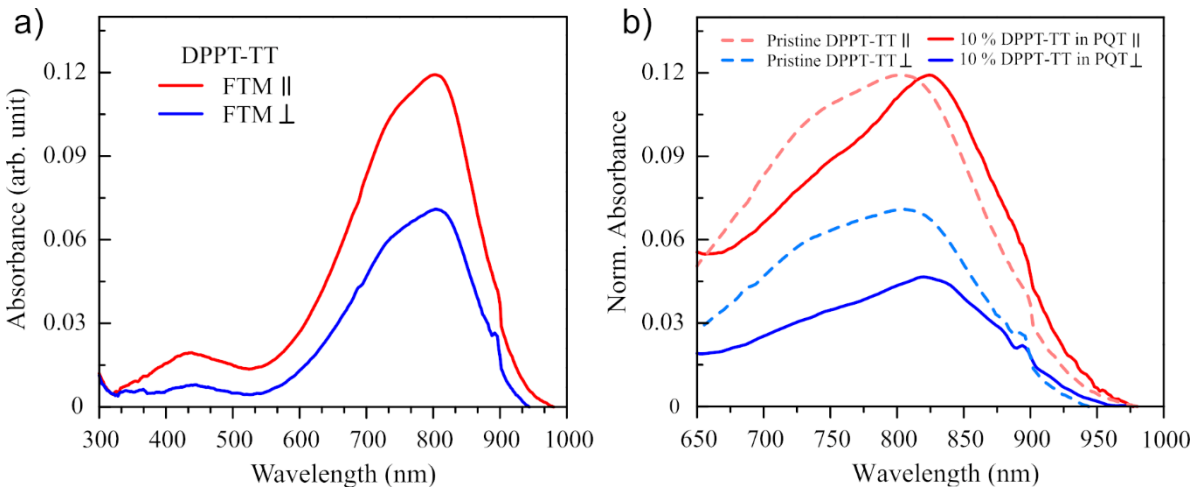


**Figure 5.5. (a) Polarized UV-Vis-NIR spectra of FTM coated pristine DPPT-TT (b) Polarized UV-Vis-NIR spectra of FTM coated film with DPPT-TT 10% in DPPT-TT:PQT blend. The dotted line in (b) represents the spectra of FTM coated pristine DPPT-TT for comparison. In each case, || and ⊥ represent light polarization parallel and perpendicular to the polymer orientation direction, respectively.**

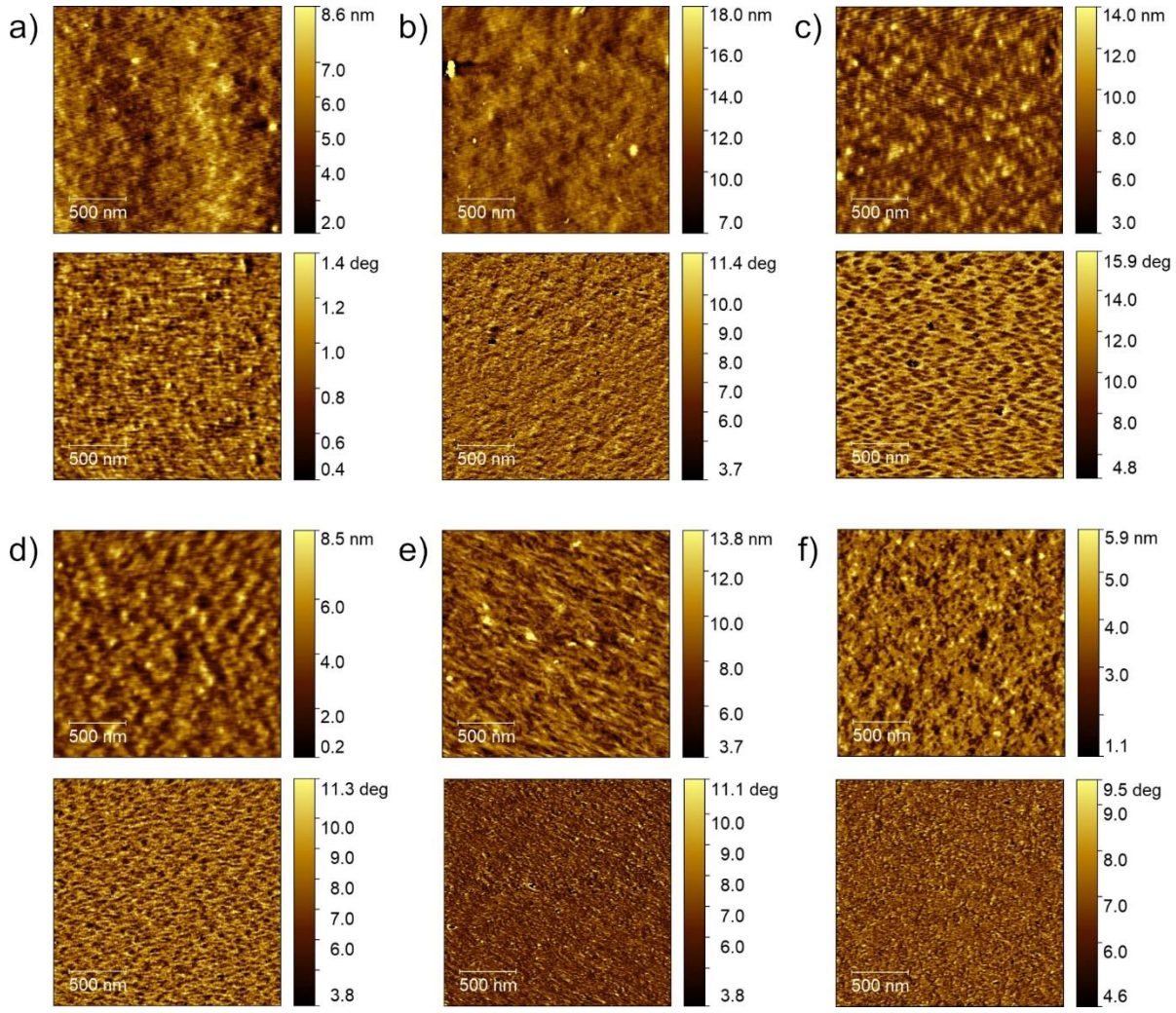


**Figure 5.6. AFM height and phase image of FTM films. (a) Pristine PQT, (b) Pristine PFO, (c) PFO 25% in PFO:PQT blend (d) PFO 40% in PFO:PQT blend, (e) Pristine DPPT-TT, and (f) 25% DPPT-TT in DPPT-TT:PQT blend. Scan area is 4 μm$^2$, and the scanning direction was parallel to the polymer alignment direction.**

The results of the AFM scan are presented in **Figure 5.6** AFM images generated from pristine polymers or films with a lower proportion of PFO in PQT show featureless and no particular texture. This is because the surface roughness of the polymer blends be in between the roughness of the individual pristine polymer films and seen no phase separation along the lateral direction due to the high solubility of the polymer in chloroform. It is believed that even if there is a nanoscale phase separation, it must be reflected in the form of increased interchain

interactions. Therefore, these results agree with the results obtained with the absorption spectrum shown in **Figure 5.4,** where we see a decrease in intermolecular interactions between the individual polymers.

## 5.4 Conclusions

In conclusion, the alignment of the guest polymers can be easily controlled in the FTM method using a polymer blending approach. Blending PFO into PQT helps improve PFO alignment; DR of PFO increased ~ 2 – 4 times. The increasing DR also found in another CP DPPT-TT having no LC-characteristic when it blended into PQT polymer. Both PFO and DPPT-TT as a guest polymer were well-mixed into the PQT as host polymer without any phase separation. Assisting ability of polymer alignment could be maintained even with increasing film thickness. The polymer blending approach in FTM provides a strategy to investigate future electronic properties and offer low-cost and large-area films in terms of fabrication.

# Chapter 6. General Conclusion and Future Work

## 6.1 General Conclusion

This thesis presents the work's results to investigate the characteristics and orientation mechanism of the oriented semiconducting polymer thin films formed by UFTM. The method under development is solution-based and is capable of producing highly oriented and large-area thin films. With the capabilities that have been presented, this method seems to have good potential for making significant contribution in the development of the organic electronics device fabrication. Several characterization methods have been utilized to investigate the characteristics of oriented thin films, including; polarized UV-vis-NIR absorption spectroscopy, atomic force microscopy, and X-ray diffraction. In addition, to analyze the effect of thin-film microstructure on electrical parameters, various types of organic thin-film transistors (OFETs) have been fabricated and analyzed.

The first chapter of this thesis provides brief information about the motivation in developing the electronics sector in the global industrial market and the reasons for the electronics industry players to develop electronic products based on organic semiconductor materials. Examples for electronic products based on organic materials, reports on its total trade in 2020 along with its predictions in 2030, and companies that produce electronic products made from organic are given in the first subsection. In addition, this chapter also provides a brief introduction to semiconductor organic materials, a brief introduction to the orientation of semiconductor polymer molecules in thin films to obtain improved performance of polymer-based electronic devices, and a brief theory of the organic device of field-effect transistors. Finally, at the end of this chapter, the writer gives a brief motivation for doing this research work and outlines this thesis.

The second chapter contains information on the polymers and chemicals used, sample preparation techniques, and characterizations carried out in work reported in this thesis.

In the third chapter, we demonstrated the ability of UFTM to produce highly uniform oriented PQT thin films with a large area (≈40 $cm^2$). The uniformity of the resulting large-area films was revealed by the results of 2-D position mapping of the absorption peaks and AFM images. We reveal that most of the central regions covering 70% of the entire film width have uniform orientation characteristics. In edges regions, the molecular orientation directions were nearly orthogonal to those observed in the center. Furthermore, the orientation characteristics of the polymer molecular using angle-dependent UV-vis absorbance spectrum measurements correspond to the results of angle-dependent field-effect mobility measurements. This chapter also showed that OFETs fabricated in two rows along a single film with an area of ≈15 × 2.5 $cm^2$ had uniform field-effect mobility, with an average of 0.0262±0.0033 $cm^2$/Vs. In addition, PQT FETs fabricated from UFTM films did not show significant performance differences concerning film thickness variations, and even 10 nm thick films offer highly reproducible results in terms of device performance.

The fourth chapter discussed the growth mechanism of highly oriented thin films and the anisotropy of charge mobility at the surface interfaces, i.e., the liquid interface and the air interface. For this purpose, OFETs with BGTC and TGBC configurations were fabricated, and their mobility anisotropy was analyzed. The mobility anisotropy of OFET with BGTC and TGBC configurations represents the anisotropy of charge mobility at the liquid interface and the air interface, respectively. Although the film thickness increased up to ~30 nm, there was no significant difference in charge transport anisotropy or field-effect mobility for the overall film thickness, indicating that the SCPs in UFTM were oriented at both interfaces. In other words, the orientation of the polymer in the UFTM film is uniform throughout the film thickness.

These results simultaneously validate that UFTM could be utilized to fabricate OFETs with BGTC and TGBC configurations and provide performance that is not much different.

In chapter five, the discussion focuses on testing the versatility of UFTM in assisting guest SCP orientation in a well-oriented host SCP blend. In this work, thin films were prepared by UFTM using a blending solution of PFO and/or DPPT-TT with PQT. Interestingly, the orientation of PFO and/or DPPT-TT can be in-situ assisted by blending with PQT during film formation, as evidenced by the increased DR of the two guest polymers (PFO/DPPT-TT). Furthermore, the DR of the host SCP decreases monotonically with an increase in the guest SCPs proportion, suggesting that guest polymers are well mixed in the host matrix without any phase separation. Finally, although the film thickness is increased by increasing the polymer solution concentration, assisting capabilities of the polymer can be maintained. With these results, we believe the characteristics of FTM are favorable, and many unique properties can be found in devices using this approach.

### 6.2 Future work

Recently, many researcher achieve the OFET mobility of conjugated polymers > 10 $cm^2/(V\ s)$ by molecular design strategies such as side chain engineering, chemical substitution, and donor-acceptor polymer-based. However, such polymers are difficult to get in the market. Our motivation in this work is in dept study of a new developed method to prepare a large area thin film with high orientation. PQT is a conjugated polymer that has been reported to have high orientation capability when prepared using the floating film transfer method (FTM) and is easy to obtain. This report shows that the PQT films prepared using the FTM method have the mobility of 10 times greater than those prepared using the spin-coating method. This increased mobility is due to the film prepared using the FTM method having a polymer backbone arrangement in one direction. As a result, the charge transport is maximum along this conjugate

chain. Further work of interest is to use the FTM method to prepare thin films of polymers that are reported to have high mobility.

UFTM offers several advantages in preparing polymer thin films, such as; easy to control the film thickness, the resulting film is large and highly oriented, does not require sophisticated equipment, and low production costs. In addition, the characteristics of the film formed are not affected by the substrate used because the transferred film already solidified. Furthermore, transferring solidified film has the advantage of making multilayers because it will not damage the underlying layer. In addition, this report also demonstrates the uniformity of OFET devices fabricated from a single floating film with large-area.

Until now, UFTM films are still being prepared manually, which may result in variations, depending on who prepares the UFTM films. An interesting job in the future is to make the UFTM film preparation process automatic. **Figure 6.1** illustrates the process of automating film preparation on a flexible substrate using the UFTM method. First, to get a wider floating film, the size of the slider is enlarged, and the polymer solution flows from a reservoir with a wide, narrow slit at the bottom. This polymer reservoir design allows the solution to drop simultaneously, followed by forming a wide and oriented floating film. The floating film is then transferred on the flexible substrate assisted by a rotating cylinder with a speed similar to floating film growth. This automated UFTM design makes it possible to mass-produce thin films on flexible substrates.

It has been demonstrated that this method resulted in the thin film of the p-type semiconducting polymer with high orientation. Furthermore, the n-type semiconducting polymer can also be prepared similarly to produce a high-performance n-channel OFET. Thus, incorporating highly oriented n-type and p-type polymer semiconductors in multilayer structures can develop flexible high-performance inverters.

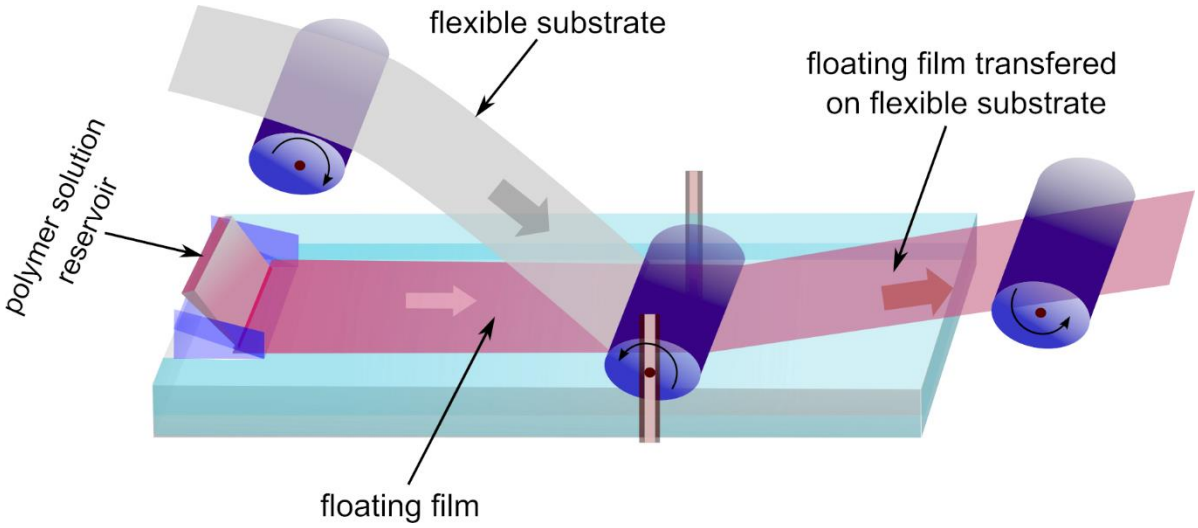


**Figure 6.1. Illustration of automation of thin-film preparation on the flexible substrate in UFTM method**

# References


(1) R. Das, X. He, K. G. Flexible, Printed and Organic Electronics 2020-2030: Forecasts, Technologies, Markets: IDTechEx https://www.idtechex.com/en/research-report/flexible-printed-and-organic-electronics-2020-2030-forecasts-technologies-markets/687 (accessed Jun 25, 2021).

(2) Marketsandmarkets.com. Organic Electronics Market by Material (Semiconductor, Conductive, Dielectric and Substrate), by Application (Battery, Conductive Ink, Display, Lighting, Logic/Memory, Sensor, OPV, ORFID and Others), Geography - Global Analysis and Forecast (2014 - 2020) http://www.marketsandmarkets.com/Market-Reports/organic-electronics-market-144113962.html (accessed Jun 25, 2021).

(3) Rühle, V.; Lukyanov, A.; May, F.; Schrader, M.; Vehoff, T.; Kirkpatrick, J.; Baumeier, B.; Andrienko, D. Microscopic Simulations of Charge Transport in Disordered Organic Semiconductors. *J. Chem. Theory Comput.* **2011**, *7* (10), 3335–3345. https://doi.org/10.1021/ct200388s.

(4) Gryn'ova, G.; Lin, K.-H.; Corminboeuf, C. Read between the Molecules: Computational Insights into Organic Semiconductors. *J. Am. Chem. Soc.* **2018**, *140* (48), 16370–16386. https://doi.org/10.1021/jacs.8b07985.

(5) Wang, Y.; Sun, L.; Wang, C.; Yang, F.; Ren, X.; Zhang, X.; Dong, H.; Hu, W. Organic Crystalline Materials in Flexible Electronics. *Chem. Soc. Rev.* **2019**, *48* (6), 1492–1530. https://doi.org/10.1039/C8CS00406D.

(6) Coropceanu, V.; Cornil, J.; da Silva Filho, D. A.; Olivier, Y.; Silbey, R.; Brédas, J.-L. Charge Transport in Organic Semiconductors. *Chem. Rev.* **2007**, *107* (4), 926–952. https://doi.org/10.1021/cr050140x.

(7) Anthony, J. E. Functionalized Acenes and Heteroacenes for Organic Electronics. *Chem. Rev.* **2006**, *106* (12), 5028–5048. https://doi.org/10.1021/cr050966z.

(8) Nagar, R.; Varrla, E.; Vinayan, B. P. Photocatalysts for Hydrogen Generation and Organic Contaminants Degradation. In *Multifunctional Photocatalytic Materials for Energy*; Elsevier, 2018; pp 215–236. https://doi.org/10.1016/B978-0-08-101977-1.00011-9.

(9) Yuan, Y.; Giri, G.; Ayzner, A. L.; Zoombelt, A. P.; Mannsfeld, S. C. B.; Chen, J.; Nordlund, D.; Toney, M. F.; Huang, J.; Bao, Z. Ultra-High Mobility Transparent Organic Thin Film Transistors Grown by an off-Centre Spin-Coating Method. *Nat. Commun.*

**2014**, *5* (1), 3005. https://doi.org/10.1038/ncomms4005.

(10) Bucella, S. G.; Luzio, A.; Gann, E.; Thomsen, L.; McNeill, C. R.; Pace, G.; Perinot, A.; Chen, Z.; Facchetti, A.; Caironi, M. Macroscopic and High-Throughput Printing of Aligned Nanostructured Polymer Semiconductors for MHz Large-Area Electronics. *Nat. Commun.* **2015**, *6* (1), 8394. https://doi.org/10.1038/ncomms9394.

(11) Steyrleuthner, R.; Schubert, M.; Howard, I.; Klaumünzer, B.; Schilling, K.; Chen, Z.; Saalfrank, P.; Laquai, F.; Facchetti, A.; Neher, D. Aggregation in a High-Mobility n-Type Low-Bandgap Copolymer with Implications on Semicrystalline Morphology. *J. Am. Chem. Soc.* **2012**, *134* (44), 18303–18317. https://doi.org/10.1021/ja306844f.

(12) Pandey, M.; Kumari, N.; Nagamatsu, S.; Pandey, S. S. Recent Advances in the Orientation of Conjugated Polymers for Organic Field-Effect Transistors. *J. Mater. Chem. C* **2019**, *7* (43), 13323–13351. https://doi.org/10.1039/c9tc04397g.

(13) Jimison, L. H.; Toney, M. F.; McCulloch, I.; Heeney, M.; Salleo, A. Charge-Transport Anisotropy Due to Grain Boundaries in Directionally Crystallized Thin Films of Regioregular Poly(3-Hexylthiophene). *Adv. Mater.* **2009**, *21* (16), 1568–1572. https://doi.org/10.1002/adma.200802722.

(14) Tumbleston, J. R.; Collins, B. A.; Yang, L.; Stuart, A. C.; Gann, E.; Ma, W.; You, W.; Ade, H. The Influence of Molecular Orientation on Organic Bulk Heterojunction Solar Cells. *Nat. Photonics* **2014**, *8* (5), 385–391. https://doi.org/10.1038/nphoton.2014.55.

(15) Yang, H.; LeFevre, S. W.; Ryu, C. Y.; Bao, Z. Solubility-Driven Thin Film Structures of Regioregular Poly(3-Hexyl Thiophene) Using Volatile Solvents. *Appl. Phys. Lett.* **2007**, *90* (17), 172116. https://doi.org/10.1063/1.2734387.

(16) Sirringhaus, H.; Brown, P. J.; Friend, R. H.; Nielsen, M. M.; Bechgaard, K.; Langeveld-Voss, B. M. W.; Spiering, a. J. H.; Janssen, R. a. J.; Meijer, E. W.; Herwig, P.; de Leeuw, D. M. Two-Dimensional Charge Transport in Self-Organized, High-Mobility Conjugated Polymers. *Nature* **1999**, *401* (6754), 685–688. https://doi.org/10.1038/44359.

(17) Pandey, R. K.; Takashima, W.; Nagamatsu, S.; Dauendorffer, A.; Kaneto, K.; Prakash, R. Macroscopic Self Ordering of Solution Processible Poly(3,3‴-Dialkylquaterthiophene) by Floating Film Transfer Method. *J. Appl. Phys.* **2013**, *114* (5). https://doi.org/10.1063/1.4817288.

(18) Kumari, N.; Tripathi, A. S. M.; Sadakata, S.; Pandey, M.; Nagamatsu, S.; Hayase, S.; Pandey, S. S. 2D Positional Profiling of Orientation and Thickness Uniformity in the Semiconducting Polymers Thin Films. *Org. Electron.* **2019**, *68*, 221–229. https://doi.org/10.1016/j.orgel.2019.02.011.

(19) Kumari, N.; Pandey, M.; Syafutra, H.; Nagamatsu, S.; Nakamura, M.; Pandey, S. S. Solvent-Assisted Friction Transfer Method for Fabricating Large-Area Thin Films of Semiconducting Polymers with Edge-On Oriented Extended Backbones. *ACS Appl. Mater. Interfaces* **2020**, *12* (49), 55033–55043. https://doi.org/10.1021/acsami.0c14874.

(20) Chabinyc, M. L.; Toney, M. F.; Kline, R. J.; McCulloch, I.; Heeney, M. X-Ray Scattering Study of Thin Films of Poly(2,5-Bis(3-Alkylthiophen-2-Yl)Thieno[3,2- b ]Thiophene). *J. Am. Chem. Soc.* **2007**, *129* (11), 3226–3237. https://doi.org/10.1021/ja0670714.

(21) Chabinyc, M. L. X-ray Scattering from Films of Semiconducting Polymers. *Polym. Rev.* **2008**, *48* (3), 463–492. https://doi.org/10.1080/15583720802231734.

(22) Noriega, R.; Rivnay, J.; Vandewal, K.; Koch, F. P. V.; Stingelin, N.; Smith, P.; Toney, M. F.; Salleo, A. A General Relationship between Disorder, Aggregation and Charge Transport in Conjugated Polymers. *Nat. Mater.* **2013**, *12* (11), 1038–1044. https://doi.org/10.1038/nmat3722.

(23) Nahid, M. M.; Gann, E.; Thomsen, L.; McNeill, C. R. NEXAFS Spectroscopy of Conjugated Polymers. *Eur. Polym. J.* **2016**, *81*, 532–554. https://doi.org/10.1016/j.eurpolymj.2016.01.017.

(24) Chang, J.; Lin, Z.; Zhang, C.; Hao, Y. Organic Field-Effect Transistor: Device Physics, Materials, and Process. In *Different Types of Field-Effect Transistors - Theory and Applications*; InTech, 2017. https://doi.org/10.5772/intechopen.68215.

(25) Tsumura, A.; Koezuka, H.; Ando, T. Macromolecular Electronic Device: Field-effect Transistor with a Polythiophene Thin Film. *Appl. Phys. Lett.* **1986**, *49* (18), 1210–1212. https://doi.org/10.1063/1.97417.

(26) Lee, B. H.; Bazan, G. C.; Heeger, A. J. Doping-Induced Carrier Density Modulation in Polymer Field-Effect Transistors. *Adv. Mater.* **2016**, *28* (1), 57–62. https://doi.org/10.1002/adma.201504307.

(27) Paterson, A. F.; Singh, S.; Fallon, K. J.; Hodsden, T.; Han, Y.; Schroeder, B. C.; Bronstein, H.; Heeney, M.; McCulloch, I.; Anthopoulos, T. D. Recent Progress in High-Mobility Organic Transistors: A Reality Check. *Adv. Mater.* **2018**, *30* (36), 1801079. https://doi.org/10.1002/adma.201801079.

(28) Ji, D.; Li, L.; Fuchs, H.; Hu, W. Engineering the Interfacial Materials of Organic Field-Effect Transistors for Efficient Charge Transport. *Accounts Mater. Res.* **2021**, *2* (3), 159–169. https://doi.org/10.1021/accountsmr.0c00112.

(29) Guo, S.; Wang, Z.; Chen, X.; Li, L.; Li, J.; Ji, D.; Li, L.; Hu, W. Low-voltage Polymer-dielectric-based Organic Field-effect Transistors and Applications. *Nano Sel.* **2021**,

nano.202100051. https://doi.org/10.1002/nano.202100051.

(30) Tang, W.; Huang, Y.; Han, L.; Liu, R.; Su, Y.; Guo, X.; Yan, F. Recent Progress in Printable Organic Field Effect Transistors. *J. Mater. Chem. C* **2019**, *7* (4), 790–808. https://doi.org/10.1039/C8TC05485A.

(31) Khim, D.; Luzio, A.; Bonacchini, G. E.; Pace, G.; Lee, M. J.; Noh, Y. Y.; Caironi, M. Uniaxial Alignment of Conjugated Polymer Films for High-Performance Organic Field-Effect Transistors. *Advanced Materials*. Wiley-VCH Verlag May 17, 2018. https://doi.org/10.1002/adma.201705463.

(32) Tripathi, A. S. M.; Pandey, M.; Sadakata, S.; Nagamatsu, S.; Takashima, W.; Hayase, S.; Pandey, S. S. Anisotropic Charge Transport in Highly Oriented Films of Semiconducting Polymer Prepared by Ribbon-Shaped Floating Film. *Appl. Phys. Lett.* **2018**, *112* (12), 123301. https://doi.org/10.1063/1.5000566.

(33) Tripathi, A. S. M.; Gupta, R. K.; Sharma, S.; Nagamatsu, S.; Pandey, S. S. Molecular Orientation and Anisotropic Charge Transport in the Large Area Thin Films of Regioregular Poly(3-Alkylthiophenes) Fabricated by Ribbon-Shaped FTM. *Org. Electron.* **2020**, *81*. https://doi.org/10.1016/j.orgel.2020.105687.

(34) Tripathi, A. S. M.; Kumari, N.; Nagamatsu, S.; Hayase, S.; Pandey, S. S. Facile Fabrication of Large Area Oriented Conjugated Polymer Films by Ribbon-Shaped FTM and Its Implication on Anisotropic Charge Transport. *Org. Electron.* **2019**, *65*, 1–7. https://doi.org/10.1016/j.orgel.2018.10.043.

(35) Li, Y.; Singh, S. P.; Sonar, P. A High Mobility P-Type DPP-Thieno[3,2-b]Thiophene Copolymer for Organic Thin-Film Transistors. *Adv. Mater.* **2010**, *22* (43), 4862–4866. https://doi.org/10.1002/adma.201002313.

(36) Lim, E.; Jung, B.-J.; Shim, H.-K. Synthesis and Characterization of a New Light-Emitting Fluorene−Thieno[3,2- b ]Thiophene-Based Conjugated Copolymer. *Macromolecules* **2003**, *36* (12), 4288–4293. https://doi.org/10.1021/ma034168r.

(37) Dauendorffer, A.; Miyajima, S.; Nagamatsu, S.; Takashima, W.; Hayase, S.; Kaneto, K. One-Step Deposition of Self-Oriented β-Phase Polyfluorene Thin Films for Polarized Polymer Light-Emitting Diodes. *Appl. Phys. Express* **2012**, *5* (9), 092101. https://doi.org/10.1143/APEX.5.092101.

(38) Morita, T.; Singh, V.; Nagamatsu, S.; Oku, S.; Takashima, W.; Kaneto, K. Enhancement of Transport Characteristics in Poly(3-Hexylthiophene) Films Deposited with Floating Film Transfer Method. *Appl. Phys. Express* **2009**, *2* (11), 111502. https://doi.org/10.1143/apex.2.111502.

(39) Pandey, M.; Gowda, A.; Nagamatsu, S.; Kumar, S.; Takashima, W.; Hayase, S.; Pandey, S. S. Rapid Formation and Macroscopic Self-Assembly of Liquid-Crystalline, High-Mobility, Semiconducting Thienothiophene. *Adv. Mater. Interfaces* **2018**, *5* (6), 1700875. https://doi.org/10.1002/admi.201700875.

(40) Sanda, S.; Nagase, T.; Kobayashi, T.; Takimiya, K.; Sadamitsu, Y.; Naito, H. High-Performance Didodecylbenzothienobenzothiophene-Based Top-Gate Organic Transistors Processed by Spin Coating Using Binary Solvent Mixtures. *Org. Electron.* **2018**, *58*, 306–312. https://doi.org/10.1016/j.orgel.2018.04.013.

(41) Chang, J. F.; Sun, B.; Breiby, D. W.; Nielsen, M. M.; Sölling, T. I.; Giles, M.; McCulloch, I.; Sirringhaus, H. Enhanced Mobility of Poly(3-Hexylthiophene) Transistors by Spin-Coating from High-Boiling-Point Solvents. *Chem. Mater.* **2004**, *16* (23), 4772–4776. https://doi.org/10.1021/cm049617w.

(42) Zhang, F. J.; Di, C. A.; Berdunov, N.; Hu, Y.; Hu, Y.; Gao, X.; Meng, Q.; Sirringhaus, H.; Zhu, D. Ultrathin Film Organic Transistors: Precise Control of Semiconductor Thickness via Spin-Coating. *Adv. Mater.* **2013**, *25* (10), 1401–1407. https://doi.org/10.1002/adma.201204075.

(43) Endo, T.; Nagase, T.; Kobayashi, T.; Takimiya, K.; Ikeda, M.; Naito, H. Solution-Processed Dioctylbenzothienobenzothiophene-Based Top-Gate Organic Transistors with High Mobility, Low Threshold Voltage, and High Electrical Stability. *Appl. Phys. Express* **2010**, *3* (12). https://doi.org/10.1143/APEX.3.121601.

(44) Kim, N. K.; Jang, S. Y.; Pace, G.; Caironi, M.; Park, W. T.; Khim, D.; Kim, J.; Kim, D. Y.; Noh, Y. Y. High-Performance Organic Field-Effect Transistors with Directionally Aligned Conjugated Polymer Film Deposited from Pre-Aggregated Solution. *Chem. Mater.* **2015**, *27* (24), 8345–8353. https://doi.org/10.1021/acs.chemmater.5b03775.

(45) Roberts, M. E.; Queraltó, N.; Mannsfeld, S. C. B.; Reinecke, B. N.; Knoll, W.; Bao, Z. Cross-Linked Polymer Gate Dielectric Films for Low-Voltage Organic Transistors. *Chem. Mater.* **2009**, *21* (11), 2292–2299. https://doi.org/10.1021/cm900637p.

(46) Yilbas, B. S.; Al-Sharafi, A.; Ali, H. Surfaces for Self-Cleaning. In *Self-Cleaning of Surfaces and Water Droplet Mobility*; Elsevier, 2019; pp 45–98. https://doi.org/10.1016/B978-0-12-814776-4.00003-3.

(47) DeLongchamp, D. M.; Kline, R. J.; Lin, E. K.; Fischer, D. A.; Richter, L. J.; Lucas, L. A.; Heeney, M.; McCulloch, I.; Northrup, J. E. High Carrier Mobility Polythiophene Thin Films: Structure Determination by Experiment and Theory. *Adv. Mater.* **2007**, *19* (6), 833–837. https://doi.org/10.1002/adma.200602651.

(48) Nagamatsu, S.; Takashima, W.; Kaneto, K.; Yoshida, Y.; Tanigaki, N.; Yase, K.; Omote, K. Backbone Arrangement in "Friction-Transferred" Regioregular Poly(3-Alkylthiophene)S. *Macromolecules* **2003**, *36* (14), 5252–5257. https://doi.org/10.1021/ma025887t.

(49) Nagamatsu, S.; Misaki, M.; Chikamatsu, M.; Kimura, T.; Yoshida, Y.; Azumi, R.; Tanigaki, N.; Yase, K. Crystal Structure of Friction-Transferred Poly(2,5-Dioctyloxy-1,4-Phenylenevinylene). *J. Phys. Chem. B* **2007**, *111* (17), 4349–4354. https://doi.org/10.1021/jp067555m.

(50) Sirringhaus, H. 25th Anniversary Article: Organic Field-Effect Transistors: The Path beyond Amorphous Silicon. *Adv. Mater.* **2014**, *26* (9), 1319–1335. https://doi.org/10.1002/adma.201304346.

(51) Kim, N. K.; Shin, E. S.; Noh, Y. Y.; Kim, D. Y. A Selection Rule of Solvent for Highly Aligned Diketopyrrolopyrrole-Based Conjugated Polymer Film for High Performance Organic Field-Effect Transistors. *Org. Electron.* **2018**, *55*, 6–14. https://doi.org/10.1016/j.orgel.2018.01.006.

(52) Oh, J. Y.; Rondeau-Gagné, S.; Chiu, Y. C.; Chortos, A.; Lissel, F.; Wang, G. J. N.; Schroeder, B. C.; Kurosawa, T.; Lopez, J.; Katsumata, T.; Xu, J.; Zhu, C.; Gu, X.; Bae, W. G.; Kim, Y.; Jin, L.; Chung, J. W.; Tok, J. B. H.; Bao, Z. Intrinsically Stretchable and Healable Semiconducting Polymer for Organic Transistors. *Nature* **2016**, *539* (7629), 411–415. https://doi.org/10.1038/nature20102.

(53) Wang, S.; Xu, J.; Wang, W.; Wang, G. J. N.; Rastak, R.; Molina-Lopez, F.; Chung, J. W.; Niu, S.; Feig, V. R.; Lopez, J.; Lei, T.; Kwon, S. K.; Kim, Y.; Foudeh, A. M.; Ehrlich, A.; Gasperini, A.; Yun, Y.; Murmann, B.; Tok, J. B. H.; Bao, Z. Skin Electronics from Scalable Fabrication of an Intrinsically Stretchable Transistor Array. *Nature* **2018**, *555* (7694), 83–88. https://doi.org/10.1038/nature25494.

(54) Pandey, M.; Pandey, S. S.; Nagamatsu, S.; Hayase, S.; Takashima, W. Solvent Driven Performance in Thin Floating-Films of PBTTT for Organic Field Effect Transistor: Role of Macroscopic Orientation. *Org. Electron.* **2017**, *43*, 240–246. https://doi.org/10.1016/j.orgel.2017.01.031.

(55) Pandey, M.; Nagamatsu, S.; Takashima, W.; Pandey, S. S.; Hayase, S. Interplay of Orientation and Blending: Synergistic Enhancement of Field Effect Mobility in Thiophene-Based Conjugated Polymers. *J. Phys. Chem. C* **2017**, *121* (21), 11184–11193. https://doi.org/10.1021/acs.jpcc.7b03416.

(56) Pandey, M.; Nagamatsu, S.; Pandey, S. S.; Hayase, S.; Takashima, W. Enhancement of

Carrier Mobility along with Anisotropic Transport in Non-Regiocontrolled Poly (3-Hexylthiophene) Films Processed by Floating Film Transfer Method. *Org. Electron.* **2016**, *38*, 115–120. https://doi.org/10.1016/j.orgel.2016.08.003.

(57) Brinkmann, M.; Hartmann, L.; Biniek, L.; Tremel, K.; Kayunkid, N. Orienting Semi-Conducting Pi-Conjugated Polymers. *Macromol. Rapid Commun.* **2014**, *35* (1), 9–26. https://doi.org/10.1002/marc.201300712.

(58) Kumari, N.; Pandey, M.; Nagamatsu, S.; Nakamura, M.; Pandey, S. S. Investigation and Control of Charge Transport Anisotropy in Highly Oriented Friction-Transferred Polythiophene Thin Films. *ACS Appl. Mater. Interfaces* **2020**, *12* (10), 11876–11883. https://doi.org/10.1021/acsami.9b23345.

(59) Hartmann, L.; Tremel, K.; Uttiya, S.; Crossland, E.; Ludwigs, S.; Kayunkid, N.; Vergnat, C.; Brinkmann, M. 2D versus 3D Crystalline Order in Thin Films of Regioregular Poly(3-Hexylthiophene) Oriented by Mechanical Rubbing and Epitaxy. *Adv. Funct. Mater.* **2011**, *21* (21), 4047–4057. https://doi.org/10.1002/adfm.201101139.

(60) Pandey, M.; Sadakata, S.; Nagamatsu, S.; Pandey, S. S.; Hayase, S.; Takashima, W. Layer-by-Layer Coating of Oriented Conjugated Polymer Films towards Anisotropic Electronics. *Synth. Met.* **2017**, *227*. https://doi.org/10.1016/j.synthmet.2017.02.018.

(61) Pandey, M.; Wang, Z.; Kapil, G.; Baranwal, A. K. A. K.; Hirotani, D.; Hamada, K.; Hayase, S. Dependence of ITO-Coated Flexible Substrates in the Performance and Bending Durability of Perovskite Solar Cells. *Adv. Eng. Mater.* **2019**, *21* (8), 1900288. https://doi.org/10.1002/adem.201900288.

(62) Clark, J.; Silva, C.; Friend, R. H.; Spano, F. C. Role of Intermolecular Coupling in the Photophysics of Disordered Organic Semiconductors: Aggregate Emission in Regioregular Polythiophene. *Phys. Rev. Lett.* **2007**, *98* (20), 206406. https://doi.org/10.1103/PhysRevLett.98.206406.

(63) Clark, J.; Chang, J.-F.; Spano, F. C.; Friend, R. H.; Silva, C. Determining Exciton Bandwidth and Film Microstructure in Polythiophene Films Using Linear Absorption Spectroscopy. *Appl. Phys. Lett.* **2009**, *94* (16), 163306. https://doi.org/10.1063/1.3110904.

(64) Gaudin, O. P. M.; Samuel, I. D. W.; Amriou, S.; Burn, P. L. Thickness Dependent Absorption Spectra in Conjugated Polymers: Morphology or Interference? *Appl. Phys. Lett.* **2010**, *96* (5). https://doi.org/10.1063/1.3294636.

(65) Fox, M. *Optical Properties of Solids*; Oxford University Press, 2001.

(66) Pandey, R. K.; Singh, A. K.; Upadhyay, C.; Prakash, R. Molecular Self Ordering and

Charge Transport in Layer by Layer Deposited Poly (3,3‴-Dialkylquarterthiophene) Films Formed by Langmuir-Schaefer Technique. *J. Appl. Phys* **2014**, *116*, 94311. https://doi.org/10.1063/1.4894515.

(67) Kline, R. J.; DeLongchamp, D. M.; Fischer, D. A.; Lin, E. K.; Richter, L. J.; Chabinyc, M. L.; Toney, M. F.; Heeney, M.; McCulloch, I. Critical Role of Side-Chain Attachment Density on the Order and Device Performance of Polythiophenes. *Macromolecules* **2007**, *40* (22), 7960–7965. https://doi.org/10.1021/ma0709001.

(68) Hosokawa, Y.; Misaki, M.; Yamamoto, S.; Torii, M.; Ishida, K.; Ueda, Y. Molecular Orientation and Anisotropic Carrier Mobility in Poorly Soluble Polythiophene Thin Films. *Appl. Phys. Lett.* **2012**, *100* (20), 203305. https://doi.org/10.1063/1.4718424.

(69) Tripathi, A. S. M.; Sadakata, S.; Gupta, R. K.; Nagamatsu, S.; Ando, Y.; Pandey, S. S. Implication of Molecular Weight on Optical and Charge Transport Anisotropy in PQT-C12 Films Fabricated by Dynamic FTM. *ACS Appl. Mater. Interfaces* **2019**, *11*, 28088–28095. https://doi.org/10.1021/acsami.9b06568.

(70) O'Connor, B. T.; Reid, O. G.; Zhang, X.; Kline, R. J.; Richter, L. J.; Gundlach, D. J.; Delongchamp, D. M.; Toney, M. F.; Kopidakis, N.; Rumbles, G. Morphological Origin of Charge Transport Anisotropy in Aligned Polythiophene Thin Films. *Adv. Funct. Mater.* **2014**, *24* (22), 3422–3431. https://doi.org/10.1002/adfm.201303351.

(71) Lee, M. J.; Gupta, D.; Zhao, N.; Heeney, M.; Mcculloch, I.; Sirringhaus, H. Anisotropy of Charge Transport in a Uniaxially Aligned and Chain-Extended, High-Mobility, Conjugated Polymer Semiconductor. *Adv. Funct. Mater.* **2011**, *21* (5), 932–940. https://doi.org/10.1002/adfm.201001781.

(72) Kushida, T.; Nagase, T.; Naito, H. Angular Distribution of Field-Effect Mobility in Oriented Poly[5,5???-Bis(3-Dodecyl-2-Thienyl)-2,2???-Bithiophene] Fabricated by Roll-Transfer Printing. *Appl. Phys. Lett.* **2014**, *104* (9), 093304. https://doi.org/10.1063/1.4867980.

(73) Pingel, P.; Zen, A.; Neher, D.; Lieberwirth, I.; Wegner, G.; Allard, S.; Scherf, U. Unexpectedly High Field-Effect Mobility of a Soluble, Low Molecular Weight Oligoquaterthiophene Fraction with Low Polydispersity. *Appl. Phys. A Mater. Sci. Process.* **2009**, *95* (1), 67–72. https://doi.org/10.1007/s00339-008-4994-0.

(74) O'Connor, B.; Kline, R. J.; Conrad, B. R.; Richter, L. J.; Gundlach, D.; Toney, M. F.; DeLongchamp, D. M. Anisotropic Structure and Charge Transport in Highly Strain-Aligned Regioregular Poly(3-Hexylthiophene). *Adv. Funct. Mater.* **2011**, *21* (19), 3697–3705. https://doi.org/10.1002/adfm.201100904.

(75) Walser, M. P.; Kalb, W. L.; Mathis, T.; Brenner, T. J.; Batlogg, B. Stable Complementary Inverters with Organic Field-Effect Transistors on Cytop Fluoropolymer Gate Dielectric. *Appl. Phys. Lett.* **2009**, *94* (5), 92–95. https://doi.org/10.1063/1.3077192.

(76) Shaari, S.; Naka, S.; Okada, H. Effect of Interfacial Layers on Physical and Electrical Properties of Dinaphtho[2,3-b:2′,3′-d]Thiophene Organic Thin-Film Transistors. *Jpn. J. Appl. Phys.* **2017**, *56* (3), 03BB04. https://doi.org/10.7567/JJAP.56.03BB04.

(77) Lee, S.; Koo, B.; Shin, J.; Lee, E.; Park, H.; Kim, H. Effects of Hydroxyl Groups in Polymeric Dielectrics on Organic Transistor Performance. *Appl. Phys. Lett.* **2006**, *88* (16), 162109.

(78) Yang, J.; Zhao, Z.; Wang, S.; Guo, Y.; Liu, Y. Insight into High-Performance Conjugated Polymers for Organic Field-Effect Transistors. *Chem* **2018**, *4* (12), 2748–2785. https://doi.org/10.1016/j.chempr.2018.08.005.

(79) Schott, S.; Gann, E.; Thomsen, L.; Jung, S. H.; Lee, J. K.; McNeill, C. R.; Sirringhaus, H. Charge-Transport Anisotropy in a Uniaxially Aligned Diketopyrrolopyrrole-Based Copolymer. *Adv. Mater.* **2015**, *27* (45), 7356–7364. https://doi.org/10.1002/adma.201502437.

(80) Yang, Y.; Hong, Y.; Wang, X. Utilizing the Diffusion of Fluorinated Polymers to Modify the Semiconductor/Dielectric Interface in Solution-Processed Conjugated Polymer Field-Effect Transistors. *ACS Appl. Mater. Interfaces* **2021**, *13* (7), 8682–8691. https://doi.org/10.1021/acsami.0c23058.

(81) Takagi, K.; Nagase, T.; Kobayashi, T.; Kushida, T.; Naito, H. High-Performance and Electrically Stable Solution-Processed Polymer Field-Effect Transistors with a Top-Gate Configuration. *Jpn. J. Appl. Phys.* **2015**, *54* (1), 011601. https://doi.org/10.7567/JJAP.54.011601.

(82) Rumer, J. W.; Rossbauer, S.; Planells, M.; Watkins, S. E.; Anthopoulos, T. D.; McCulloch, I. Reduced Roughness for Improved Mobility in Benzodipyrrolidone-Based, n-Type OFETS. *J. Mater. Chem. C* **2014**, *2* (41), 8822–8828. https://doi.org/10.1039/c4tc01790k.

(83) Pei, M.; Guo, J.; Zhang, B.; Jiang, S.; Hao, Z.; Xu, X.; Li, Y. Semiconductor/Dielectric Interface in Organic Field-Effect Transistors: Charge Transport, Interfacial Effects, and Perspectives with 2D Molecular Crystals. *Advances in Physics: X*. Taylor and Francis Ltd. January 1, 2020. https://doi.org/10.1080/23746149.2020.1747945.

(84) Usta, H.; Facchetti, A. *Polymeric and Small-Molecule Semiconductors for Organic*

*Field-Effect Transistors*; 2015.

(85) Khim, D.; Ryu, G. S.; Park, W. T.; Kim, H.; Lee, M.; Noh, Y. Y. Precisely Controlled Ultrathin Conjugated Polymer Films for Large Area Transparent Transistors and Highly Sensitive Chemical Sensors. *Adv. Mater.* **2016**, *28* (14), 2752–2759. https://doi.org/10.1002/adma.201505946.

(86) Jurchescu, O. D. Large-Area Organic Electronics: Inkjet Printing and Spray Coating Techniques. In *Organic Electronics*; Wiley-VCH, 2013; pp 319–339. https://doi.org/https://doi.org/10.1002/9783527650965.ch13.

(87) Zeidell, A. M.; Filston, D. S.; Waldrip, M.; Iqbal, H. F.; Chen, H.; McCulloch, I.; Jurchescu, O. D. Large-Area Uniform Polymer Transistor Arrays on Flexible Substrates: Towards High-Throughput Sensor Fabrication. *Adv. Mater. Technol.* **2020**, *5* (8), 1–7. https://doi.org/10.1002/admt.202000390.

(88) Huang, F.; Li, M.; Xu, Y.; Cui, A.; Li, W.; Xu, Y.; Chu, J.; Noh, Y. Y. Understanding Thickness-Dependent Electrical Characteristics in Conjugated Polymer Transistors with Top-Gate Staggered Structure. *IEEE Trans. Electron Devices* **2019**, *66* (6), 2723–2728. https://doi.org/10.1109/TED.2019.2910116.

(89) Himmelberger, S.; Dacuña, J.; Rivnay, J.; Jimison, L. H.; McCarthy-Ward, T.; Heeney, M.; McCulloch, I.; Toney, M. F.; Salleo, A. Effects of Confinement on Microstructure and Charge Transport in High Performance Semicrystalline Polymer Semiconductors. *Adv. Funct. Mater.* **2013**, *23* (16), 2091–2098. https://doi.org/10.1002/ADFM.201202408.

(90) Harper, A. F.; Diemer, P. J.; Jurchescu, O. D. Contact Patterning by Laser Printing for Flexible Electronics on Paper. *npj Flex. Electron. 2019 31* **2019**, *3* (1), 1–6. https://doi.org/10.1038/s41528-019-0055-3.

(91) Wang, H.; Tang, Q.; Zhao, X.; Tong, Y.; Liu, Y. Ultrasensitive Flexible Proximity Sensor Based on Organic Crystal for Location Detection. *ACS Appl. Mater. Interfaces* **2018**, *10* (3), 2785–2792. https://doi.org/10.1021/acsami.7b15352.

(92) Chen, H.; Zhang, W.; Li, M.; He, G.; Guo, X. Interface Engineering in Organic Field-Effect Transistors: Principles, Applications, and Perspectives. *Chem. Rev.* **2020**, *120* (5), 2879–2949. https://doi.org/10.1021/acs.chemrev.9b00532.

(93) Yang, D. S.; Barłóg, M.; Park, J.; Chung, K.; Shanker, A.; Sun, J.; Kang, J.; Lee, K.; Al-Hashimi, M.; Kim, J. Alignment of Lyotropic Liquid Crystalline Conjugated Polymers in Floating Films. *ACS Omega* **2018**, *3* (11), 14807–14813. https://doi.org/10.1021/acsomega.8b02205.

(94) Vohra, V.; Anzai, T. Molecular Orientation of Conjugated Polymer Chains in Nanostructures and Thin Films: Review of Processes and Application to Optoelectronics. *Journal of Nanomaterials*. Hindawi Limited 2017. https://doi.org/10.1155/2017/3624750.

(95) Hamidi-Sakr, A.; Biniek, L.; Fall, S.; Brinkmann, M. Precise Control of Lamellar Thickness in Highly Oriented Regioregular Poly(3-Hexylthiophene) Thin Films Prepared by High-Temperature Rubbing: Correlations with Optical Properties and Charge Transport. *Adv. Funct. Mater.* **2016**, *26* (3), 408–420. https://doi.org/10.1002/adfm.201504096.

(96) Pandey, R. K.; Singh, A. K.; Prakash, R. Directed Self-Assembly of Poly(3,3$_v$-Dialkylquarterthiophene) Polymer Thin Film: Effect of Annealing Temperature. *J. Phys. Chem. C* **2014**, *118* (40), 22943–22951. https://doi.org/10.1021/jp507321z.

(97) Choi, D.; An, T. K.; Kim, Y. J.; Chung, D. S.; Kim, S. H.; Park, C. E. Effects of Semiconductor/Dielectric Interfacial Properties on the Electrical Performance of Top-Gate Organic Transistors. *Org. Electron.* **2014**, *15* (7), 1299–1305. https://doi.org/10.1016/j.orgel.2014.02.026.

(98) Tsao, H. N.; Müllen, K. Improving Polymer Transistor Performance via Morphology Control. *Chem. Soc. Rev.* **2010**, *39* (7), 2372. https://doi.org/10.1039/b918151m.

(99) Chang, S. S.; Rodríguez, A. B.; Higgins, A. M.; Liu, C.; Geoghegan, M.; Sirringhaus, H.; Cousin, F.; Dalgleish, R. M.; Deng, Y. Control of Roughness at Interfaces and the Impact on Charge Mobility in All-Polymer Field-Effect Transistors. *Soft Matter* **2008**, *4* (11), 2220. https://doi.org/10.1039/b810278c.

(100) Gu, K.; Loo, Y. The Polymer Physics of Multiscale Charge Transport in Conjugated Systems. *J. Polym. Sci. Part B Polym. Phys.* **2019**, *57* (23), 1559–1571. https://doi.org/10.1002/polb.24873.

(101) Pingel, P.; Zen, A.; Abellón, R. D.; Grozema, F. C.; Siebbeles, L. D. A.; Neher, D. Temperature-Resolved Local and Macroscopic Charge Carrier Transport in Thin P3HT Layers. *Adv. Funct. Mater.* **2010**, *20* (14), 2286–2295. https://doi.org/10.1002/adfm.200902273.

(102) Bolsée, J.-C.; Oosterbaan, W. D.; Lutsen, L.; Vanderzande, D.; Manca, J. The Importance of Bridging Points for Charge Transport in Webs of Conjugated Polymer Nanofibers. *Adv. Funct. Mater.* **2013**, *23* (7), 862–869. https://doi.org/10.1002/adfm.201102078.

(103) Crossland, E. J. W.; Tremel, K.; Fischer, F.; Rahimi, K.; Reiter, G.; Steiner, U.; Ludwigs,

S. Anisotropic Charge Transport in Spherulitic Poly(3-Hexylthiophene) Films. *Adv. Mater.* **2012**, *24* (6), 839–844. https://doi.org/10.1002/adma.201104284.

(104) Diao, Y.; Zhou, Y.; Kurosawa, T.; Shaw, L.; Wang, C.; Park, S.; Guo, Y.; Reinspach, J. A.; Gu, K.; Gu, X.; Tee, B. C. K.; Pang, C.; Yan, H.; Zhao, D.; Toney, M. F.; Mannsfeld, S. C. B.; Bao, Z. Flow-Enhanced Solution Printing of All-Polymer Solar Cells. *Nat. Commun.* **2015**, *6* (1), 1–10. https://doi.org/10.1038/ncomms8955.

(105) Hidayat, A. T.; Benten, H.; Ohta, N.; Na, Y.; Muraoka, A.; Kojima, H.; Jung, M. C.; Nakamura, M. Enhancement of Short-Range Ordering of Low-Bandgap Donor-Acceptor Conjugated Polymer in Polymer/Polymer Blend Films. *Macromolecules* **2020**. https://doi.org/10.1021/acs.macromol.0c00623.

(106) Han, H.; Nam, S.; Seo, J.; Lee, C.; Kim, H.; Bradley, D. D. C.; Ha, C. S.; Kim, Y. Broadband All-Polymer Phototransistors with Nanostructured Bulk Heterojunction Layers of NIR-Sensing n-Type and Visible Light-Sensing p-Type Polymers. *Sci. Rep.* **2015**, *5*, 16457. https://doi.org/10.1038/srep16457.

(107) Lee, C.; Kim, J.-J. Enhanced Light Out-Coupling of OLEDs with Low Haze by Inserting Randomly Dispersed Nanopillar Arrays Formed by Lateral Phase Separation of Polymer Blends. *Small* **2013**, *9* (22), 3858–3863. https://doi.org/10.1002/smll.201300068.

(108) Nikzad, S.; Wu, H. C.; Kim, J.; Mahoney, C. M.; Matthews, J. R.; Niu, W.; Li, Y.; Wang, H.; Chen, W. C.; Toney, M. F.; He, M.; Bao, Z. Inducing Molecular Aggregation of Polymer Semiconductors in a Secondary Insulating Polymer Matrix to Enhance Charge Transport. *Chem. Mater.* **2020**, *32* (2), 897–905. https://doi.org/10.1021/acs.chemmater.9b05228.

(109) Liu, C.; Minari, T.; Li, Y.; Kumatani, A.; Lee, M. V.; Athena Pan, S. H.; Takimiya, K.; Tsukagoshi, K. Direct Formation of Organic Semiconducting Single Crystals by Solvent Vapor Annealing on a Polymer Base Film. *J. Mater. Chem.* **2012**, *22* (17), 8462–8469. https://doi.org/10.1039/c2jm15747k.

(110) Ejima, H.; Ogita, K.; Yamamoto, M.; Sasaki, S.; Hikima, T.; Takata, M.; Yoshie, N. Epitaxy-Driven Nanostructure Formation in Polymer Blend Thin Films Containing Regioregular Poly(3-Hexylthiophene). *Chem. Lett.* **2016**, *45* (6), 604–606. https://doi.org/10.1246/cl.160068.

(111) Pandey, M.; Pandey, S. S.; Nagamatsu, S.; Hayase, S.; Takashima, W. Influence of Backbone Structure on Orientation of Conjugated Polymers in the Dynamic Casting of Thin Floating-Films. *Thin Solid Films* **2016**, *619*, 125–130. https://doi.org/10.1016/j.tsf.2016.11.015.

(112) Misaki, M.; Chikamatsu, M.; Yoshida, Y.; Azumi, R.; Tanigaki, N.; Yase, K.; Nagamatsu, S.; Ueda, Y. Highly Efficient Polarized Polymer Light-Emitting Diodes Utilizing Oriented Films of B -Phase Poly(9,9-Dioctylfluorene). *Appl. Phys. Lett.* **2008**, *93* (2). https://doi.org/10.1063/1.2959073.

(113) Chu, P. H.; Zhang, L.; Colella, N. S.; Fu, B.; Park, J. O.; Srinivasarao, M.; Briseño, A. L.; Reichmanis, E. Enhanced Mobility and Effective Control of Threshold Voltage in P3HT-Based Field-Effect Transistors via Inclusion of Oligothiophenes. *ACS Appl. Mater. Interfaces* **2015**, *7* (12), 6652–6660. https://doi.org/10.1021/am509090j.

(114) Mori, D.; Benten, H.; Kosaka, J.; Ohkita, H.; Ito, S.; Miyake, K. Polymer/Polymer Blend Solar Cells with 2.0% Efficiency Developed by Thermal Purification of Nanoscale-Phase-Separated Morphology. *ACS Appl. Mater. Interfaces* **2011**, *3*, 2924–2927. https://doi.org/10.1021/am200624s.

(115) Pandey, M.; Pandey, S. S.; Nagamatsu, S.; Hayase, S.; Takashima, W. Controlling Factors for Orientation of Conjugated Polymer Films in Dynamic Floating-Film Transfer Method. *J. Nanosci. Nanotechnol.* **2017**, *17* (3), 1915–1922. https://doi.org/10.1166/jnn.2017.12816.

(116) Pace, G.; Bargigia, I.; Noh, Y. Y.; Silva, C.; Caironi, M. Intrinsically Distinct Hole and Electron Transport in Conjugated Polymers Controlled by Intra and Intermolecular Interactions. *Nat. Commun.* **2019**, *10* (1). https://doi.org/10.1038/s41467-019-13155-9.

(117) Vezie, M. S.; Few, S.; Meager, I.; Pieridou, G.; Dörling, B.; Ashraf, R. S.; Goñi, A. R.; Bronstein, H.; McCulloch, I.; Hayes, S. C.; Campoy-Quiles, M.; Nelson, J. Exploring the Origin of High Optical Absorption in Conjugated Polymers. *Nat. Mater.* **2016**, *15* (7), 746–753. https://doi.org/10.1038/nmat4645.

(118) Chen, L.; Zhao, K.; Cao, X.; Liu, J.; Yu, X.; Han, Y. Diketopyrrolopyrrole-Based Polymer Fibrils Formation by Changing Molecular Conformation during Film Formation. *J. Polym. Sci. Part B Polym. Phys.* **2018**, *56* (15), 1079–1086. https://doi.org/10.1002/polb.24609.

# List of Publications

## 1. Scientific Papers

**Syafutra, H.**; Pandey, M.; Kumari, N.; Pandey, S. S.; Benten, H.; Nakamura, M. Assisted Alignment of Conjugated Polymers in Floating Film Transfer Method Using Polymer Blend. *Thin Solid Films* **2021**, 734, 138814.

Pandey, M.*; **Syafutra, H.***; Kumari, N.; Pandey, S. S.; Abe, R.; Benten, H.; Nakamura, M. Extreme Orientational Uniformity in Large-Area Floating Films of Semiconducting Polymers for Their Application in Flexible Electronics. *ACS Appl. Mater. Interfaces* **2021**, 13 (32), 38534–38543.
*Equal contribution

**Syafutra H.**, Pandey M, Benten H., Nakamura M.. *Perfectness of the main-chain alignment in the π-conjugate polymer films prepared by the floating film transfer method*.
**(under preparation)**

Kumari, N.; Pandey, M.; **Syafutra, H.**; Nagamatsu, S.; Nakamura, M.; Pandey, S. S. Solvent-Assisted Friction Transfer Method for Fabricating Large-Area Thin Films of Semiconducting Polymers with Edge-On Oriented Extended Backbones. *ACS Appl. Mater. Interfaces* **2020**, *12* (49), 55033–55043.

## 2. Scientific Conferences

### a. International Conference (* Presenting Author)

*1) Oral Presentation*

Pandey M. ,* **Syafutra H.**, Kumari N., Pandey S. S. ,* Nakamura M: "Characteristics of Large-Area Floating Films of Oriented Polymeric Semiconductors for Flexible Electronics", The Eighth International Symposium on Organic and Inorganic Electronic Materials and Related Nanotechnologies (EM-NANO 2021), Jun. 1-3, 2021, No. A3-1-2 (Online, Oral Video).

**Syafutra H.,*** Kumari N., Shugita Y.,. Pandey S. S, Jung M. -C, Benten H., Pandey M., Nakamura M.: "Preparation and Characterization of Large-Area Oriented Ribbon-Shaped Floating Films of Conjugated Polymers", The 33rd International Microprocesses and Nanotechnology Conference (MNC2020), Nov. 9-12, 2020, No. 2020-25-1 (Online, Oral Video).

*2) Poster Presentation*

**Syafutra H.,*** Pandey M., Kumari N., Pandey S. S., Benten H., Nakamura M.: "Assisting Polymer Orientation using Polymer Blend in FTM", The Eighth International Symposium on Organic and Inorganic Electronic Materials and Related Nanotechnologies (EM-NANO 2021), Jun. 1-3, 2021, No. P1-33 (Online, Oral Video).

**b. Domestic Conference** (* Presenting Author)

*1) Oral Presentation*

**Syafutra H.,*** Kumari N., Pandey S. S., Benten H., Pandey M., Nakamura M.:"Orientation Characteristics of Large-area Thin Films of Conjugated Polymers", 第 68 回応用物理学会春季学術講演会, オンライン開催, 2021.3.16～19 (2021.3.16) 16a-Z17-7

Pandey M.,* **Syafutra H.**, Sugita Y., Kumari N., Pandey S. S., Benten H., Nakamura M.: "Floating film transfer method: an effective method for macroscopically oriented large-area films of conjugated polymers", 第 68 回応用物理学会春季学術講演会, オンライン開催, 2021.3.16～19 (2021.3.16) 16a-Z17-6.